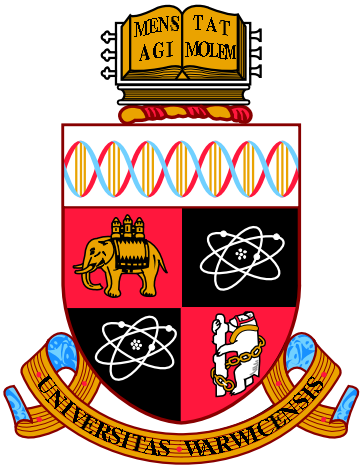

Developing Force Measurement Techniques for Cell Mechanics and Contractility in Ageing Dermal Fibroblasts

by

Zhuonan Yu

Thesis

Submitted to the University of Warwick

for the degree of

Doctor of Philosophy

School of Engineering

February 2021

WARWICK
THE UNIVERSITY OF WARWICK

Contents

List of Tables

List of Figures

Acknowledgements

Foremost I express my deep sense of gratitude and profound respect to my supervisor Dr Isaac Kuo-Kang Liu, who has helped and inspired me at all stages of my time as his student with great patience. I have been incredibly fortunate to have such a great supervisor who has shown immense care towards my research and wellbeing beyond his obligation and my expectation. He has always responded to my queries, addressed my needs very promptly, and tirelessly reviewed and commented on pieces of my writings. I thank him for the dedications and efforts he has put in and the personal time he sacrificed to guild me through the entire PhD.

My sincere thank also goes to Dr Richard Siow and Dr Matthew Smith at King's College London for the collaboration with wonderful outcomes and their time in training me on cell culture skills. Their insightful guidance and expert knowledge in biology have been indispensable to the project. Also, I would like to thank Dr Ken Mao for helpful discussions and valuable suggestions on the finite element analysis. Moreover, it has been a great pleasure to receive help from Dr Tianrong Jin and Lidong Liu on the experiments regarding cell-embedded collagen hydrogel and the finite element modelling of hydrogel indentation. I acknowledge the financial support from the School of Engineering, University of Warwick for consumables and travel costs towards training workshops and conferences, and the technical support from the technicians within the school in building experiment instruments.

Throughout my PhD, I have been incredibly lucky to have shared the experience with colleagues and comrades: Dr Sam, Dr Sarah, Matt, Rhys, Punit, Joe and Sam (2.0). The day-to-day research student life shared with them will forever

be the invaluable experiences I treasure for the rest of my life. Special thanks to my dear friends Jacqui, Jincheng and Meng for keeping the most frustrating days of COVID-19 lockdown bearable. Thank you for the weekend walks in Stratford-upon-Avon, social bubble dinners, 'face-2m-face' catch-ups and the mobile games nights filled with laughter.

I owe a debt of thanks to my parents, Binsheng Yu and Zhongli Wang, for their unrelenting emotional support throughout my studies and years of unconditional love. I can not express how much I appreciate the informative yet somehow philosophical discussion regarding my work with my dad, and the encouragements and emotional supports I had received from my mum when I experienced ups and downs. Without you, I wouldn't be who I am and where I am now.

Last but not least, my special thanks are reserved for amore mio and soulmate, Lingzan for her continued inspiration, tolerance, support and encouragement during the thesis writing, correction and viva preparation process.

Zhuonan Yu

University of Warwick

February, 2021

Declarations

I hereby declare that the work on this thesis, submitted in partial fulfilment of the requirements for the degree of Doctor of Philosophy at the University of Warwick, is original work of my own. The thesis has not been previously submitted to any other institution for any degree, diploma or other qualification.
Parts of this thesis have been published by the author:

- Zhuonan Yu, Matthew J. Smith, Richard C.M. Siow, and Kuo-Kang Liu. Ageing modulates human dermal fibroblast contractility: Quantification using nano-biomechanical testing. Biochimica et Biophysica Acta (BBA) - Molecular Cell Research, Volume 1868, Issue 5 (2021): 118972.
  doi: 10.1016/j.bbamcr.2021.118972

Parts of this thesis have been presented by the author:

- Zhuonan Yu, Matthew J. Smith, Richard C.M. Siow, Lidong Liu and Kuo-Kang Liu. A novel collagen-based assay for measuring dermal fibroblast contractility influenced by natural ageing. 30^{th} Annual Conference of the European Society for Biomaterials, Dresden, Germany, 9^{th} - 13^{th} September, 2019.

Published work is contained in Appendix A.

Abstract

Cellular contraction force plays a crucial role in the normal function of a biological cell. Such importance is greatly enhanced in dermal fibroblasts' function as contraction force generation is directly related to fibroblast's ability in migration and the maintenance of the extracellular matrix. In other words, the contractility of dermal fibroblasts has a close link to the physiological function of the skin as a physical barrier and regulatory organ for the homeostasis of the human body. Despite the fact that the ageing-associated changes in dermal tissue have been studied extensively, there remains a paucity in quantitatively characterising the contractility changes of dermal fibroblasts as an effect of ageing.

The primary goal of this research project is to develop a viable technique in differentiating the contraction force generated by young and aged dermal fibroblasts, which are both highly quantitative and cell-friendly. A novel nano-biomechanical technique has been developed to measure the contraction force exerted by dermal fibroblasts embedded in collagen hydrogels. The collagen hydrogel provides cells with a 3D matrix that mimics physiological conditions in the native tissue, which can be further modified by the residing cells, promoting natural behaviours of the cells. The technique can estimate the contraction force of the embedded cells over a given culture time (up to 48 hours) by accurately measuring the elasticity and the geometrical change of the hydrogel disk. A tailored indentation tester system achieves the measurements in combination with mathematical modelling based on material properties and contact mechanics. The model is further verified by finite element analysis in the prediction of force-displacement of the gel under indentation. The bio-nano-biomechanical tester developed in the project has resolutions of 10 nN and 100 nm in force and displacement, respectively, and can be used in characterising the mechanical behaviours of other soft biological tissues and biomaterials.

The novel technique was applied to measure the contraction force of dermal fibroblasts derived from 'young' ($<$ 30 years old) and 'aged' ($>$ 60 years old) donors and transforming growth factor $\beta 1$ was used as agonist to stimulate contraction. Aged cells showed larger basal contractility while young donors responded to stimulation significantly more. The nano-biomechanical technique demonstrated its ability to differentiate the contraction force of young and aged dermal fibroblasts and the potential of extending the technique further into the study of cell mechanics.

Abbreviations

ADP	Adenosine Diphosphate
AFM	Atomic Force Microscopy
αSMA	α Smooth Muscle Actin
ANOVA	Analysis Of Variance
Arp2/3	Actin Related Protein 2/3
ASCII	American Standard Code for Information Interchange
ATP	Adenosine Triphosphate
CCD	Charge Coupled Device
CFM	Culture Force Monitor
CGCA	Collagen Gel-based Contraction Assay
DAQ	Data Acquisition
DMEM	Dulbeccos' Modified Eagle's Medium
DNA	Deoxyribonucleic Acid
ECM	Extracellular Matrix
EDTA	Ethylenediaminetetraacetic Acid
EMP	Elastic Micro-Pillar
F-actin	Filamentous Actin
F-D	Force-Displacement
FA	Focal Adhesion
FBS	Foetal Bovine Serum
FEA/FEM	Finite Element Analysis/ Finite Element Methods
FPCM	Fibroblast-Populated Collagen Microspheres

G-actin	Globular Actin
GPa	Gigapascal
h	Hour(s)
HDPE	High-density Polyethylene
HSB	Hue-Saturation-Brightness
kg	Kilo-gram
kPa	Kilo-pascal
min	Minute(s)
ml	Millilitre
mM	Millimolar
MMP	Matrix Metalloproteinase
mN	Milli-newton
mRNA	Messenger Ribonucleic Acid
MSC	Mesenchymal Stem Cell
NHDF	Normal Human Dermal Fibroblast
Nlgeom	Nonlinear Geometry
nm	Nano-meter
nN	Nano-newton
OT	Optical Tweezer
OCM	Optical Coherence Microscopy
P-value	Value of Statistical Significance
PBS	Phosphate-Buffered Saline
PDE	Partial Differential Equation
PDMS	Polydimethylsiloxane
PEG	Polyethene Glycol
Pi	Inorganic Phosphate
PMMA	Polymethylmethacrylate
pN	Pico-newton
R^2-value	Coefficient of Determination
RGB	Red-Green-Blue

ROS	Reactive Oxygen Species
s.e.m	Standard Error of the Mean
SLS	Standard Linear Solid
TFM	Traction Force Microscopy
TGF	Transforming Growth Factor
μm	Micro-meter
μN	Micro-newton
UV	Ultraviolet
VI	Virtual Instrument

Chapter 1

Introduction to cell mechanics and contractility measurement in hydrogel

1.1 Introduction

Since the last quarter of the 20^{th} century, we have seen unprecedented shifts and transformations of research methodologies in biological sciences as a result of advancements and breakthroughs in imaging technology, computational power and instrument design. Quantitative studies are now more dominant over that of qualitative and observational nature. These transformations in biological sciences also call for interdisciplinary integrations with traditionally quantitative subjects, such as mathematics, statistics, physics and engineering. As a result, biophysics and biomechanics have been increasingly important and attracted many attentions as it bridges together biology and physics.

Over the past few decades, biomechanical studies have branched into the study of cell mechanics as the reciprocal interactions between mechanical behaviours of cells and their biological functions have been recognised [142, 210]. For example, the contraction of cells can apply a traction force to the extracellular matrix (ECM), and the mechanical cues can be sensed by cells in regulating contraction and indirectly influence migration, growth and differentiation [100]. The contractility of cells determines its ability to exert forces onto the ECM, respond to mechanical stimulations and undergo locomotions. The changes in contractility affect tissue organisation and function through altering cells' ability in dynamically restructure the micro-environment. Also, the importance of the contractility of cells is manifested in tissues such as muscle and skin where tension is key to their functions. The study of contractility of cells within the context of cell-matrix interactions can provide us new perspectives into how contractility of cells changes along with other mechanical parameters, contributing towards various processes such as ageing [31, 182] and disease development [158, 170].

The primary goal of this chapter is to outline the implications of mechanical behaviour of cells such as cell contraction force and cell-matrix elasticity in understanding pathological and ageing states. Furthermore, the physiological relevance of measuring cell contraction force in detecting ageing, along with the current challenges, will be introduced in the following sections. Chapter 2, systematically reviews the mechanisms of ageing of the skin and the changes that occur during dermal fibroblast ageing. In Chapter 3, a number of techniques in measuring cellular forces are presented in detail together with their benefits and limitations in applications. The details regarding the development of a novel bio-nano-indentation tester are presented in Chapter 4 and followed by the measurement and modelling of the mechanical behaviours of collagen gel hydrogel in Chapter 5. The work and results on the investigation of changes of contractility of naturally aged dermal fi-

broblasts are presented in Chapter 6. Lastly, the summaries of this project and future outlooks in future developments of the research topic is outlined in Chapter 7.

1.2 Mechanical behaviours and contractility of cells in disease and ageing

Conventionally, the approaches in studying the changes in disease and ageing have been focused on the biochemical factors. Recently, a significant amount of attention has been shifted to the study of their relationship with the mechanical behaviour of the cell. Moreover, the mechanical characteristics of cells are indicative of the capability of cells in force generation as well as exerting and sensing forces from the surrounding environment. These abilities are crucial to cells' ability to contract, migrate and adapt to changes in the mechanical environments, which is indispensable to regulating the physiological functions [72, 156]. The study of the mechanical behaviours of cells will provide an alternative approach to understanding disease and ageing. Below are few examples showing how disease and ageing processes relate to the changes of cell's ability to sustain, generate and sense mechanical forces.

- The skeletal system is constantly subjected to various mechanical loadings. As the primary functioning cells, osteocytes can sense the mechanical loadings and dynamically respond to the mechanical stimulations. Adequate mechanical stimulation to bone tissue promotes matrix remodelling activities of osteocytes (*e.g.* osteoblast, osteoclast) in health keeping [192]. While the lack of mechanical stimulation due to prolonged immobilisation of an individual is recognised as the primary cause of disease such as osteoporosis [5]. Also, evidence shows that the age-related changes in the force generation and force

sensing abilities of chondrocytes and osteocytes contribute significantly to the development and progression of age-related musculoskeletal disorders [209].

- Dysfunctions in the cardiovascular system often have a strong correlation to cell contractility as contractile forces are required for directing blood flow. Also, its functions are easily influenced by the changes of mechanical behaviours of cells such as stiffness. Evidence has shown that vascular endothelium cells can discriminate various fluid mechanical forces generated by pulsatile blood flow. The resulted phenotypic modulation of the endothelium can lead to cardiovascular diseases such as atherosclerosis [74]. Contractility changes and the lose of regulation to contractility in cardiomyocytes caused by malfunctioning sarcomeric proteins have been recognised to contribute to cardiomyopathies [234]. During ageing, the increase in flow velocity and blood pressure can lead to increased shear stress in arteries, which causes blood vessel cells to undertake structural change, reflected in the increase in stiffness and contractility [198, 251].

- Erythrocytes (*i.e.* red blood cells) are the most abundant cells present in the blood, and their mechanical properties largely govern their functions. The mechanical stability of the biconcave shape allows oxygen transport and the highly elastic and deformable nature enable them to pass through narrow capillaries one-third of their diameter [203]. Stiffening and the loss of their standard biconcave shape are the primary function limiting pathological alterations to the erythrocytes in sickle cell anaemia and malaria [135, 174, 211]. Ageing of the erythrocyte is accompanied by a reduction in the elastic modulus [129] and membrane deformability [40], suggesting consequent functional changes to occur.

- The visual system provides us with a distinctive way to sense the world. To form a sharp image on the retina, focusing power of the lens is adjusted simul-

taneously through contraction of ciliary muscle cells. Presbyopia is the most well-known age-related vision change. It is a result of the decline in ciliary muscle contractility combined with a diminished ability for the lens to accommodate deformation due to stiffening with age [91,92]. Also, from mechanosensing point of view, a previous study has demonstrated that elevated hydrostatic pressure within the eye can cause stress on retinal ganglion cells leading to premature apoptosis and as a consequence causing glaucoma [215].

Generally speaking, the mechanical behaviour of the cells plays a vital role in maintaining homeostasis and ensuring the functionality of the cells. As cells are the basic structural and functional building blocks of tissue, their mechanical behaviours have direct influences over tissue functions. The above example demonstrated how pathological and ageing states relate to the changes in mechanical behaviour and response of cells. The mechanical behaviours of cells include yet not limited to stiffness, adhesion, rheology, shape and the ability to migrate and modify matrix. Despite the variety, all of these are closely related to the malfunction of the cytoskeleton, which forms the structural support of cells. The generation of contraction force requires highly synchronised activities of dynamic assembly of the cytoskeleton and molecular motors, intracellular transport and focal adhesion (see Section 1.3). Thus cell contractility can reflect mechanical behaviours of cells, suggesting the importance of its studies. Especially in the study of ageing, cell contractility can be a great parameter in summarising the multitude of changes in the process.

1.3 Cytoskeleton and contraction force

1.3.1 Elements of the cytoskeleton

The cytoskeleton is a dynamic structural scaffold within the cell. It can undergo remodelling in response to external stimuli and enables cellular contraction. The cytoskeleton is a crucial component for maintaining the structural integrity, defining the mechanical properties and behaviours of a cell. Among which, the high order meshes and fibre bundles of the cytoskeleton is the major contributor in providing the abilities for cells to withstand external mechanical forces and maintain the cellular morphology. Besides, the cytoskeleton also serves in generating and transmitting cellular forces through its dynamic structure [68, 152]. The cytoskeleton comprises three components: microfilaments, microtubules and intermediate filaments (Figure 1.1).

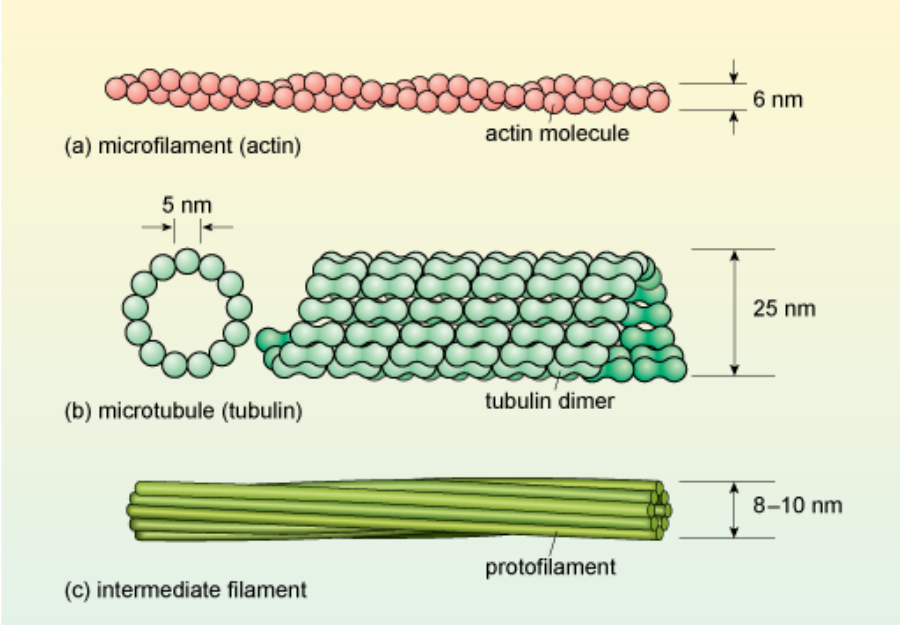

Figure 1.1: Three major components of the cytoskeleton. (a) microfilament, (b) microtubule, (c) intermediate filament. [220]

Microfilament

Microfilaments are also known as actin filaments (Figure 1.1(a)). They are the major structural component of the cytoskeleton and the origin of the forces required for cell contraction and migration [217]. Microfilament is a polarised double-helical actin polymer chain that makes up to 5% of the entire cell protein content. They are widely present throughout the cytoplasm but found to be the most concentrated in the cell cortex. A typical microfilament has a diameter around 6 nm and a length of more than 10 μm [52], interacting with other filaments to form a network. Also, with an elastic modulus of 2 GPa microfilaments are very strong [244]. One of the key functions for microfilaments in relation to cell contraction is the binding with myosins to generate contractile forces, allowing cells to maintain its morphology and sustaining cellular functions. The detailed mechanism is introduced below (Section 1.3.2).

Within the cytoplasm, actins exist as two forms, filamentous F-actin and its monomer globular G-actin. The mechanical behaviour of the microfilament is dependent on both the molecular structure of the G-actin and the network formation of the F-actin. The polymerisation and depolymerisation of the G-actin give the microfilament its dynamic nature. In the process depicted as 'treadmilling', the association of G-actin occurs at 'barbed' end of the F-actin and the dissociation happens at 'pointed' end. The association of G-actins, as well as its reverse action, is facilitated by proteins such as profiling and cofilin. Also, proteins such as gelsolin will serve to cap the end of the microfilament and prevents further modifications. The coordination of these proteins can create various monomer-polymer interaction scenarios, resulting in different growth patterns to the microfilaments. These mechanisms are manifested in the formation of lamellipodia and filopodia during cell migration of proliferation. Moreover, branches in F-actin can be created by Arp2/3 proteins, which provides additional polymerisation site to G-actins [161]. The re-

sulted crosslinked F-actin meshwork offers structural support for the cell membrane. Lastly, when the polymerisation and depolymerisation of G-actin reach equilibrium or capped with proteins at both ends, a stable microfilament is formed. Stable microfilaments are critical components in force generation, stress fibre formation and intracellular transport.

Microtubule

Microtubule is a hollow helical tube with a diameter of approximately 25 nm, composed of basic units of α and β-tubulin (see Figure 1.1(b)) [240]. The construction of microtubule gives it rigidity, and it is resistant to bending and compression, as demonstrated by Kurachi *et al.* through optical trapping [122]. It is believed that the microtubule contributes to the viscous properties of the cell and can resist cellular compressive force, which gives it a crucial role in cell morphogenesis and organisation. Similar to microfilament, microtubules are also subject to dynamic polymerisation and depolymerisation of tubulin. It is recognised that mechanical loading has regulatory functions to the assembly of microtubule [179]. Within the cell, the assembly of microtubules originate from the centrosome, which is a structure located at the centre of a cell, and extend its length by polymerisation at the far-end [51]. Since the network of microtubules radiates outwards from the centre of the cell, it plays an essential role in intracellular transport, where motor proteins such as dynein and kinesin bind onto and shift along the length of the structure [94]. Moreover, evidence shown that microtubule has a crucial function in cell division as inhibition of microtubule polymerisation led to interrupted mitosis [149].

Intermediate filaments

Intermediate filaments play a role in facilitating intracellular transport, maintaining mechanical integrity and signal transductions. It has a bundled structure composed of many subunits of α-helix-rich protofilaments, which undergoes phosphorylation and dephosphorylation. The diameter of intermediate filament falls in between that of microfilament and microtubule at around 10 nm. The structure of intermediate filament gives it a unique ability to be highly sensitive to mechanical strain and undergo a series of structural changes during deformation and act compliant to small deformations while stiffens at large deformations [32]. The mesh network of intermediate filament acts as a 'stress absorber' and resist severe deformation to occur on cells [89, 180]. Moreover, intermediate filaments are directly linked to the cell nucleus, therefore also serves a role of directly transmitting the force between nucleus and cytoskeleton [75].

1.3.2 Cell contraction force generation

The contraction force generation of cells primarily involves the conversion of chemical energy to kinetic energy. The most widely accepted mechanism of cell contraction is based on actomyosin interaction within the stress fibre (Figure 1.2). As first demonstrated in striated muscle cells by Huxley *et al* [101], motorheads at both ends of the myosin bundle are able to interact with and walk along actin filaments towards the '+ end' (barbed end) and slide the antiparallel actin filaments together towards the centre (M line). Briefly, the classical model of contraction force generation has myosin II functioning as a molecular motor, converting energy from adenosine triphosphate (ATP) hydrolysis into a directed motion of the actin filament within the stress fibre. It relies on the assembly of myosin II into a bundled higher-order structure [64, 125], where bipolar myosin bundles are formed through

phosphorylation of the myosin II light chain [86]. The relative motion between actin and myosin shortens the stress fibre and creates local stress, while global scale shortening of the stress fibre causes cytoskeletal network contraction and generates contraction force [102].

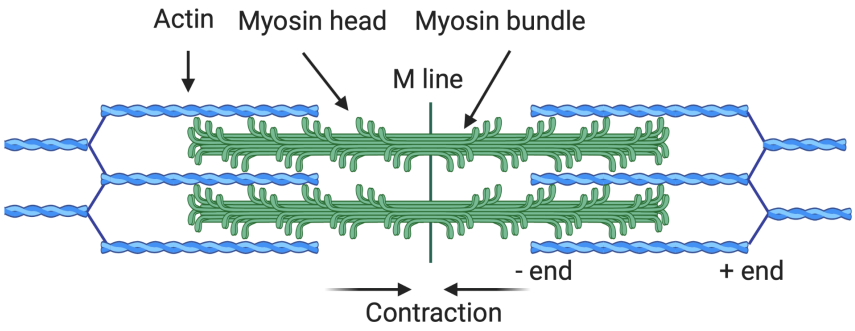

Figure 1.2: Schematic showing the organisation of actomyosin stress fibre.

Figure 1.3 demonstrated how chemical energy is converted to mechanical energy and mobilise the actin filament at an individual actomyosin junction. The cycle starts at the top of the schematic diagram. At the initial phase (phase 1), the myosin head is at a low energy state separate from the actin filament. Between phase 1 and 2, an ATP molecule is introduced and bind to the myosin head. As shown in phase 3, the hydrolysis of the ATP releases energy and promotes myosin head to a high-energy configuration. In this process, the neck of the myosin extends, resulting in the head displacement of around 5 nm opposite to the direction of contraction (to the right in the case presented in the diagram). It is worth mentioning that adenosine diphosphate (ADP) and the inorganic phosphate (Pi) are attached to the myosin head in this phase as the hydrolysis product of ATP. The 'high-energy' myosin head is subsequently bound to the actin (phase 4). At phase 5, the actin mediated release of Pi triggers the energy release of myosin head and change in configuration. This phase is termed as 'power stroke', generating a force of around 3-4 pN per myosin head [34], dragging the actin fibre to move (to the left in the case presented in the diagram). Followed by this, ADP molecule detaches from the myosin head, where it

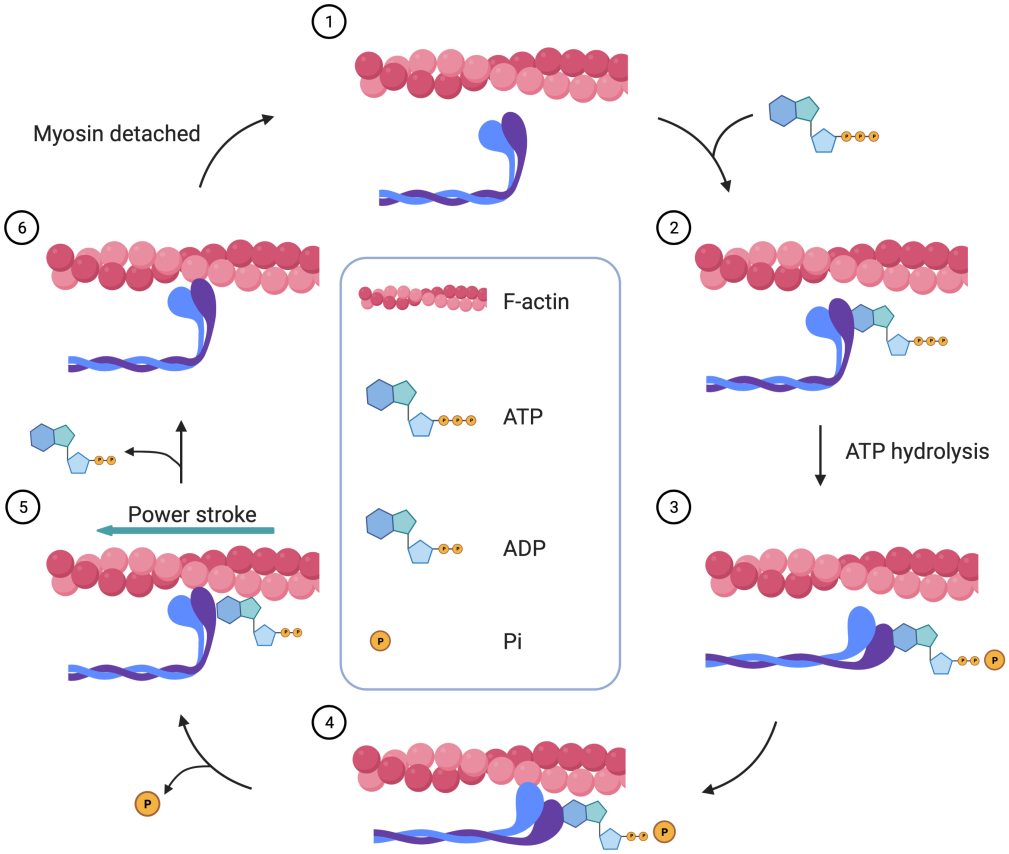

Figure 1.3: The mechanisms of actomyosin-based contraction at the molecular level (the actin molecule slides from right to left).

enters a low-energy 'rigour' state (phase 6). The subsequent dissociation of myosin head with the actin filament marks the end of the force-generating cycle and the beginning of the next one. During the entire cycle, force generation occurs at the fourth phase (*i.e.* power stroke), while biochemical changes take place during other phases to restore the force generation capability of the myosin head. In this system, the rate-limiting factor for contraction is the time taken for such 'restoration'. As the hydrolysis of ATP is a catalytic event, the ATPase activity of the myosin motor determines the speed of contraction at the molecular level, which is observed in both myocyte contraction [14] and *in vitro* motility assays [250].

The myosin molecular motor-based mechanism demonstrated a sophisticated way of contractile force generation. Alternatively, the mechanism of actomyosin-based contraction can also be myosin motor independent. Based on the highly oriented F-actin assembly mechanism, the contraction force can be provided by simultaneous 'treadmilling' motion of the actin filament. During this process, myosin can simply act as a crosslinker and allow actin filaments to drive the contraction. The myosin-independent contractility is observed by many during cytokinesis in ring closure [141, 247]. Xue *et al* have demonstrated the intertwined connection between myosin dependent and independent contraction force generation [247]. This suggests that the two mechanisms could individually contribute to the contraction as well as jointly affect contraction. It is hard to distinguish the contributions of these mechanisms in contraction force generation as both mechanism requires the assembly of myosin bundle and ATP. Myosin molecular motor dependent model remains to be recognised as the dominant mechanism in contraction force generation.

1.4 Collagen hydrogel-based contraction force sensing for ageing

1.4.1 Cell-matrix interaction in collagen-based assay contraction

Human cells generate and reside in a complex bioactive hydrogel scaffold (*i.e.* ECM). It comprises structural proteins such as collagen, fibronectin, and laminin offering a mechanically stable micro-environment. Hydrated proteoglycan fills up the pores created by the structural proteins acting as storage and medium for the diffusion of homeostasis-critical soluble molecules [222]. Cells are continuously remodelling their surrounding matrix and cause the mechanical and chemical environment to change. These changes reciprocally regulate cellular processes through mechanosensing. The functions of cells such as fibroblasts and chondrocytes are primarily dependent on the ability of matrix remodelling, and the dependency becomes pronounced during states such as ageing [38, 242].

Cells exert and transmit internal tension and forces to the outside environment through cell-to-matrix adhesions. Cell-to-matrix adhesions mainly occur at the sites of focal adhesions (FA), where the extended ends of cytoskeletal proteins aggregate join with FA proteins (*e.g.* talin, vinculin) through transmembrane receptors (*i.e.* integrins) [139]. Integrins will then binds to ligands present in the ECM, forming connections enabling transmission of mechanical signals. The mechanosensing of cells provides the basis of substrate elasticity influencing cellular behaviours. Studies on glioma cells show that rigid substrates can promote cell division, where the division rate increased by 5-folds when situated on rigid substrates [229]. Also, sudden changes in ECM stiffness has been shown to be an important factor in promoting malignant transformation, tumorigenesis and metastasis [106], and also shown to be related to the changes of cytoskeletal tension in tumours cells [99]. Moreover,

the behaviours of specific cells on a substrate with altered stiffness is characteristic of particular phenotypes. For example, cancerous cells can be distinguished by their ability to grow on substrates softer than their corresponding healthy tissues [55].

FA allows the contraction force generated by the molecular machinery of actomyosin interactions to be exerted onto the matrix as traction force. Cells also possess the ability to sense force from the matrix and regulate contraction. The mechanical cues within the ECM promote the assembly of cytoskeleton into actin stress fibres, strengthen FAs and induce a range of signalling cascades for contraction regulation [214, 252]. Overall, the cell-matrix interaction forms an intercellular feedback loop in the coordination of cellular contraction force. The mechanisms of cell force sensing and matrix regulated contraction within ECM is reviewed in detail by Humphrey *et al* [100].

The *in vitro* cell-mediated collagen hydrogel share the same principle with cellular contraction within the ECM. As the cells spread and evenly distributing inside the collagen matrix, they form FA-like link with collagen fibril through integrin and pull onto the collagen fibrils. Consequently, isometric tension is developed on the collagen fibrils as resistance to the deformation, and the tension stimulates further contraction. The individual forces exerted onto the individual collagen fibril will translate and propagate along with the interconnected collagen network, resulting in overall observable contraction of the hydrogel matrix. Also, as the hydrogel contracts, cells will come to alignment with the principle strain of the hydrogel deformation to reach tensional homeostasis [183], providing the basis of using hydrogel as a tool for studying cell contraction.

1.4.2 3D collagen hydrogel mimics the native extracellular matrix

It has been noticed that the interaction with the ECM can result in cells to display a different phenotype to that defined otherwise by their genotype [177]. Such discovery suggests that a cell does not act as a solitary individual and any cellular behaviour should be assessed in the context of the ECM, as the dynamic extracellular environment will trigger intercellular signal transduction in the regulation of cell behaviours.

A common approach for *in vitro* study of cellular behaviours is adopting three-dimensional (3D) cell-embedded collagen hydrogels. A difference can be found between traditional two-dimensional (2D) approach and 3D hydrogel gel matrix in how cells sense the micro-environment. For instance, cells are only partially in contact with the substrate and the neighbouring cells in a 2D substrate, causing polarised mechanotransduction and unnatural behaviour of the cells [73]. Also, the rest of the cell surface is in direct exposure to the culturing media for nutrition and waste exchange. However, the homogeneous culture media does not create a concentration gradients of nutrients, growth factors and cytokines as that *in vivo*. It is shown that the dynamic spatial concentration gradients of soluble factors in the ECM have influences on cell migration, communication, and differentiation.

Thus, for the study of cellular behaviours such as contractility, a 3D hydrogel model should be used to best recapitulate the mechanical and biochemical stimulation present in native ECM. As collagen is one of the most abundant fibrous proteins present within the ECM, 3D collagen hydrogel can best mimic native ECM, providing physiological behaviours of the cells. The benefits of using 3D collagen hydrogel in studying the contractility of aged dermal fibroblasts are especially prominent, as the ageing of fibroblasts is a complex process involving changes in many aspects which changes its matrix remodelling and mechanosensing abilities [223].

1.4.3 Mechanical properties of collagen hydrogel influences contraction force measurement

Hydrogels are water-swollen crosslinked polymeric network promoting cell function. They are highly customisable in terms of stiffness, viscoelasticity, water content, oxygen permeability and porosity. It can also be functionalised with specific bioactive molecules in accommodating and promoting particular cell type and cellular activities.

The stiffness of a homogeneous hydrogel is dependent on the concentration of the polymer and the crosslinking density. Influences of hydrogel stiffness can vary between different cell types. Marklein *et al* [143] demonstrated increased proliferation and migration of mesenchymal stem cells (MSC) on 3D hyaluronic acid scaffolds with higher stiffness, while Banerjee *et al* [11] concluded opposite for neuronal stem cells. In terms of the cell contractility measured using collagen-based assay, fibroblasts in stiffer hydrogel have shown reduced contraction [109]. However, the influences of hydrogel stiffness in contraction force measurement can not be simply assessed in isolation. As a dynamic system, cells embedded in the collagen hydrogel are constantly remodelling their surroundings, changing the matrix stiffness. The remodelling rate is dependent on the initial stiffness of the collagen hydrogel, demonstrated separately by Zhu *et al* [256] and Ahearne *et al* [3] on fibroblasts with lung and corneal origin. Based on the mechanism of cell-mediated collagen contraction, if the collagen fibrils buckle under the force applied by the cells due to insufficient strength, they will not reciprocally stimulate contraction, resulting in decreased contraction. It suggests that hydrogel matrix with low stiffness tends to reduce the cell contraction as it is more likely for the polymer (*e.g.* collagen) fibrils to buckle under increased traction force as a result of reduced fibril density. Also, the difference in hydrogel stiffness can affect hydrogel's oxygen and nutrient permeability, available focal adhesion sites, which is key to cellular activ-

ities. Such complication also indicates the benefits of measuring contraction force of aged fibroblast with collagen hydrogel as the measurements are done in the context with consideration of the ability of aged cells in modifying surrounding matrix, providing better assessment of the ageing process.

Hydrogel often contains a large amount of water, thus often exhibit viscoelastic behaviours. Also, given the molecular structures of their polymer chains, the viscoelastic properties vary among different hydrogels. Collagen hydrogels are shown to be significantly viscoelastic among few commonly used natural hydrogels (*e.g.* agarose and alginate). How viscoelasticity of the hydrogel affects the embedded cells remains unclear [1] and shown to change during contraction and matrix remodelling [3]. Although viscoelasticity of collagen should not post an issue in contraction force measurement, the characterisation of its viscoelastic behaviours remains useful to evaluate the matrix's mechanical influences on cell contraction.

1.5 Outlook in hydrogel-based contraction force measurement

A significant advantage of using hydrogel is to provide the cells with a physiologically-biomimetic 3D matrix. In the study of contraction force, it is especially important to construct hydrogels with matching mechanical properties to native tissues. Within the human body, the stiffness of ECM can vary by several orders of magnitude between the softest brain tissue to the hardest bone tissue. However, cells commonly used in contractility studies are sourced from tissues with Young's modulus range upwards of tens of kilo-Pascal (kPa). The hydrogels with similar stiffness are often very soft and require delicate handling skills throughout the study. Usually, quantitative analysis involves the measurement of displacement response of an applied force to the hydrogel. Thus requiring measurement instruments with milli-Newton

(mN) and micro-meter (μm) level sensitivity respectively, which inevitably prone to environmental perturbations. Also, in macro-scale mechanics, it can be reasonably assumed that materials are homogeneous, and the size and shape of the probe are negligible. In the study of contractility with hydrogels, the heterogeneity in hydrogel caused by cell's remodelling and contraction as well as the geometrical profiles of the probe can no longer be neglected. However, both issues can be addressed with the application of a relatively simple mechanical model and making an appropriate assumption based on the aim of the study.

As introduced in the previous section, ECM comprises a complex hierarchy of a wide variety of proteins and proteoglycans with multiple types of cells. Although the hydrogel construction can largely mimic the native ECM, a complete replication remains extremely difficult to achieve. However, techniques for creating inhomogeneous anisotropic hydrogel to mimic fibrous protein alignment in tissue have been developed [1]. Moreover, with the application of 3D bioprinting, we can create hydrogel-based engineered tissue substitute to resemble physiological conditions best. Lastly, as many factors are involved (*e.g.* collagen digestion, FA formation, etc.) in determining the cell-mediated hydrogel contraction, it remains challenging to distinguish exact contributing parameter. However, these factors may turn out to be useful in detecting ageing as the measured contractility is a reflection of many changes in cellular processes during ageing.

Chapter 2

Ageing of the skin and fibroblasts

As the work has an aim in measuring and distinguishing the contractility difference between young and aged dermal fibroblasts, it indicated importance for the focus to be laid on the basic mechanisms in ageing. Also, as skin is a highly integrated structure, the crosstalk between dermal fibroblasts and the rest of the dermal tissue holds the key to dermal fibroblast function. This chapter approaches the contractility changes of aged dermal fibroblasts in the light of functional changes of the skin tissue and fibroblasts as a consequence of ageing.

2.1 Mechanisms of ageing

Ageing is defined as a process of progressively losing the maximal functions, metabolic efficiency and reduction of adaptive potential to environmental stresses. Ageing lead to various types of diseases and is the primary reason for the finite lifespan of an individual in the absence of disease. During the process of ageing, many metabolic and

signalling pathways, gene networks and organelle functions can be altered. Thus, ageing can be described as a convergence of various chronic molecular processes on a common, uniform set of phenotypical changes. The phenotypical changes occur during ageing lower the adaptive potential of an individual and increase the vulnerability of an individual to the exposure of environmental stress [223].

The study of the mechanism associated with ageing dates back many decades with multiple theories proposed. At the very early stage of the mechanistic study of ageing, the cause of such process was believed to be simplex and isolated, such as the accumulated free radical damages [82]. However, with more studies over the years, the current view is that ageing is caused by a mixture of different interconnected factors instead of being attributed to any single cause. The recognition of the interconnections between the modulating factors of ageing has led to the categorisation of the 'hallmarks' of ageing which systematically summaries the alterations of molecular and cellular processes during ageing [9, 138].

It is commonly agreed that ageing has two principal determinants: intrinsic disposition and extrinsic factors. Intrinsic disposition mainly consists of the genetic makeup and the somatic composition of an individual, which is the fundamental driven force of the ageing process, determining what is ultimately possible. The influences of an individual's adoption to different lifestyles, the nutritional level and the environmental exposures being subjected to are categorised and termed extrinsic factors.

The genetic formation of an individual is frequently under threat from factors from both external (*e.g.* electromagnetic radiations, chemicals, pathogens) and internal (*e.g.* errors in DNA replication, by-products of biochemical pathways) origins. The vast majority of the genetic lesions are repaired by sophisticated and efficient biochemical responses tackling DNA damages, which can eliminate the negative im-

pacts of such damages [169]. Despite the sophistication, if the DNA damage occurs too close to the event of proliferation, the lesion can be carried on and incorporated into the genome as a mutation due to insufficiency of time for adequate DNA repair. In some unfortunate cases, the combination of mutations can lead to pathological processes such as cancer and autoimmune disease, but more often, the mutations have minimal and negligible influences on biological functions. However, when allowed time, these otherwise negligible effects of the individual mutations combine and impact the stability of the genome. Hence, the stability of the genome negatively relates to age, rendering an aged individual vulnerable when exposed to stressors.

The vast majority of different types of cells have a limited number of cell cycles they can undergo before going into senescence [85]. DNA is duplicated by a type of enzyme called DNA polymerase during the proliferation process. Although the duplication of DNA is highly accurate, with each successive DNA duplication, part of the telomere, which is a non-coding repetitive gene sequence at the end of the chromosome is left uncopied. The reason for this is believed to be the physical space required for the interactions between the molecular machinery of the DNA polymerase and the DNA chain. Such phenomenon leaves the resultant DNA chain to be slightly shorter, which is often benign. However, as cells go through enough number of cell cycles, the telomere becomes too short, and part of the gene-coding DNA is left uncopied, triggering cell senescence and terminates further proliferation. Many phenotypical changes can be seen on senescent cells. One of the representative ones is developing age-associated secretory phenotype, where extraneous inflammatory cytokines and matrix metalloproteinases (MMPs) are secreted by the senescent cell and having paracrine effects on adjacent cells [46, 165].

Many stimuli can activate senescence through the aforementioned DNA damage response. Other than the shortening of telomere as mentioned above, senescence can also be triggered by overprescribed exposure of reactive oxygen species

(ROS) [49], as well as the activation of tumour related genes as reported by Chandeck *et al* [37] and Li *et al* [132]. Often, the senescent cells are removed from the tissue by phagocytosis of the immune cells; however, the cumulative number of senescent cells was shown to increase with individual's ageing process. It is believed that such an increase is associated with both increases in senescent cell production and a decrease in the removal capability. The increased prevalence of senescent cells is reported to be causing low-level chronic inflammations, which is often seen on aged individuals [42].

Inflammation response is a good indicator of the ageing process. Increased inflammation with age reflects the reduction of an individual's ability in responding to and cope with environmental stresses [69]. Inflammation is a multi-step complex series of biological events of protective nature, involving multiple molecular pathways in response to cellular and tissue damages. In simple words, inflammation is a two-step process. First, aggregation and activation of immune cells are accompanied by the increase in blood flow to the damaged site. With less severe damage, it enters into 'resolution' phase until the damaged cells and tissue are regenerated. While with more severe damage, macrophages and lymphocytes are recruited, and chronic inflammation occurs and gradually transition into the 'resolution' phase. It has shown that ageing not only leads to inflammation caused by prevalent senescent cells but also have negative impacts on the inflammation resolution, which results in more aggressive progression of diseases observed on ageing individuals [16, 245].

As indicated by Lopez-Otin *et al* [138], changes on the biomolecules are also observed during ageing. As an example, the amount of DNA methylation has shown to increase with age. Although having no direct effect on the expression of genes, hypermethylation and methylation patterns with certain characters have been shown to make an individual more susceptible to diseases through affecting genomic stability [111]. Proteins are critical to the vast majority of the biological

process as it plays a vital role in nearly all biochemical pathways. Sophisticated processes are in place for proteostasis, which dynamically regulates the production, transport and degradation of the protein to achieve a balanced, functional proteome. Associated with age, the accumulation and aggregation of dysfunctional proteins can disrupt cellular processes, leading to degenerative diseases such as Parkinson's and Alzheimer's disease [196]. Also, during ageing, proteostasis is negatively impacted by ROS damage, the decline in immune cells, attributing to the ageing process [148].

An extensive amount of evidence indicates that ageing is a joint result of interconnected factors such as DNA damage, cellular senescence, telomere attrition, ageing associated inflammation, epigenetic changes and loss of proteostasis. The above listed several representative factors associated with ageing in general, while the following sections will look into the ageing of the skin at tissue level, as well as addressing the alteration of dermal fibroblasts during ageing

2.2 Ageing of skin tissue

Particular characteristics make the skin tissue and functional dermal cells (*e.g.* fibroblasts, melanocytes, mast cells) an essential area of ageing study, especially in terms of distinguishing the effects of extrinsic and intrinsic ageing processes. Similar to other organs, the entire skin is subject to intrinsic ageing, while extrinsic ageing is limited to the area exposed to environmental elements. As an example, the primary causes of the extrinsic ageing of the skin are photo-oxidative stress due to ultraviolet (UV) radiation and toxic hydrocarbons within tobacco fume and smokes from industrial establishments [121]. The nature of these harmful exposures dictates that they are relatively easy to be shielded from, thus creating areas of adjacent skin tissues that has the same intrinsic dispositions and only differs in the levels of exposure to extrinsic factors.

At the tissue level, the skin is primarily composed of three layers (shown in Figure 2.1). The epidermis is a superficial stratified epithelium containing a highly proliferative population of keratinocytes, acting as a barrier against pathogens and preventing excessive dehydration. Below is a thick dermis layer which consists of the majority of the fibroblast populations within the skin. The fibroblasts make and control the dermal matrix, which determines the mechanical strength of the skin and structurally support the epidermis. Beneath the epidermis and the dermis is the subcutis, which primarily consists of fat tissues acting as energy storage and shock absorber for the protection of internal organs. The layered structure of the skin also promotes the interest in the study of the ageing process in the skin. The differences in the proliferation characteristics of dominant cells types in each tissue layer resulted in the intrinsic and extrinsic ageing process of the skin to involve different compartments of the organ, which makes it easier for discriminating the two ageing processes [223].

Upon overall evaluation of the aged skin, many phenotypical changes can be observed. At the cellular level, it has reduced capacity for healing and DNA repair as well as a reduced cell turnover. At the tissue level, aged skin has less and disorganised collagen and elastin networks, impaired dermal vasculature, reduced melanocyte concentrations and flatter dermal papillae. Regarding the functional decline of aged skin, it has been reported to have reduced capacity for sensory perception, thermoregulation and immunosurveillance. Lastly, from an appearance perspective, aged skin is often dry, rough with uneven pigmentation accompanied by wrinkle and impaired hair growth [63, 206]. The dryness, roughness, and wrinkle can all be found to be related to the disrupted dermal ECM, which has a proven link to the functional decline of the fibroblast. The following subsections describe morphological changes on epidermis and dermis in aged skin.

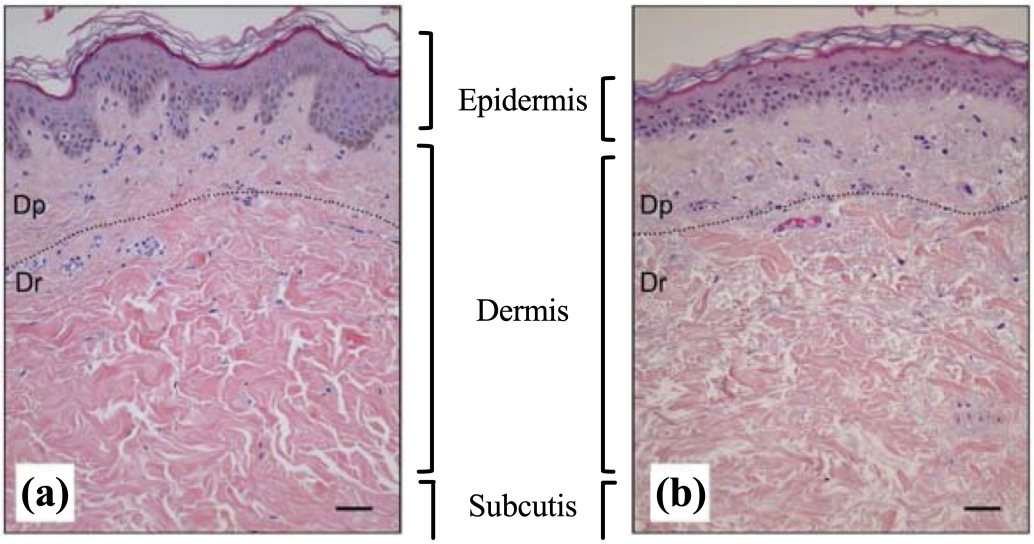

Figure 2.1: Histology of skin with marking of primary layers. (a) 19-year-old donor. (b) 74-year-old donor. Dp and Dr denote papilary and reticular dermis, respectively. Scale bar = 50 μm. Figures were produced by Mine *et al* [150] and reproduced under the creative commons licence (CC BY 4.0).

2.2.1 Epidermis

As introduced above, the primary function of the epidermis is acting as a barrier and the first line of defence towards harmful external elements. However, the function of epidermis extends beyond the barrier function thanks to the various substructures. For example, the sweat glands and hair follicles can serve in the regulations of body temperature [163], water and electrolyte exchange [104, 110]. Also, the melanocyte present in the epidermis will produce melanin, which can absorb the UV radiation, reduce the intensity of harmful rays to reach deeper tissue. Epidermis also hosts various receptors for transducing sensations critical to the wellbeing of an individual, such as pain, temperature, pressure and itchiness to the central nervous system [113].

With high cell turn out rate, it is continuously in a state of regeneration through proliferation and exfoliation. As the new cells develop, older cells are pushed to the superficial side of the epidermis and eventually reaches stratum corneum,

which is at the surface of the skin. The cells at the surface of the skin are constantly being shed at the same rate as the replenish rate of new cells, thus under normal conditions, the thickness of the epidermis remains constant. The process of cell shedding ensures the stratum corneum is at its optimal states for its functions as a barrier and permeability control. More importantly, the cell shedding also eliminates most of the damages to the cells caused by extrinsic stressors.

Morphologically, the aged epidermis is different from young ones in several different aspects. As shown in Figure 2.1, the interface between epidermis and dermis has interdigitations. These interdigitations stabilise the epidermal cells and strengthen the adherence between the dermis and epidermis layer by increase the contact surface area. In aged tissue, the interdigitation becomes flat, leading to loss of adherent strength. Also, as shown by Breitenbach *et al* [29], the basement membrane in young epidermal tissue is much better defined than that of aged tissue. Such differences suggest that the proliferation of keratinocytes in the aged tissue are largely disturbed, leading to the observed thinning of the epidermis in aged tissue.

2.2.2 Dermis

The basement membrane defines the border between the epidermis and the dermis tissue. The construction and upkeep of the membrane are joint efforts of keratinocytes from both epidermis and dermis. The basements membrane is rich in collagen IV and is a critical component of the dermal-epidermal junction, which is vital for the integrity of the skin. The function of the dermal-epidermal junction includes the regulation of nutrient transport and signal transduction [33]. Unlike the epidermis, the dermis has a much lower cell density, and the majority of the tissue volume is predominantly a fibrous ECM, consists of macromolecules such as collagen, elastin, fibronectin, fibrillin, glycoproteins and proteoglycans [140].

There are two sub-layers of dermis named papillary dermis and reticular dermis respectively (see Figure 2.1). No clear border is present between the two sub-layers, yet they are distinguished by their locations and the structural composition of the ECM. Collagen is the major fibrous protein within the dermis, with type III collagen primarily located in the papillary dermis and type I collagen being ubiquitous in the reticular dermis [147]. Overall, the collagen composition ratio of type I and III is believed to be 4:1 across the entire dermis, forming a structural mesh with other fibrillar components, jointly responsible for the structural integrity of the dermal ECM. Dermal fibroblasts are responsible for the production and maintenance of ECM. Collagens are secreted by dermal fibroblasts as short peptide chains and incorporated into the existing network of fibrous protein mesh through the spontaneous formation of collagen cross-linking [44].

Both damages in the collagen and elastin networks were observed in the aged dermal tissue, especially within the regions of photo exposure [7, 44]. The damages to the fibrous networks is reflected in the loss of strength and elasticity of the ECM and disorganisation of the tissue structures. Seite *et al* [201] have shown a shift of the morphology of elastin fibres within dermis from thin and single-stranded to beaded when age, as well as reported on its decline in connectivity with the epidermis. In terms of the level of collagen in the dermis, the deficit caused by a high level of degradation and low replenishment rate results in the loss of collagen density and integrity [181]. Moreover, as introduced in Chapter 1, fibroblast function is largely dependent on the mechanosensing of the external stimuli, which is critical for the adaptation of fibroblasts to a normal healthy morphology [232]. The decrease in fibrous protein content and damages to the ECM structure in aged dermis leads to the globular non-adherent morphology of dermal fibroblasts [44,181]. The resultant lack of fibroblast function in ECM maintenance will further reduce the ECM integrity, hence entering a feedback loop resulting in accelerated worsening

of aged dermal tissue conditions.

2.3 Ageing of dermal fibroblasts

Dermal fibroblasts play an irreplaceable role in the formation and maintenance of the ECM in the dermis, which makes them directly responsible for the structural integrity of the skin. Their direct link with the functions of the skin makes them one of the most important functional cells among all dermal cells. Also, dermal fibroblasts have long lifespans and rarely proliferate, making them excellent carriers of the cumulative stresses of both endogenous and exogenous nature over time. As a highly integrated system with numerous biochemical pathways and molecular machinery, the mechanism of cellular function is complex per se. However, the following subsections aim to list several typical changes that occur during the ageing of dermal fibroblasts in different categories, as well as how they affect the functionalities of the fibroblast and the dermal tissue.

2.3.1 Genetic and chromosome changes in ageing dermal fibroblasts

One of the major causes of ageing is the accumulation of otherwise trivial and benign damages to the DNA and the instabilities in the nuclear genome. *In vitro* induced senescent dermal fibroblasts has shown increased centrosome aberrations [168], chromosomal instability associated with demethylation of DNA [212] and the activation of transposable elements [50], causing inaccurate replication of the DNA. However, as fibroblasts rarely proliferate in dermal tissues, it remains unclear that observations on the induced senescent cells fully reflects the situation of fibroblasts in dermal tissue of aged human [223]. Also, the DNA repair capacity was seen

to decline significantly on aged primary human dermal fibroblasts [213]. A study conducted by Herbig *et al* [88] demonstrated telomere DNA damage due to lack of repair capability on primate dermal fibroblasts, which observation shall be easily translated to human dermal fibroblasts.

Previous works have also shown ageing-related disruptions of pre-mRNA processing within fibroblasts. As an example, altered splicing of lamin A pre-mRNA observed in fibroblasts found *in vivo* in the aged human dermis is believed to have facilitating effects in skin ageing [146]. The miss-splicing of lamin A pre-mRNA creates progerin, which is an altered form of lamin with different structures. Progerin lacks the necessary binding site for crucial biochemical pathways, which prohibits the correct distribution of lamin within the cell nucleus. Also, the altered structure of progerin has adverse effects on nuclear architecture and epigenetic chromatin control, as well as causing the accumulation of oxidative DNA damages [186, 204]. Similar to that observed in other ageing cells, epigenetic alterations were also seen in aged fibroblasts. DNA hypermethylation was observed in dermal fibroblasts from aged donors [116] and meta-analysis conducted by Horvath *et al* [97] suggests that the level of DNA methylation is closely correlated with age. However, Gronninger *et al* [78] reported negative evidence through the study of human dermal fibroblasts, suggesting that dermal fibroblasts are an exception to the methylation-age correlation, which probably is a reflection on opposing influences of chronological and extrinsic ageing on DNA methylation in dermal tissue.

2.3.2 Disrupted proteostasis and respiration

Also introduced in Section 2.1, proteostasis is crucial in the function of cells. As the name suggests, one of the most important roles of fibroblasts is the production of fibrous proteins and the maintenance of ECM. It was shown that UV radiation of

dermal fibroblasts could stimulate the production of MMPs [66], which are capable of degrading all kinds of ECM proteins. It is believed that the enhanced production of MMPs and decreased expression of the endogenous inhibitor of dermal fibroblasts are mainly responsible for the degradation of ECM observed in the extrinsically aged skin [30]. Moreover, evidence has shown the changes in remodelling activities of ECM proteoglycan by dermal fibroblasts [115, 188], which can further lead to the structural and functional change of collagen networks within the ECM.

Moreover, at the organelle level, mitochondrial dysfunctions have also been shown in aged fibroblast. Greco *et al* [76] have demonstrated a progressive decrease in respiration rate and uncoupling of oxidative phosphorylation of dermal fibroblasts harvested from donors of advanced age, suggesting inefficiency aerobic ATP production of aged fibroblasts. Moreover, mitochondrial ROS level is increased in dermal fibroblasts from old donors, which is believed to be related to the reduction of anti-oxidative capacity [119, 184].

2.3.3 Changes in the cytoskeleton and mechanical properties

In addition to the production of various fibrous proteins and MMPs for ECM remodelling, the mechanical aspects of the dermal fibroblast properties are also at great importance for the study of the ageing process of dermal fibroblasts. As detailed in Section 1.3, the cytoskeleton is a dynamic structural scaffold made up of various proteins. Therefore it is directly related to mechanical properties of the cells. Pieces of evidence have shown that the actin filament formation of the aged dermal fibroblasts is altered without a significant decrease in actin content [26]. In detail, aged fibroblasts have an increased expression of cofilin, which depolymerises F-actin into G-actin, resulting in higher G-actin to F-actin ratio in aged fibroblasts in comparison to young cells [26, 39]. It is worth noting that cofilin can be activated by UV

radiation, which suggests a mechanistic link between intrinsic ageing and extrinsic photoageing of dermal fibroblasts through analysing the changes of G-actin level.

Due to cytoskeletal changes in aged dermal fibroblasts, studies have shown an increase in cell surface and volume, decline in mobility and exhibited less plasticity upon mechanical manipulation [103, 199]. Indentation of dermal fibroblasts from donors with different age shown a significant increase in Young's modulus of the cells with higher donor age [59], which may be a cause of reduced mobility.

2.4 Summary

The ageing of dermal fibroblasts entitles complex changes in multiple systems at the sub-cellular level. With increasing knowledge in the changes of biochemical pathways and their interactions during the ageing process, we can paint a good picture of dermal fibroblasts ageing in that aspect. However, the mechanical property changes dermal fibroblasts during ageing has still not yet reached the same level of understanding.

With more understanding of the cytoskeletal structure through advancement in instruments, we gathered more evidence in how mechanical properties of fibroblasts will change during ageing. The alterations of cytoskeleton structure and property can be the cause of many alterations in the mechanical changes observed in aged cells, yet each mechanical property is somewhat isolated. In light of this, contractility is an excellent measure of the combined effect of different alterations in mechanical properties. On one hand, the generation of contraction force requires highly coordinated cellular event (see Section 1.3), and on the other hand, the level of contractility can be affected by many other mechanical properties of the cell such as stiffness and cell adhesion. Moreover, the study of how ageing influences dermal

fibroblast contractility has great practical implications as fibroblasts constitute a significant type of contractile cells within the skin and regulate dermal matrix, responsible for the major phenotypical changes in aged skin. However, due to various difficulties, the assessment of cellular contractility has been suboptimal with many assessments remained qualitative. Therefore, it remains a paucity in comparing the contraction force generated by young and aged dermal fibroblasts, where a quantitative technique is required to accurately determine the contraction force of young and aged dermal fibroblasts while providing appropriate dermal matrix equivalent to the cells.

The next chapter will focus on the past techniques used in sensing and measuring cellular forces.

Chapter 3

Cell force sensing technique

3.1 Introduction

In the study of cellular mechanics, manipulation and testing of forces directly or indirectly at a cellular level is often essential. In the past fifty years, the biomedical field experienced a breakthrough. Combined with the advancement of instrumentation and software engineering such breakthrough has led to some state-of-the-art biomechanical tools and their current applications along with many advanced mathematical and mechanical models [13, 133, 191, 231]. The selection of a suitable mechanical tester and the adaptation of a measuring technique is based upon the size of the biological structure and the information required to be extracted from such studies. Figure 3.1 shows the typical size range and the displacement measuring capabilities of some typical techniques used in the study of biomechanics. Displacement is in the range of micrometres for cell mechanics study while the nanometre level of measuring capabilities is required for the studies of biomolecules as well as sub-cellular structures. In this study, the focus is mainly on the mechanical investigations at the cellular level (*i.e.* microscale). Several approaches are applicable to

study cell mechanics. Though techniques vary greatly, the underlying principle is to achieve the measurement of force and displacement, directly or indirectly.

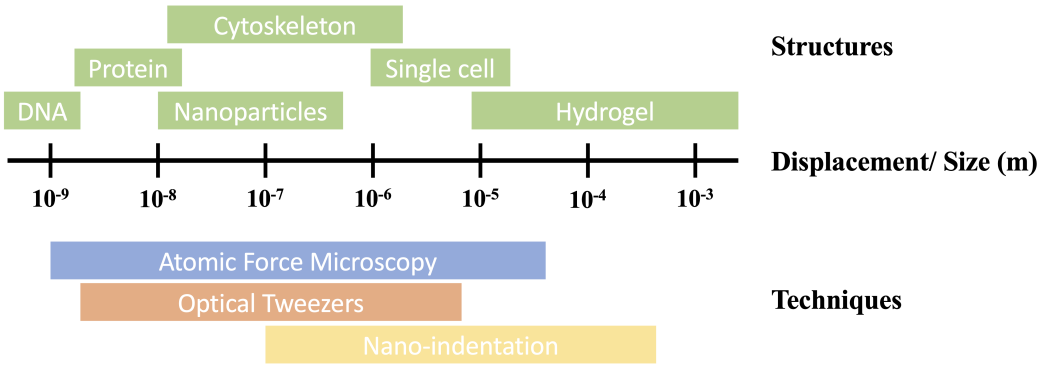

Figure 3.1: Typical size of biological structures and displacement measuring capabilities of techniques used in the study of biomechanics. [134]

3.2 Techniques in the mechanical study on a single cell

The mechanical study on a single cell includes the measurement material properties of the cell (*e.g.* cell elasticity) as well as forces involved in cellular activities (*e.g.* adhesion force). The magnitude of forces for studying material properties are in the range of nano-newtons (nN) to micro-newtons (μN) as a typical cell is considered as soft material, while forces during cellular events are down to pico-newton range as the origin of such forces are often protein-protein interactions [134]. With advancements of force-sensing devices capable of resolving forces and displacements at micro-/nanoscale (shown in Figure 3.1), it is possible to conduct studies on mechanical properties of cellular structures and the biomechanical and biophysical event of interest on a single cell with high precision. Among plentiful of instruments and techniques, atomic force microscope (AFM) and optical tweezer (OT) are the most prevailing techniques in their category. The former has an unrivalled advantage in spontaneously measure both displacement and applied force at piconewton (pN) precision, while the latter excel in its non-contact and cell-friendly nature [191,238].

3.2.1 Atomic force microscope

AFM mainly comprises a flexible cantilever beam with a fine tip mounted on the free end. A laser beam is shined on the cantilever and subsequently reflected onto a photodetector for detecting cantilever deflection due to tip-surface interaction (Figure 3.2). As the tip lowered by the piezoelectric stage (not shown in the figure) and come into contact with the sample, reaction force will cause the cantilever deflection and combined with parameters such as the cantilever stiffness, a force-displacement (F-D) curve is obtained. In the application of studying material properties of cells, tip shape and indentation depth are also supplemented and used in estimating material properties of cells, such as cell elasticity/viscoelasticity [123].

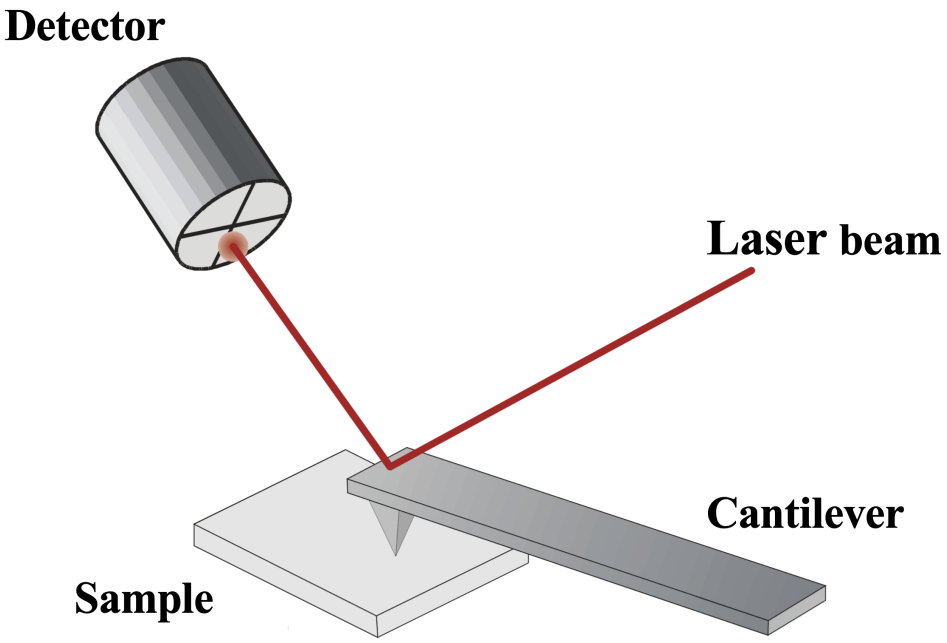

Figure 3.2: Schematics of AFM working principle.

AFM system was originally developed for visualising atomic and surface properties of materials [20]. It can provide surface scans with an atomic level of reso-

lution. In the vertical direction, it has displacement sensitivity down to less than 0.1 nm [35]. AFM has a vast detection range for forces, yet the sensitivity remains at piconewton level throughout its range [35, 235]. To expand its application in cell mechanics measurement, it has been adapted with environmental control chambers and has been incorporated into microscope systems allowing it to take measurements *in vitro*.

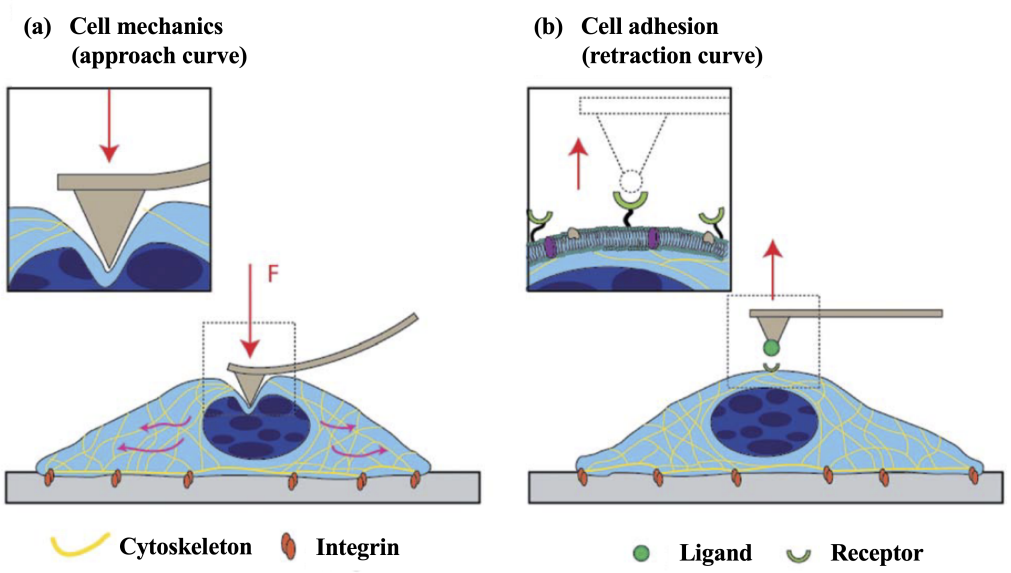

Figure 3.3: Schematic diagram of AFM in cell mechanics studies. (a) cell elasticity measurement; (b) Cell adhesion measurement. (modified from [58])

Figure 3.3 shows the two typical AFM applications in cell mechanics studies. Apart from indenting the cell with a tip, with an altered setup to the AFM system, cell adhesion force measurement can be achieved by functioning the tip with protein molecules and recording the *F-D* data during the upward motion of cantilever (shown in Figure 3.3(b)) [205]. So far AFM has been used to examine the mechanics of membrane proteins [159], cell nucleus [93], as well as investigating mechanical changes during differentiation and disease progression [45, 124, 194]. Further to the application in cellular mechanical studies, the advantage of the high spatial resolution of AFM has also been exploited in applying local stress to a point-of-interest

on the cell. Assessing the localised mechanical behaviour of the indented part will help better understand the mechanical functions of cytoskeleton within that specific part of the cell [176, 195]. Additionally, cytoskeletons protein can be marked with fluorescent dyes, AFM in combination with an optical microscope can detect the fluorescent light for further analysis of cytoskeleton [96]. Moreover, by attaching various biological substances (*e.g.* protein, hydrogel, second cell), applications of AFM can be further extended to investigate force generation during contraction, migration etc.

AFM is an invaluable tool in the study of cell mechanics, yet its disadvantages are also noticeable. While providing precise measurement during indentation, it can only measure on the cell at one given point, which significantly limits the number of points it can conduct measurements within a given period. Also, the measurement is highly dependent on the properties and geometry of the cantilever and its tip, which determines the tip-cell contact profile. These parameters are critical to the selection of appropriate mechanical models based on their underlining mechanisms, thus results from different AFM systems are not usually comparable.

3.2.2 Optical tweezers

OT technique uses photon trapping mechanism to apply forces to a cell and mechanically manipulate the cell. Such a technique uses radiation pressure originating from the electromagnetic field to trap particles, which gives it non-contact nature (Figure 3.4). As photons from a focused laser beam pass through a particle with a comparatively higher refractive index to the surrounding, directional change of the photons will result in changes of the momentum of the photons creating a net trapping force ranging from 0.1 to 100 pN [253]. Such a technique was invented and developed through the 1970s and uses an infrared laser and microscope system to

trap and control the movement of viruses and bacteria [8]. OT has the advantages of being a non-contact method with high force resolution while being cell-friendly due to measurement conducted in aqueous solutions [77].

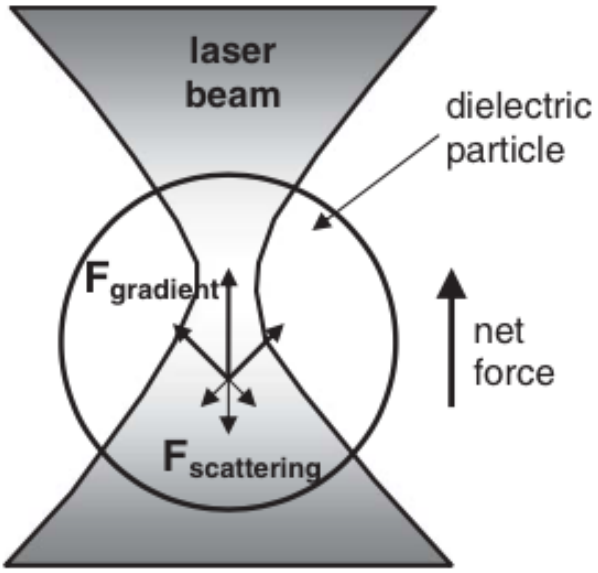

Figure 3.4: Working principals of optical tweezer. [133]

For characterising the mechanical property of a single cell, two opposed silica beads with a radius of several micrometres are attached to the cell acting as 'handles' for the laser beam [238]. Silica beads which are coated with surface proteins (*e.g.* fibronectin) will form focal adhesion with cells through ligand-receptor binding. A known force can be exerted to the cell through trapping of the silica beads and displacement of the cell can be gathered through analysis of time-lapse video or images.

The application of OT in the study of single-cell mechanics is extensive. So far, it has been used in investigating whole-cell mechanical properties on blood cells, tumour cells, epithelial cells and mesenchymal stem cells (MSCs) [79, 80, 226]. To further take advantage of its piconewton level sensitivity and non-contact nature, it has been used to determine the mechanical properties of proteins and nucleoids

[87], as well as measuring forces generated by the subcellular mechanisms during intracellular transport [22]. Moreover, by attaching multiple spherical beads [130] and using multiple laser beams [189] for trapping, more complex loading scenario can be created which will significantly help with studying the cellular mechanics with multiple dimensions.

Disadvantages and limitations of OT are also worth noting. As mentioned above, the trapping force is generated by the change of momentum of the photons, despite utilising the high-intensity lasers, the overall trapping force is small and easily subject to the perturbation to the light path [191]. However, the perturbation could be minimised as the vast majority of the applications of optical tweezers are conducted in the aqueous phase. Lastly, the high-power laser beam will cause local heating and photodamage. Although increasing the wavelength of the laser source can mitigate the damage [253], prolonged trapping still has adverse effects on the trapped cell, consequently altering the mechanical properties of the cell.

3.3 Techniques in measuring cell contraction force

Cell contraction plays a vital role in wound healing, inflammation, angiogenesis and metastasis [108]. Assessing cell contraction force will provide a unique insight into the contractility of the cells. Contraction force measurement can be performed on both single-cell and populated cells. Single-cell measurement techniques include deformable membrane, traction force microscopy (TFM) and elastic micro-pillar (EMP) technique. Although the detail designs of these techniques vary, they all share the same underlying principle of analysing contraction force through measurement of a deformable substrate. On the other hand, multiple cell measurement techniques require cells to be embedded into hydrogels to form a 3D matrix and measure contraction force based on geometrical changes of the cell-embedded hy-

drogel. These techniques include collagen gel-based contraction assay and culture force microscope (CFM).

3.3.1 Deformable membrane

Harris *et al* [84] developed the first technique for measuring traction force produced by cells. When cells were seeded onto a thin silicon rubber film, the cells contract and pulled on the film, causing visible wrinkles to form. The length and patterns of the formed microscopic wrinkles were used to locate and follow where cells are under contraction and extension, and the relative magnitude of force generated by different types of cells during contraction was estimated [83]. Although laid foundation on measuring cell contraction force through the deformable substrate, this technique cannot quantitatively determine the magnitude and directions of the contraction force. Also, surface defects and non-uniformity of the film thickness can easily introduce errors into the measurement due to the utilisation of the thin film [191].

3.3.2 Traction force microscopy

2D TFM

2D Traction force microscopy (TFM) addressed the limitations of the wrinkling membranes method by assessing the substrate deformation with the displacement of embedded microbeads. Pelham *et al* [172] used a flexible collagen-coated polyacrylamide substrate to study the locomotions of fluorescent-labelled cells seeded on the surface. Based on this, Munevar *et al* [162] improved on the quantitation and introduced the TFM technique by embedding a large number of fluorescent microbeads for measuring substrate deformation. A typical TFM analysis involves optically imaging the bead distribution before and after (or various time points in

the case of dynamic analysis) cell contraction. Computer algorism compare the images and calculate the bead displacements, which is used in quantitatively resolve contraction force by incorporating with the substrate stiffness.

TFM gained popularity as a versatile technique and has been used to measure forces produced by various cell types such as osteoblasts [48], Keratinocyte [56], smooth muscle cells [166, 254] and HeLa cells [239]. As the size of the embedded fluorescent beads (≤ 1 μm) are typically much smaller than the size of a cell, it allows force distribution to be mapped with subcellular resolution [178], and studies such as determining the contribution of active cytoskeletal contraction to traction force generation can be conducted [105]. Also, application of TFM can be extended to measuring forces at focal adhesions [19], traction forces during migration [137, 162] as well as to elucidate how pathological events influence the traction force [193, 236].

The limitations of 2D TFM primarily exist around its unsatisfactory cell-friendliness. First of all, the substrate used in the study is often synthetic polyacrylamide or polyethylene glycol (PEG) hydrogel as opposed to biologically relevant materials for their isotropic, homogeneous, time-invariant mechanical properties [178]. Also, 2D nature of the technique making it far from ideal to study physiological behaviours of cells, as many cellular processes are removed and cells exhibit dramatically different mechanical behaviours when removed from 3D environments and maintained on 2D substrates [47]. Secondly, as force is resolved through the measured elasticity of a homogenous, isotropic and linearly elastic substrate, any errors in the process can be carried on and cause discrepancies in the resolved force. Thirdly, the resolution of traction force through the displacements of discrete markers do not adequately describe the deformation of the continuous substrate surface, and such task is often computationally heavy due to the propagation of the deformation [200, 237]. Lastly, although the elastic properties can be tailored to different test conditions by altering chemical compositions, it may affect

the surface properties of the substrate [43].

3D TFM

The physiological environment of most cells *in vivo* is in 3D matrix as opposed to being on the surface of 2D substrate. 3D TFM is developed as a means to investigate traction fields and measuring contraction force in a more physiologically relevant conditions (*i.e.* cells embedded in a fibrous matrix). In essence, 3D TFM adds extra dimension in the vertical direction to 2D TFM by embedding cells and beads within the matrix and measuring substrate deformation with embedded beads in all three dimensions.

The needs for tracking fiduciary markers in 3D constitute the majority of the added difficulties to 3D TFM, yet so far several approaches have been developed. Bloom *et al* tracked the displacements of embedded fluorescent beads along z axis (vertical direction) using the patterns of diffraction rings generated by beads that are out of the focus plane of the optical system [23]. The tracking of the beads through this method can be accomplished through ordinary microscopy technique. With this method it requires only 5 seconds to track the bead displacements around the vicinity of a single cell, effectively 'freezing' the motion of the cell during the process and minimises the error as a result. However, the tracking resolution along z axis is relatively low at around 120 nm [23]. Laser-scanning confocal microscopy has became ubiquitous in the study of cell morphology due to its high imaging resolution in 3D, which also makes it a viable tool for tracking beads in 3D TFM. Legant *et al* [128] have first demonstrated 3D traction force measurement with polyethene glycol (PEG) hydrogel and confocal microscopy. It offers great spatial resolution, yet the acquisition process is slow, at approximately 3 min per volume per cell, with optimisation of resolution versus acquisition speed [128]. During the time of scan-

ning, changes to the matrix by cellular activities are beyond negligible, inevitably introducing uncertainty to the reliability of the results. Also, the reconstruction process of 3D TFM through confocal microscopy is often very computationally intense. Moreover, as observed by Maskarinec *et al* [144] laser beams used in confocal microscopy are phototoxic to cells, hence the time interval for each image acquisition sequence needs to be kept above 30 mins, limiting its potential in dynamic studies in 3D TFM. Optical coherence microscopy (OCM), which is a variant of optical coherence tomography, can also be applied to tracking of beads in 3D. OCM offers rapid volumetric acquisition rate and utilises near-infrared wavelengths to mitigate light scattering and phototoxicity. However, the spatial resolution of such system is less ideal and prone to the introduction of speckles [160].

Although, many improvements in mimicking the *in vivo* environments have been made during the shift from 2D to 3D TFM, it still does not adequately represent physiological conditions. Firstly, cells are usually seeded at very low density to avoid interference of traction fields surrounding each cells and matrix remodelling [117, 144]. As the contraction of cell is largely regulated via mechanosensing during cell-cell and cell-matrix interactions, very low cell density will unavoidably hinder such processes. Secondly, unlike that in 2D TFM, the substrate not only serves as a measuring device but also a matrix to sustain cellular activities, causing local degradation, precludes the reconstruction of the matrix deformation and resolve contraction force generated by the cells [23]. The difficulties in force resolution is more pronounced in the studies on 3D TFM with physiologically relavent matrix (*e.g.* collagen), as the nonlinear fibrillar nature of the gel prevents the resolution of forces from local matrix deformations through classical mechanics approaches [178].

3.3.3 Elastic micro-pillar technique

In 2003, Tan *et al* [216] developed microfabricated elastomeric arrays, (*i.e.* microneedle-like posts) (Figure 3.5), to spatially track the forces produced by cells attached to their tips. Such a technique was invented to address the inherent limitations of TFM. Deflection of the beam can be measured optically, and contraction force can be resolved by applying elastic beam theory (Equation 3.1), knowing Young's modulus and dimensions of the micro-pillars (Figure 3.5(a)).

$$F = (\frac{3EI}{L^3})\delta \tag{3.1}$$

where E, I, L and δ are Young's modulus, the moment of inertia, length and the horizontal deflection of the micro-pillar.

Since the introduction of EMP technique, it has seen applications in studies for measuring cellular forces on many different types of cells, such as epithelial cells [57], endothelial cells [136], fibroblasts [127], various myocytes [27,190,197,216,241] and dendritic cells [185].

Compared to TFM, this technique excels in the customisability of the micro-pillars while keeping the surface properties constant [216]. By controlling the length and diameter of the pillars, the compliance of the pillars can be altered for different cells types. Meanwhile, variation in the moment of inertia can be achieved for different force directions by changing the cross-section of the micro-pillar (Figure 3.5(g)). Furthermore, different constructions of the micro-pillar array (Figure 3.5(c-f)) will also affect how cells attach to, spread across and deflect the micro-pillars. As the pillar deflect independently by the cell during contraction, therefore reflecting the subcellular distribution of traction forces directly [216]. Additionally, the micro-pillar arrays can be fabricated by casting in a cost-effective manner (Figure 3.5(b))

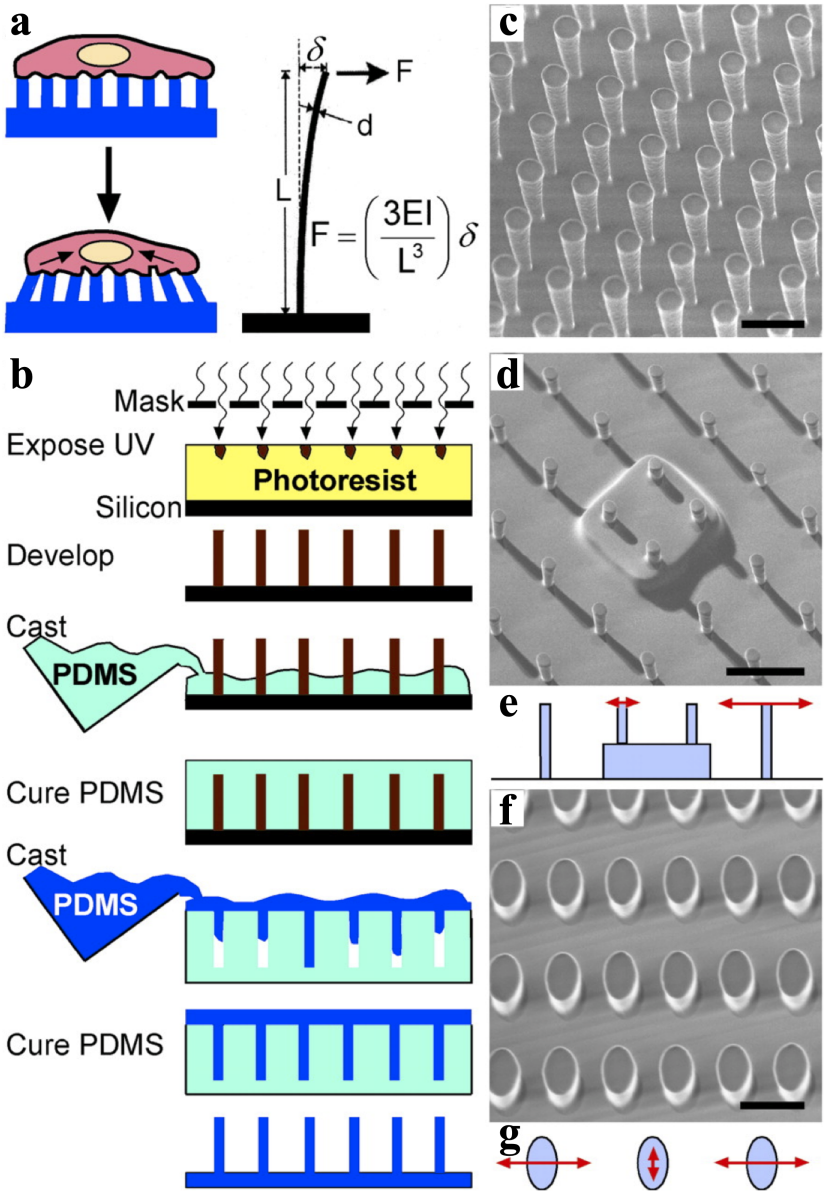

Figure 3.5: Schematic and scanning electron micrographs of EMP. (a) schematic of working principals of EMP; (b) the schematic on the fabrication process; (c-g) scanning electron micrographs and schematics of fabricated arrays (scale bar indicate 10 μm). (modified from [216])

[191].

However, such a technique also has disadvantages. Firstly, the non-physiological material and the topology of the array substrate bears the potential of stimulating unwanted cell responses. Secondly, as an optical microscope is required to observe the pillar deflection, the substrate can only be fabricated with a limited amount of optically transparent materials such as polydimethylsiloxane (PDMS) and polymethylmethacrylate (PMMA), and the casting nature of the fabrication inevitably cause defects in the process [249].

3.3.4 Collagen gel-based contraction assay

Although single-cell techniques such as TFM and EMP are highly quantitative, they all measure contraction forces by placing isolated cells on the surface (two-dimensional) of a substrate fabricated with synthetic materials. However, within the body cells are populated in the ECM, which is a 3D networks of proteins (*e.g.* collagen, glycoproteins) and other biomolecules to provide structural and biochemical support to cells [24,221]. Therefore the 2D single-cell contraction force measurement techniques lack cell-friendliness and may not truly reflect *in vivo* cell behaviours. Bell *et al* [18] introduced fibroblast-populated collagen lattice to study fibroblast contraction, where he embedded fibroblasts into collagen hydrogel and measured contraction force through observing gel shrinkage due to the force exerted onto the 3D collagen matrix. It provided great cell-friendliness over single-cell measurement techniques given by its biomimetic 3D matrix construction.

Briefly, cells will form focal adhesions and exert traction force onto collagen fibrils during the spread within the collagen matrix. Since the collagen fibrils within the matrix are linked and intertwined, forces exerted onto individual fibril will propagate and transferred to cause global contraction of the collagen matrix.

To construct the contraction assay, cells are seeded into the collagen solution with desired cell density and collagen concentration at 4 ℃, followed by polymerisation period of approximately 20 mins after which culture media is added to provide nutrition to the embedded cells. Often the gel is then dislodged from the bottom of the Petri dish and allow to contract freely while suspended in media. The protocol regarding the construction of the assay is documented in detail by Ngo *et al* [167]. Cell contraction is detected by measuring the percentage reduction of gel area after a period of culturing with optical systems [18]. Since the first introduction, several variations to the technique have been developed with various timing of dislodge (shown in Figure 3.6). The most common method is to dislodge after polymerisation immediately (Figure 3.6(a)), and obtain measurements after a period of contraction. Such a method will result in radial shrinkage of the gel. Figure 3.6(b) demonstrated a method in which gels are not dislodged from the dish, and as the gel remains in contact with rigid Petri dish, tension within the gel will primarily lead to a reduction in the gel thickness. In comparison, the former method provides a more straightforward measurement of shrinkage with an optical system than the latter. Figure 3.6(c) demonstrated a combined method, where a period culturing is allowed to elapse before dislodging. As internal stress accumulates due to force exerted on the gel matrix before the dislodge, such method was invented and widely used in studying how external stress affects cellular behaviour [61, 227].

Due to its relative ease of application and cell-friendly nature, many studies have adapted such technique in comparing contractility of cells of different physiological origins. This technique has seen extensive usage among the study of cell contractility in pathological states such as cardiovascular disease [228], respiratory disease [67, 95], eye disease [157], as well as cells during physiological events such as ageing [248] and wound healing [98, 224].

In the early 1990s, Moon *et al* [155] developed a novel approach known

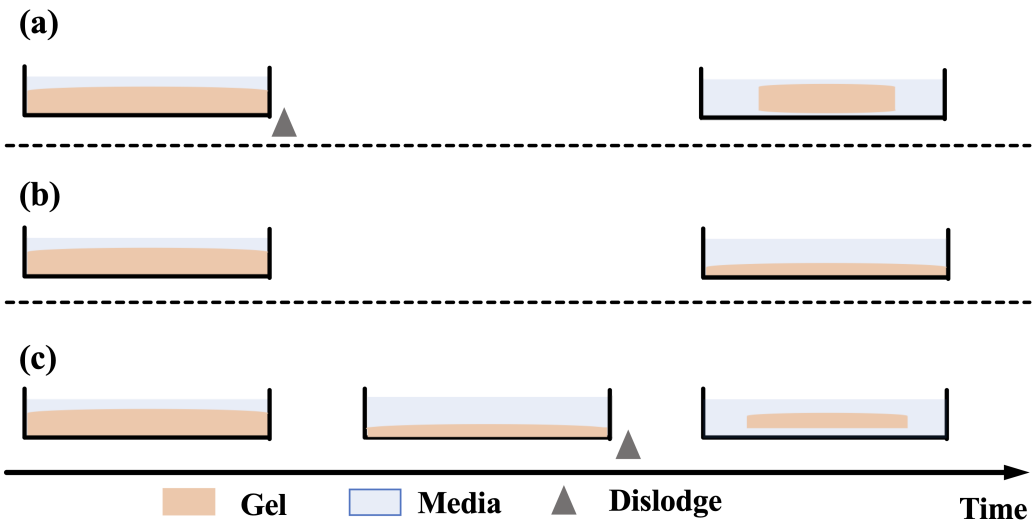

Figure 3.6: Schematics showing the variation of contraction assays based on dislodge time. (*a*) immediate dislodge; (*b*) no dislodge; (*c*) dislodge after a period of time.

as fibroblast-populated collagen microspheres (FPCM) to measure cell contraction forces by probing the interaction between cells and collagen fibrils. In comparison, the FPCM is a spherical analogue of the traditional collagen-gel based contraction assay proposed by Bell *et al*, where instead of a gel with a disk-shaped geometry, a spherical gel is constructed by pipetting cell-containing gel solution into a silicone fluid at 37 ℃. The novel approach provides a number of significant advantages over the traditional approach. Firstly, the spherical design provides a far more straightforward way of assessing the contraction force exerted onto the collagen gel. The measurement will be one-dimensional instead of two-dimensional as required in the disk-shaped gel. The spherical geometry also enables the contraction of FPCM to be mathematically described with easy to solve model that consists of only a spherically symmetric set of equations. Secondly, as reported by Modis *et al* [151], the methodology applied in constructing traditional disk-shaped gel can lead to a significant local anisotropy in the collagen matrix. It is believed to be a result of fibrillogenesis in the presence of bounding surfaces. Furthermore, as the collagen microsphere in the FPCM technique is prepared through pipetting the gel solution into silicone

fluid, the collagen fibril orientation is relatively isotropic initially. Thirdly, the diameter of the yielded microspheres can be arbitrarily small with a typical value of 1 mm [155], the small size allows diffusion gradients to be minimised and best supply embedded cells with nutrients and promptly removes cellular wastes. Lastly, from the magnitude perspective, the FPCM technique bridges the gap between single-cell contraction force measuring techniques and large scales multiple cells measurement techniques (see below sections).

Despite its cell-friendly merit and its ability to simulate various physiological conditions, collagen gel-based contraction assays can only provide a qualitative assessment on cellular contraction provided that mechanical properties, such as elasticity of the collagen matrix are unknown. Considering that collagen matrix is always under remodelling by the cells, and the elasticity of the cell embedded collagen hydrogel can be influenced by factors such as agonist treatments, the assay based exclusively on the geometrical changes of the gel fail to measure cellular contraction force accurately.

3.3.5 Culture force monitor

Collagen-based contraction assay mentioned above provides a cell-friendly and straightforward approach to assess the cellular contractility by measuring the geometric change of cell-embedded 3D biomimetic gels. Apart from its non-quantitative nature, it also lacks sensitivity as it cannot display observable radius change when the contraction force is relatively small. To improve the technique, Delvoye *et al* [53] developed CFM system, achieving direct measurements of contraction force by attaching a force transducer on the edge of the cell-embedded collagen gel.

In a typical CFM system, the sample gel is fixed to two diametrically opposed plates, which connected to a force transducer and translational stage respectively.

The stage is used to pre-stretch the gel prior to the start of the experiment (Figure 3.7).

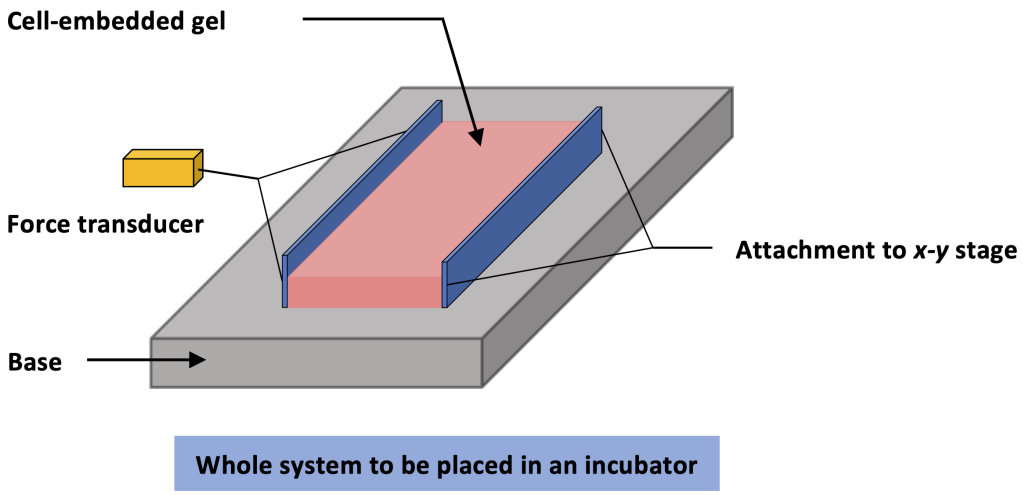

Figure 3.7: Schematic diagram of a typical CFM system.

The entire system is placed within a standard culturing incubator, and the force transducer measurements are acquired wirelessly. Alternatively, needle-like force transducer probes can be attached isometrically on the free-floating collagen hydrogel, and differential measurements can be taken between transducer pairs, such setup provides the maximum displacement sensitivity of 0.5 mm [60]. The most prominent benefit of the CFM technique is its ability to allow precise, high sensitivity measurements of multi-cellular force directly in a physiologically relevant environment and continuously detect and record changes throughout the culturing period. Also, the system enables easy application of external mechanical stimuli, providing the ability for more complex experimental design [191]. Recently, significant improvement has been made by Campbell *et al* [36] and Peperzak *et al* [175] to increase the efficiency of CFM. The multi-station dynamic CFM allows multiple gel samples to be measured simultaneously, significantly reducing the measuring time and achieved better variable controls throughout the study. Many studies have adopted CFM to measure different cell types such as fibroblasts, endothelial

cells [118], and cardiac myocytes [257].

However, there are also several disadvantages associated with CFM. One of the main disadvantages is system complexity. The setup will inevitably disturb the normal cellular processes which add uncertainty to the result, especially with protocols requiring long culture time, as well as increase the chance of infection in the culturing process. Additionally, as the force is acquired from a discrete amount of force transducers, the interpretation of the result is mostly dependent on the transducer placement. Lastly, the setup time for such a system is relatively long and complicated.

Chapter 4

Experimental setup

4.1 Introduction

The previous chapter outlined the range of magnitudes of force-sensing capability required in characterising the mechanical behaviours of cells and depicted several advanced cellular force sensing techniques. With a particular interest in the measurement of cell contraction force, the techniques used in assessing cell contractility was described in detail with their application-specific advantage and disadvantages. To investigate how ageing will affect the contraction behaviour of dermal fibroblasts, a highly quantitative technique is required. Also, as described in Chapter 2, the functional changes of ageing dermal fibroblasts are closely related to the changes of ECM. Thus, it is of great importance to measure the contraction force of dermal fibroblasts in a cell-friendly biomimetic matrix. It is indicated that the previous contraction force measurement techniques described in Chapter 3 do not fulfil the one or both requirements in differentiating the contractility of young and aged dermal fibroblasts.

Based on the concept of cell-friendly collagen gel-based contraction assay (see

Section 3.3.4), a highly quantitative technique in cell contraction force measurement suitable for differentiating contractility of young and aged dermal fibroblasts was developed. The technique achieves accurate measurement of the force responses in relation to the displacement during nano-indentation testing of cell-embedded hydrogel. The force response is used as an input parameter for mathematical modelling to determine the elasticity of cell-embedded hydrogel, which is subsequently used for the calculation of cell contraction force. In this chapter, a novel bio-nano-indentation tester achieving measurement of Young's modulus for the cell embedded hydrogel is introduced with its building components and the software structure for their coordination. Moreover, the additional features on the bio-nano-indentation tester are outlined with their prospective applications in detecting the mechanical properties of biological samples. Lastly, the designs for an optical system in hydrogel image acquisition together with image recognition and edge detection mechanism for determining the geometrical changes of the cell-embedded hydrogel is outlined.

4.2 Hardware design

The primary function of this bio-nano-indentation tester system is to achieve high precision depth-sensing indentation testing, which provides useful information regarding the deformation behaviour of the cell-embedded collagen hydrogel. The primary working mechanism is to provide high force and displacement resolutions during the nano-indentation. With the correspondent force and displacement data, a force-displacement (F-D) curve can be created. The F-D curve can be subsequently fitted with an appropriate contact mechanics model or the resultant output of a finite element simulation (see Chapter 5), through which Young's modulus of the hydrogel can be obtained. The bio-nano-indentation tester mainly consists of a force transducer, motorised x-y axis stage, motorised z axis stage, as shown in

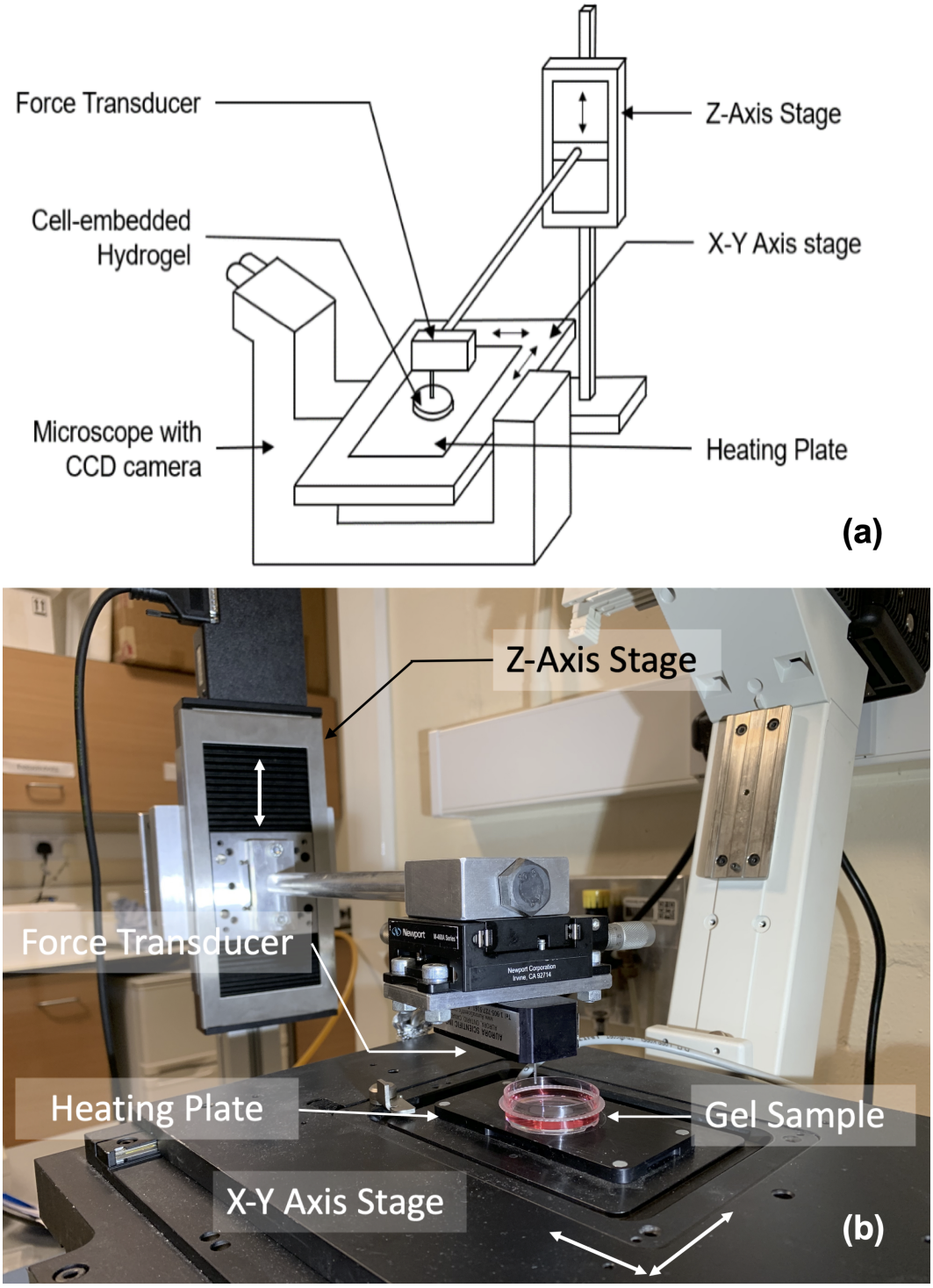

Figure 4.1: The basic force-displacement sensing component of bio-nano-indentation tester. (a) schematic diagram (not to scale); (b) image.

Figure 4.1. The tester system can achieve 10 nN and 100 nm resolution in force and displacement, respectively. As the tester system is capable of probing force and displacement at an ultra-sensitive level, the entire instrument setup is placed onto an anti-vibration table (AVT-702, Wentworth Laboratories Ltd) to isolate ambient vibrations. Through this, the likelihood of potential instability is minimised, and the force and displacement measurement accuracy is ensured. The following sections describe the feature of each component in relation to the aim in achieving high-resolution depth-sensing indentation testing, as well as the hardware architectures in data acquisition.

4.2.1 Force transducer

Force sensing mechanism

The bio-nano-indentation tester is designed to provide *F-D* curve at high resolution. The task of sensing the changes in forces is achieved by a force transducer (406A Aurora Scientific Inc. Canada). The force transducer comprises two parts, the transducer head and the electronics package, where a wired connection exists between them for signal transmission. Figure 4.2 shows the top and side view of the transducer with its dimensions. It can be seen that a silica probe with a diameter of 1 mm protrudes out of the main body of the transducer head. One end of the probe makes contact with the testing subject, while the other end of the silica probe is mounted on a cantilevered glass beam. Such configuration translates the forces into the deflection of the cantilever beam. The end of the cantilever and the base is coated with a thin layer of gold, effectively forming a capacitor. The capacitance between the cantilever and the base will change when the cantilever beam is deflected. The current generated by the change in capacitance is processed and amplified by the electronics package and output as a change in voltage. This pathway constitutes

the basic working principle of the force transducer.

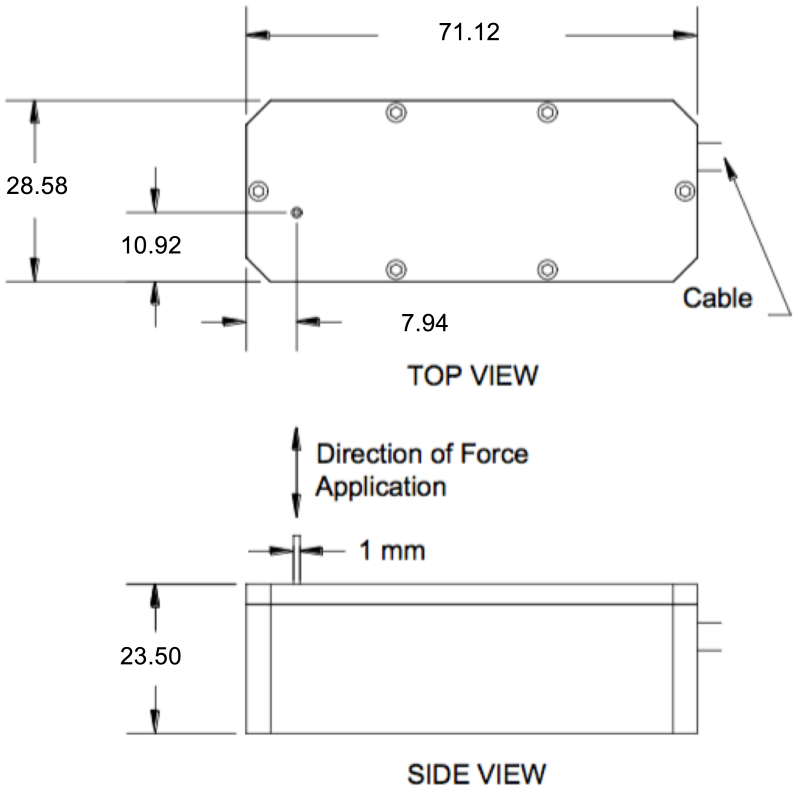

Figure 4.2: Top and side view of 406A transducer head. Unit: mm. (modified from [10])

Figure 4.3 shows the detailed circuitry in achieving the function of the force transducer. In addition to the capacitor (C_{Force}) required to achieve the translation of cantilever deflection to voltage output as introduced above, a reference capacitor ($C_{Reference}$) can be seen. The two capacitors are identical, hence the capacitance of the two capacitors is equal when no external forces are applied onto the silica probe. A difference in capacitance between C_{Force} and $C_{Reference}$ is generated when a force is applied onto the probe. In such a case, the transducer circuitry converts the current difference into voltage difference through the differential trans-impedance amplifier, which is followed by various amplifiers and eventually output as a voltage signal with an appropriate amplitude. As the deflection of the mechanically well-defined

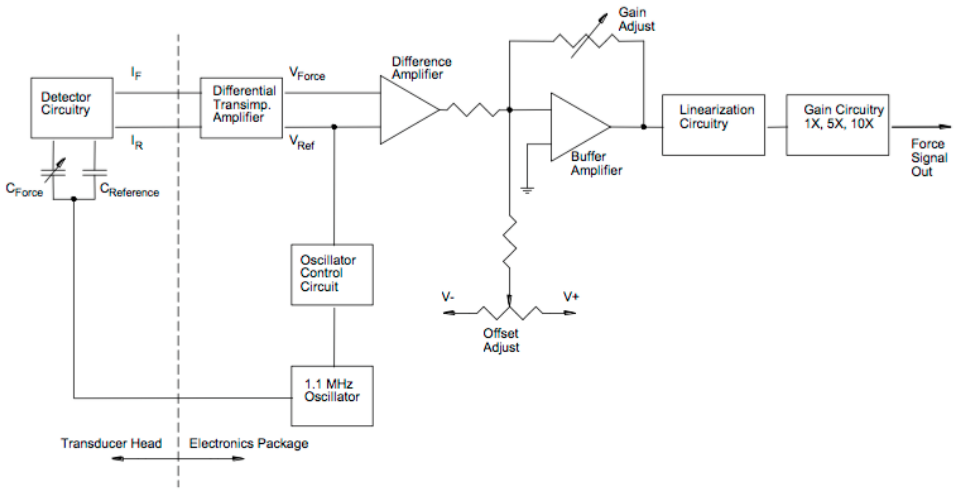

Figure 4.3: Schematics diagram shows the transducer circuitry for force detection and signal amplification. [10]

cantilever beam is within the linear elastic region, the output voltage is linearly proportional to the force subject to the silica probe.

It is worth mentioning that the two-capacitor design in the transducer head has a unique advantage in mitigating the error caused by the changes in ambient conditions. As the transducer head enclosure is neither air-tight nor thermally well-insulated, the spring constant of the glass cantilever beam differs with varying temperature [12]. Also, the nonlinear increase of capacitance along with humidity increase renders it impossible to counter react its effect by simple filters [107]. With the addition of an identical reference capacitor, the output of the measured force signal is irrelevant to the ambient condition and only determined by the amount of force subject to the silica probe.

With the change-of-capacitance based force detection design, the force transducer (406A) can provide a force resolution of 10 nN, which is at the most refined end of any transducer type of force sensing mechanism. Although a finer force resolution can be achieved through other advanced instrumentations, such as AFM and

OT (see Chapter 3), they often have more confined application scenarios. Hence, with 10 nN force resolution and ± 0.5 mN measurement range, the force transducer used in this system is more versatile and ideal for characterising the mechanical behaviours of soft biological materials and biomaterials such as collagen gel. It is also worth pointing out that force sensitivity differs among the direction of force application on the silica probe. Due to the design of the force-sensing mechanism, it can only accurately resolve forces that are applied along the central axis of the silica probe (shown in Figure 4.2: SIDE VIEW). Therefore, the transducer is mounted in such a way that the indentation is aligned with the force sensing axis of the transducer, as shown in Figure 4.1.

Probe tip modification

As the surface in contact with the test sample, the morphology of the probe tip surface is critical to sensing the applied force onto the materials. Also, the shape of the probe tip will affect how the mechanics of the contact is modelled. It also changes the methodology adopted in the fitting of the *F-D* curve in the analysis of the data acquired in the nano-indentation. Also, the silica probe is tubular, which is unsuitable for nano-indentation of soft materials, as the relatively small contact area will lead to stress concentration which may cause the puncture of the samples with small displacements.

To address the aforementioned issues, modification of the probe tip was conducted. The general action for the modification of the probe tip is to attach a piece of material with the desired shape, which contact profile is clearly defined with existing contact mechanics models. Also, as the transducer components, especially the glass cantilever beam within the transducer head is very fragile, the additional material has to be lightweight so the transducer will not be overloaded. Moreover,

the material selected for modifying the probe tip has to be rigid enough without self-deforming during the nano-indentation of soft biomaterials such as hydrogel, yet easy to be cut into the desired shape. Lastly, the bonding between additional structure and the silica probe has to be strong enough and will not cause detachment during the measurement in aqueous solutions.

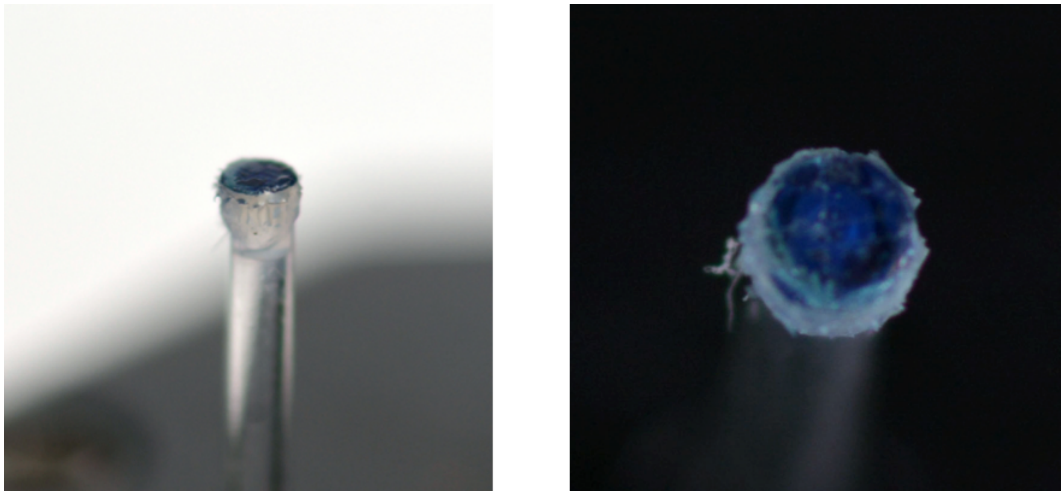

Figure 4.4: Tubular silica probe tip capped with HDPE disk.

With the above considerations, a circular high-density polyethene (HDPE) disk with 1 mm diameter was fixed onto the probe tip as a cap (shown in Figure 4.4). The material is lightweight with a smooth surface, hence its contact profile when indenting soft biomaterial can be modelled as 'cylindrical flat punch'. Also, HDPE has Young's modulus ranging between 0.6 - 1.5 GPa, it is six degrees of magnitude greater than that of the hydrogel being measured. Thus it is safe to assume the HDPE material as a rigid material in modelling and analysis (see Chapter 6). Moreover, it is believed that, with such a significant difference in the elasticity, the exact value of the Young's modulus of the material used for tip modification does not alter the result nor the assumption of it being a rigid body. As the force transducer can resolve nano-newton level forces, the forces resulting from intermolecular interaction between the HDPE cap and the gel surface are no longer negligible. However, such interactions may only come into effect when the HDPE surface is being pulled

away from the gel surface (*i.e.* reverse motion of indentation), which is irrelevant in the current design of the bio-nano-indentation tester. Hence, the characterisation of intermolecular forces between the HDPE cap surface and the hydrogel is beyond the scope of this project. Wax was selected as the choice of the adhesive for fixing the HDPE cap as it is widely available with a melting temperature which is practical and safe for the force transducer components. Also, its non-toxic nature and stability in aqueous solution provide its suitability for application in nano-indentation of soft biomaterials such as cell-embedded collagen hydrogels. Moreover, the wax provides a semi-permeant fixture between the cap and the probe, allowing the probe tip to easily provide a different contact profile by changing the cap to a spherical indenter.

4.2.2 Motorised stage

The motorised stage is an irreplaceable part of the bio-nano-indentation tester. They have very high precision and displacement resolutions, generating repeatable micro- or nano-level movements to accurately position the sample to desired locations for nano-indentation. More importantly, they can provide displacement information, which is critical for constructing an *F-D* curve for analysis. As shown in Figure 4.1, the movement of the *x-y* axis stage will position the sample to a target position for indentation, while the *z* axis stage will move the force transducer in the vertical direction, executing the motion of indentation. With the coordination of both stages, the bio-nano-indentation tester is capable of delivering depth-sensing indentation measurements at any given location on soft biomaterial samples. The resolution of both motorised stages is 100 nm.

x-y axis stage

The *x-y* stage system consists of three systems. The main component is the high precision motorised *x-y* stage (H117-series ProScan^{TM}, Prior Scientific) along with an interactive control centre joystick (PS3J100 Control Centre, Prior Scientific) for simple control of the stage motion. A modular control hub (ProScan^{TM} III, Prior Scientific) sits in between the stage and the joystick for processing commands and position feedback. The *x-y* stage used in the construction of the tester is mounted onto an inverted microscope, which also doubles as the stage for microscope functions such as epi-fluorescence analysis on stained cells. The stage has a travel range of 114 mm and 76 mm in x and y directions respectively. Hence it is capable of mobilising samples within a large area yet preserving excellent displacement resolution. The joystick is a central position controlling accessory connected to the control hub, which can achieve direct and instant control of the stage motion. It is capable of move the stage in any direction as long as the range of stage motion permits. The modular control hub is used to process the input from the joystick and coordinate the motors used in mobilising the stage. As an example, the stage is capable of precisely mimicking the motion of the joystick and moving to any direction at a constant speed. This is achieved by the control hub coordinating the output of the two motors dedicated to moving the stage in x and y directions respectively. Moreover, the control hub is a modular system, and with incorporating additional component, it can be used to control the focus of the microscope, rotating and selecting the excitation filter wheel. The ability of expansion in function may lead to further development of the functions and measurement designs of the bio-nano-indentation tester.

z axis stage

The z axis stage is used to execute the indentation and records the vertical displacement as the force transducer is directly mounted onto the stage (see Figure 4.1). The z axis system consists of a motorised linear stage (UTS 100CC, Newport) and its control unit (ESP301). The stage has a travel range of 100 mm, with a maximum speed of 40 $\mathrm{mm\,sec^{-1}}$. Such a travel range is adequate for conducting nano-indentation test on soft biomaterials with a general size, and the speed of motion is perfectly suited for measurements of viscoelastic materials (*e.g.* stress relaxation test). The motion control unit has inputs keys that can be used to control the motion of the stage, as well as featuring a screen that indicates the motor position and providing feedback to the user's manipulation. Moreover, similar to the control hub for the x-y stage, the function of the control unit can also be expanded for control and coordinate multiple stages and other components, indicating the potential of extending the function of bio-nano-indentation tester.

4.2.3 Instrument connection to the host PC

A desktop PC was chosen to be the centre of the tester, where each component is connected to, coordinated control is established, and test data is acquired and stored (see Section 4.3). Both motorised stages have a control unit, which forms two-way communication links with the host PC via USB ports. Due to the presence of the motion control unit, it is easy to gain position readings form the stages as well as controlling the stage motion with established commands. As introduced in Section 4.2.1, the output of the force transducer is in the form of voltage, which is an analogue signal by nature. The electronics package (see Figure 4.3) only serves as a power supply and an amplifier of the transducer signal. The analogue signal is passed through a terminal I/O block (SCC-68 terminal connector, National Instrument)

connected with E-series data acquisition device (DAQ) built into the host PC. This infrastructure forms the physical link for the coordination of instruments and data acquisition. The following section will lay focus on the software structure designed to achieve the functionality for fulfilling the purpose of the bio-nano-indentation tester.

4.3 Software structure for hardware coordination and data acquisition

To acquire the force-displacement data, a software infrastructure needs to be constructed for controlling and coordinating the individual component from different manufactures. The minimally required function of such software structure is to be able to mobilise z axis stage to indent the sample for a given depth, record the position of the force transducer throughout the process while acquiring the measured force value from the force transducer. With this data, an F-D curve can be formulated for analysis.

Labview (National Instrument, UK) was selected as the programming package used in building software structure of the bio-nano-indentation tester. Labview is a system engineering software for applications involving test, measurement, and control with rapid access to hardware. It is widely adopted in coordinating instrument and designing sequences in both experimental and industrial application settings. Unlike many of the programming packages, Labview is entirely based on graphical programming, where each functional programme is referred to as a virtual instrument (VI). Within each VI, primary functional blocks representing different parameters, functions and algorithms are connected via logic wires, along which the variables propagate. Also, subject to the function, each VI has input and output ports where logic lines can be drawn to achieve variable exchange. The advantage of

graphical programming is the visualisation of the data flow, which makes Labview particularly suitable for designing the software structure for coordinating hardware and acquiring data in the bio-nano-indentation tester.

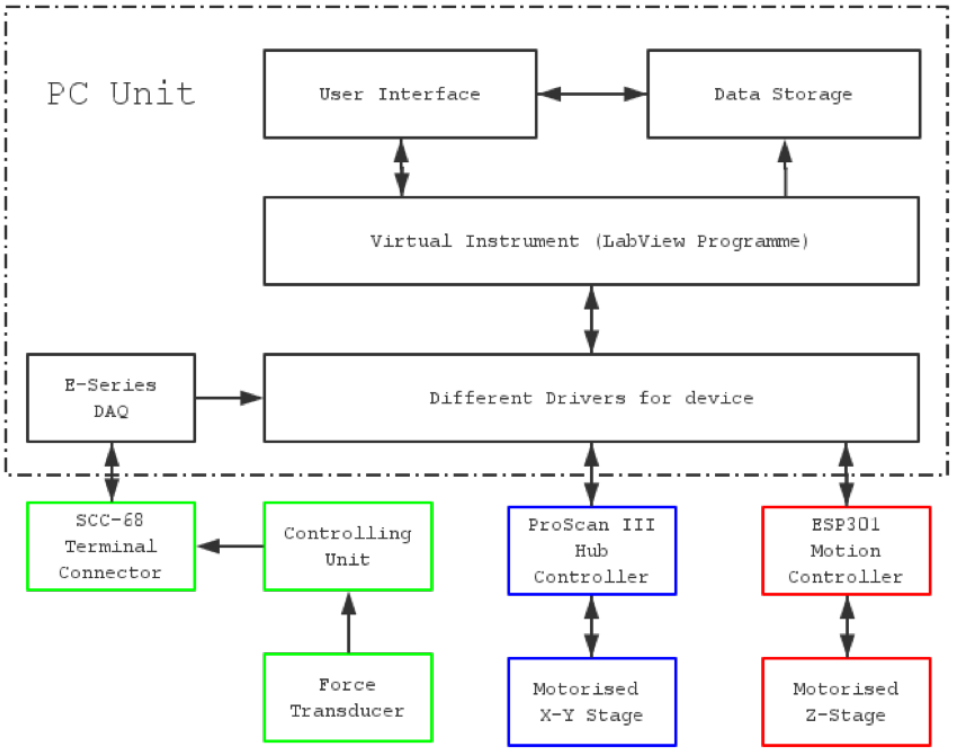

Figure 4.5: Data flow between each component of the bio-nano-indentation tester system. Green: force transducer system. Blue: x-y axis stage system. Red: z axis stage system. Items in the dotted rectangle box are contained in the host PC as indicated.

Figure 4.5 shows the basic system architecture in achieve instrument coordination and data acquisition. The arrows represent the transmission of information. The acquisition of forces is achieved through direct reading the E-series DAQ data through the built-in DAQ assistants VI of Labview. The DAQ assistants VI can log force data from the transducer at a specified sampling frequency through the connected SCC-68 terminal connector and the DAQ hardware. The sampled force data

is recorded with associated timestamps, which is achieved through programming. The z axis stage was programmed to execute a 'loading-unloading' style motion for the basic function of a depth-sensing bio-nano-indentation tester. During which, the stage is instructed to move in such way that the attached force transducer indents the sample for a specified depth at a given speed and subsequently return to its original position at the start of the test. As the velocity of stage motion is well defined, the stage position (*i.e.* displacement) can be calculated as a function of time elapsed and recorded through Labview programming. The ASCII based commands syntax to the stage motion controller to achieve various motions are clearly defined in the user's manual of the ESP 301, which is supported by the Labview. The 'loading-unloading' motion is achieved by a series of commands that involves defining the current position as 'origin', set stage speed and motion displacement as well as returning to the 'origin'. Various logic loops were applied to define the sequence of the motion and force data acquisition as well as features to improve system stability, the basic function of depth-sensing bio-nano-indentation tester can be achieved.

4.4 Additional features and prospect applications

In the nano-indentation testing of cell-embedded hydrogel, it is not always feasible to have a pre-determined indentation depth (*i.e.* displacement). Also, cellular activities within the hydrogel may lead to inhomogeneity. Thus, the need for selecting indentation sites regarding the location of cells within the sample arises. Moreover, as many nano-indentation tests in characterising mechanical behaviours of soft biomaterials use force as a constant and displacement as a variable (*e.g.* creep test), further programming was done to achieve these features to increase the testing versatility.

The x-y stage was incorporated into the software structure through communication between the host PC and control hub in a similar manner as that for the z axis stage. The x-y axis stage integration allowed the coordinates of the indentation site to be recorded, as well as specifying the location on the sample for indentation testing. Also, automated mapping of mechanical behaviour through nano-indentation can be achieved by imputing an array of coordinates for the location of interests defined by the user. The coordinate array can also be generated by defining a mapping pattern such as concentric circle, square or along a line across the sample. Moreover, the z axis stage motion is programmed to be dictated by force measured on the transducer, opens the possibility of the novel bio-nano-indentation tester being applied on a broader range of applications.

Figure 4.6 introduced the functioning sequence of the software in the nano-indentation mapping of the sample. The mapping pattern shown in the diagram is circular, yet significant similarities are shared in the software sequence when another mapping pattern is required.

As shown in Figure 4.1(b), a manual stage (M-460A-XY, Newport) with two Vernier micrometres (SM-13, Newport) is present to provide the possibility of fine adjustments in the positioning of the force transducer. This configuration allows translational movements in both x and y axis with 1 μm precision. This manual stage system addresses the need for selecting indentation points under an inverted microscope, where the fine adjustments of the location of force transducer probe are preferable than solely dependent on positioning the sample through motorised x-y axis stage.

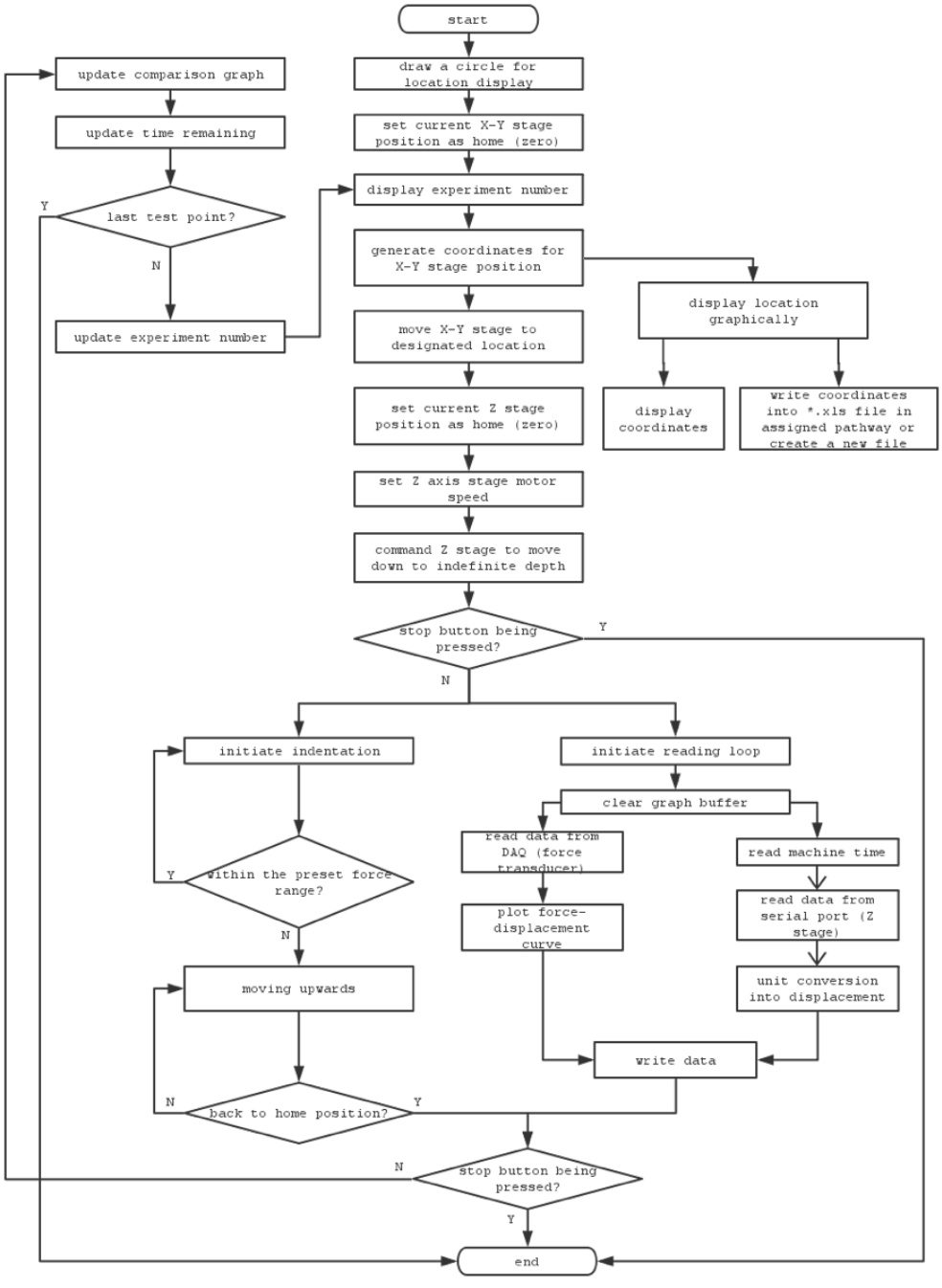

Figure 4.6: The flow chart of experimental procedures for automated mapping of mechanical properties of samples in a circular pattern.

4.5 Measurement of the geometry of the cell-embedded hydrogel

To accurately determine the contraction force generated by the cells embedded within the collagen hydrogel, both Young's modulus of and the geometrical changes of the gel as a result of cell contraction are required. The bio-nano-indentation tester, as introduced in the above sections, can execute nano-indentation while recording the force response representative of the gel material properties. However, it is necessary to obtain the thickness and the diameter of the disk-shaped cell-embedded hydrogel before and after cell contraction. Through these, Young's modulus and the geometrical change of the hydrogel can be calculated.

Measurement of hydrogel thickness

The measurement of the gel thickness is achieved through analysing the *F-D* curve of the nano-indentation test, where the indenter is allowed to penetrate the gel and reaching the surface of the rigid substrate (*e.g.* Petri-dish surface), on which the gel is placed during testing. In such test, the events that the indenter making contact with the top surface of the gel and the surface of the rigid substrate is easily distinguishable on the resultant *F-D* curve as the indenter is transitioning between materials with very different properties. Before making contact with the top surface of the gel, as the indenter tip travels within the air, the force measured is constant irrespective of the displacement. As the displacement keeps on increasing, moments before the contact with the top surface of the gel, a sudden increase of the force can be seen on the *F-D* curve due to jump-to-contact. It is described as the liquid (*e.g.* residual culture medium) on the surface of the gel fills the narrow gap between the indenter tip surface and the gel surface, forming a meniscus leading to attractive capillary force between the two surfaces [243]. As the displacement of

the indenter increases further, it makes contact with the gel surface, marked by the reversal of the direction of the force measured by the transducer. The *F-D* curve during the nano-indentation of the gel is that of a typical soft nonlinear material. Upon contact with the rigid substrate, on the *F-D* curve, the force will tend to infinity while displacement remains constant with elapsed time. With the distinct change observable on the *F-D* curve, the thickness of the gel can be obtained by the differences in the displacements measured between the top surface of the gel and the surface of the rigid substrate.

Measurement of hydrogel diameter

The measurement of the diameters of the hydrogels before and after contraction is achieved by recognition and analysing the top-view image captured by an optical system. The optical system consists of a CCD camera (Sony, XC-ST50ce) with a long focal lens (VZM 450, Edmund Industrial Optics) mounted vertically downwards on a fixation (see Figure 4.7). The base of the optical fixation is adjusted with the aid of a spirit level to ensure that the gel sample is sitting on the flat surface without tilting. The mounting of the CCD camera and the long focal lens is calibrated with a 7×9 checkerboard prior to imaging the gels to eliminate parallax error in the image acquisition process. Figure 4.8(a) and (b) show the representative images taken by the optical system used in measuring the diameter of the gel. The reduction of the gel diameter led by the contraction of embedded cells can be seen.

The diameter of the hydrogel is calculated from the measured area of the hydrogel. Although the direct measurement of the diameter can be achieved, such a method does not fully consider the potential non-circularity of post contraction gels, which remains a possibility despite the uniform distribution of the cells. The calculation of diameter through area measurement increases the versatility of the

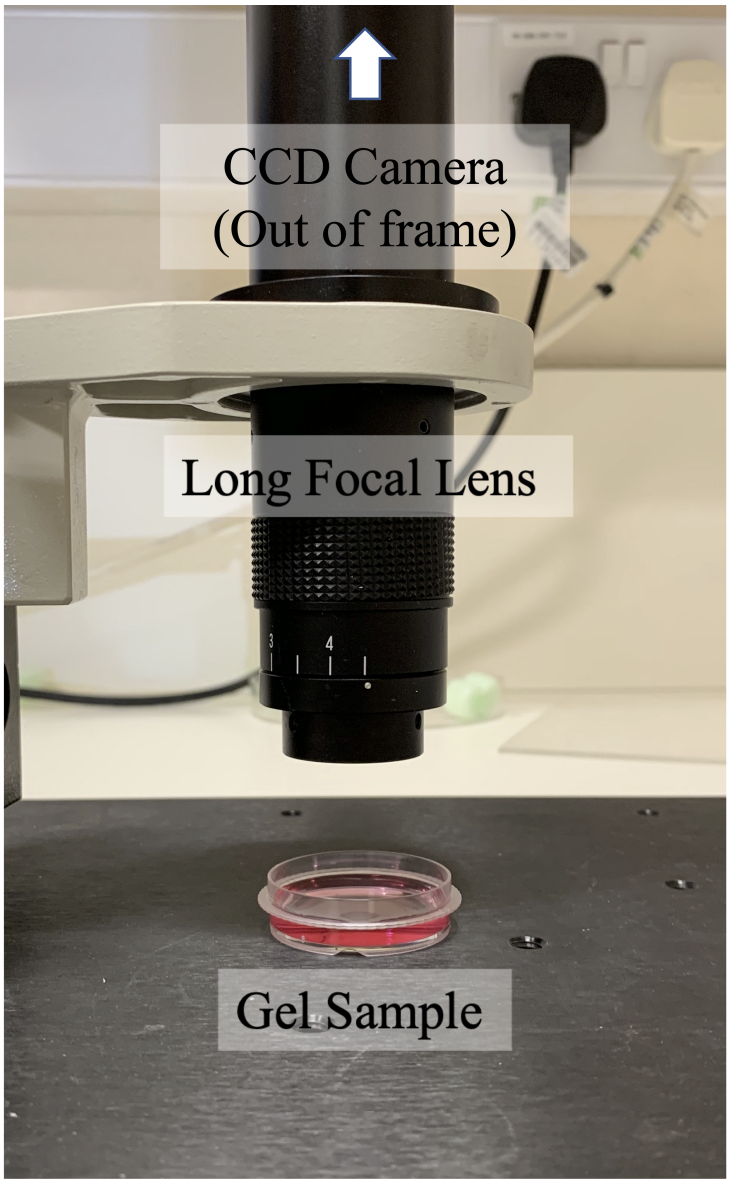

Figure 4.7: Image showing the instrument setup for obtaining the diameter of disc-shaped gel samples (CCD camera not shown).

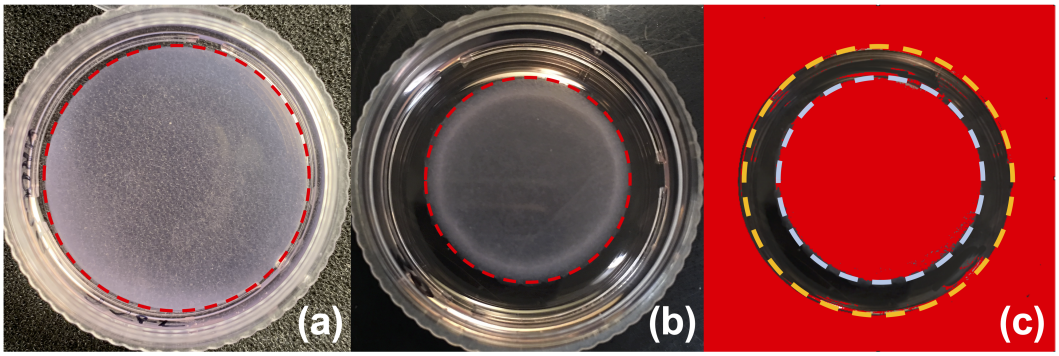

Figure 4.8: Top view of the cell-embedded hydrogels taken by the optical system. (a) and (b): sample images before and after cell contraction, dashed circle mark the edge of the gel. (c): thresholding of gel image used for calculating gel area, where yellow and light blue dashed circles mark the inner edge of the petri-dish and edge of the gel respectively.

optical system.

ImageJ programme (National Institute of Health, USA) is used in analysing the top view image of the gel through thresholding and measuring (shown in Figure 4.8(c)). Within the image, there are three distinct components, background, Petri-dish and hydrogel. As shown in Figure 4.8(b), the background is dark and the gel is light in colour, hence by applying RGB thresholding, the portion of the image covered by the gel and the background can be recognised. Also, the angle of the lighting during the imaging process created a 'halo' at the inner edge of the Petri-dish, which can be utilised as a marker in hue-saturation-brightness (HSB) thresholding. The combination of both image thresholding algorisms can effectively achieve recognition of the Petri-dish and gel area and detect the edge of each component within a top-view image of the hydrogel. As the diameter of the Petri-dish has a known value of 35 mm, the area of the Petri-dish and subsequently the area of the gel can be calculated easily. With this approach, the gel diameter can be calculated from the top view image regardless of the lens magnification, and changes in gel diameter can be assessed through comparing the diameter of the gel before and after contraction.

4.6 Summary

The bio-nano-indentation tester was designed to assess the geometrical changes and mechanical behaviour and of cell-embedded collagen hydrogels by gel image analysis and accurate measurement of the force-displacement data during nano-indentation. The fitting of the *F-D* curve in determining the Young's modulus of the cell-embedded collagen gel as well as the approaches adopted in calculating cell contraction force through the Young's modulus and geometrical change of the gel will be introduced in Chapter 6. The ability to accurately determine Young's modulus and the geometrical changes of the cell-embedded collagen hydrogel through the designed bio-nano-indentation tester system marks the distinction of this highly quantitative cell contraction force measurement technique. Overall, the development of the bio-nano-indentation tester provides the capability of differentiating contractility between young and aged dermal fibroblasts with fulfilment in both cell-friendliness and quantitativeness measurements.

Chapter 5

Mechanical behaviours of collagen hydrogel– measurement and modelling

5.1 Viscoelastic property of collagen hydrogel

As the most abundant protein within the human body, collagen plays a crucial role in many connective tissues such as skin, bone, tendon and ligaments etc. Due to its importance in native tissue, excellent biocompatibility, low toxicity and extensively studied physical and chemical properties; collagen hydrogels have been broadly adapted for applications in, tissue engineering, drug delivery and wound dressings [126]. Also, as mentioned in previous chapters, collagen hydrogel is an excellent material for mimicking the structure and biochemical environment of the ECM. Such properties are exploited in 3D cell culture, and on investigating the cell-substrate response under various conditions [17]. As a polymeric biomaterial, collagen hydrogels are structured, hierarchical and complex, which often exhibit

viscoelastic properties. Viscoelasticity is essential for biological functioning as it is essential for storage, transmission and dissipation of forces and energy within living tissues [62, 70].

Viscoelastic materials are defined as materials displays both elastic and viscous characteristics simultaneously at a considerable level when undergoing deformation [246]. Similar to soft biological tissues, hydrogels are typical biphasic materials where a solid network forms the scaffold of the structure with water filling in the porous cavities [225]. In the case of collagen hydrogel, the solid network comprises of intertwined and crosslinked collagen fibrils and water and acts as an interstitial fluid phase. It is commonly believed that the solid network is responsible for the elastic characteristics of the hydrogel, whereas the network mobility and fluid flowing within the network contributes to the viscous properties of a viscoelastic material [112]. Within collagen hydrogel, the interstitial fluid phase (*e.g.* water) can be categorised into two groups: 'free-flowing' and 'fixed'. The 'free-flowing' water can easily undergo exchanges and flow in and out of the hydrogel. The 'trapped' water (*i.e.* fixed phase) is tightly bound to collagen fibrils through hydrogen bonding and has an important role stabilising the structure of the collagen within the hydrogel and contributing greatly to the viscous properties of the collagen hydrogel. At the same time, the hierarchical structure of collagen fibres provides the elastic strength of the hydrogel.

As viscoelasticity is an important mechanical property of collagen hydrogels, it is at significant interests to characterise its viscoelastic behaviours as it will help us better understand, monitor and predict their performance as a biomaterial. Also, it will provide useful information regarding the responses in specific loading conditions, which can be used to improve and calibrate the theoretical model used in the hydrogel-based contraction force measurement technique. As mentioned in Chapter 1, highly hydrated materials are often very soft and require delicate han-

dling, which is especially true for the case in characterising viscoelastic properties of collagen hydrogel. Moreover, collagen hydrogel is particularly labile compared with other hydrogels in the biomaterial family and its mechanical properties are highly sensitive to environmental changes (*e.g.* degradation, water content loss, breakage). Therefore, the measurement technique needs to be able to reliably measure the parameters for characterising the viscoelastic property while preserving the native material properties.

There are two major categories of approaches for characterising viscoelastic behaviours: stress relaxation and creep. Stress relaxation test applies a fixed deformation to the sample and measures the stress-time response of the sample, while the creep test applies a fixed force and records the strain-time curve. The time-dependent stress and strain data from the tests and subsequently used to derive viscoelastic parameters from constitutive models. For many materials, tensile stress relaxation tests are often used to determine their viscoelastic responses, yet the nature of biomaterials, especially hydrogels, does not necessarily permit such tests to be performed. In the last decade, many alternative mechanical testing approaches have been developed to be suitable for hydrogels in particular. Ahearne *et al* demonstrated the mechanical characterisation of viscoelastic properties of biomimetic membranes through micro-shaft poking [2] and a novel method dropping a stainless steel ball onto a thin hydrogel film [4]. Cheng *et al* [41] and Mattice *et al* [145] demonstrated the technique for stress relaxation and creep tests with spherical indentation, allowing samples to be placed in an aqueous medium. Although compared to the other methods, the indentation methods are confined to measuring localised viscoelastic response rather than the bulk material; it created the least amount of disturbance to the hydrogel. For the characterisation of collagen hydrogel in this study, stress relaxation test is conducted with the indentation methods using the nano-mechanical indenter as introduced in Chapter 4, as the limitation of

localised measurement shall not affect the results as the collagen hydrogel is highly homogeneous.

5.1.1 Viscoelastic models

In general, viscoelasticity can be categorised into two regimes: linear and nonlinear. Linear viscoelasticity is usually applicable to small deformations where the governing partial differential equation describing the viscoelastic properties can be broken into a set of separate equations with lower dimensionality in both creep and stress responses and can be represented as follows:

$$\varepsilon(t) = \frac{\sigma(t)}{E_{\mathrm{c}}} + \int_0^t C(t-t')\dot{\sigma}(t')\mathrm{d}t' \tag{5.1}$$

or

$$\sigma(t) = E_{\mathrm{r}}\varepsilon(t) + \int_0^t R(t-t')\dot{\varepsilon}(t')\mathrm{d}t' \tag{5.2}$$

where t is time, σ is stress, ε is strain, E_{c} and E_{r} are instantaneous elastic modulus for creep and stress relaxation. As the deformation increases and the material properties changes under deformation, the function is no longer separable, and it enters the nonlinear viscoelastic regime. Since the majority of the materials lie in the linear regime, only the models for linear viscoelasticity will be discussed here.

Several models were used to determine the stress-strain interactions and the temporal dependencies of a viscoelastic material. The core idea of these models is to describe the elastic and viscous component of viscoelasticity as a linear combination of spring and damper elements. Where the spring element stores the energy while

the damper element dissipates energy. The key differences between the various linear viscoelastic models are the number and the combination of these elements, allowing different viscoelastic response to be described. In general, the elastic component (*i.e.* spring) can be modelled as:

$$\sigma = E\varepsilon \tag{5.3}$$

where σ is the stress, E is the spring constant and ε is stress. And the damper can be modelled as:

$$\sigma = \eta\dot{\varepsilon} \tag{5.4}$$

where σ is the stress, η is the viscosity of the damper, and $\dot{\varepsilon}$ is the time derivative of strain [208].

Maxwell model

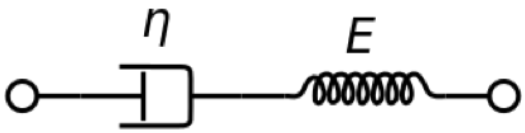

Figure 5.1: Schematic representation of Maxwell model.

Maxwell model is represented by a viscous damper and elastic spring connected in series. In such configuration, each element is subjected to the same stress as the total stress of the system, while total strain of the system is the sum of the strain on the damper and the spring. In the Maxwell model, the time (t) dependent strain-stress (ε-σ) relation can be described as:

$$\frac{1}{E} \cdot \frac{\mathrm{d}\sigma}{\mathrm{d}t} + \frac{\sigma}{\eta} = \frac{\mathrm{d}\varepsilon}{\mathrm{d}t} \tag{5.5}$$

where η is the viscosity of the damper element. The materials described by this model will exhibit gradual stress relaxation under constant strain; hence it predicts the stress relaxation behaviour rather well. However, when the model is subject to constant stress, the strain subjected to the spring element will take effect instantaneously, while the strain subjected to the damper element will exhibit linear increase as long as the stress is applied. Such phenomenon suggests that Maxwell model has limitations in predicting creep behaviours. However, due to its simplicity Maxwell model is still preferred in modelling soft solids, where strain rate can be assumed as a constant.

Voigt model

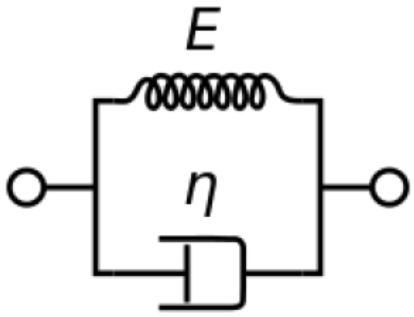

Figure 5.2: Schematic representation of the Voigt model.

Voigt model is represented by an elastic spring element and a viscous damper element connected in parallel. Unlike iso-stress between the elements in the Maxwell model, in the Voigt model, strain for each element is equal to the total strain of the system, while total stress is distributed between two parallel elements. In the Voigt model, the time (t) dependent strain-stress (ε-σ) relation can be described as:

$$\sigma(t) = E\varepsilon(t) + \eta\frac{\mathrm{d}\varepsilon(t)}{\mathrm{d}t} \tag{5.6}$$

Contrary to the Maxwell model, the Voigt model represents a solid under reversible viscoelastic strain. Under constant stress (creep scenario), the strain rate decreases with time as the elastic spring element stores more and more energy. Eventually, the strain will asymptotically approach a steady-state. This model provides a realistic prediction to the creeping behaviours of materials, yet can not achieve satisfactory predictions on the stress relaxation behaviours on materials [218]. Moreover, the model suggests that upon release of stress, the total strain of the material will gradually return to its original state. Hence, the Voigt model is widely adopted for modelling materials such as organic polymers under the loading conditions which does not exceed their elastic limits.

Standard linear solid model

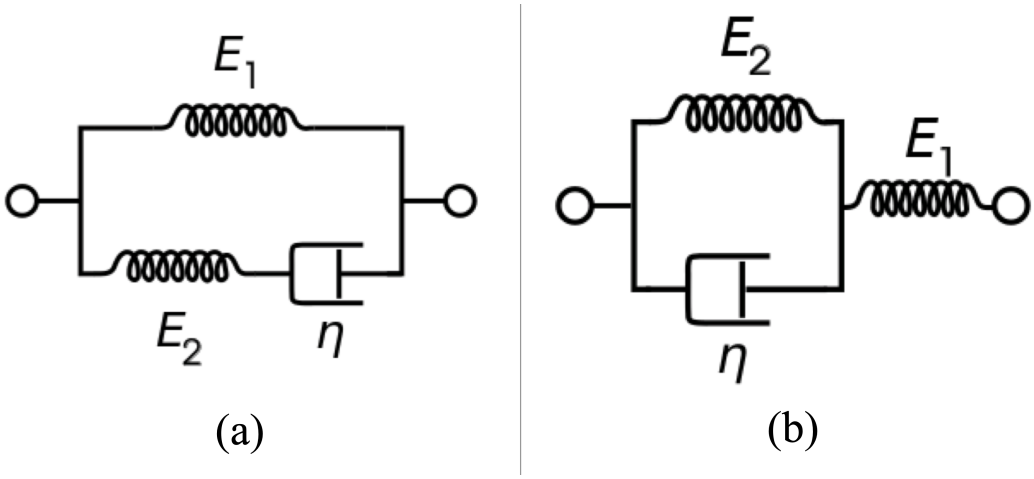

Figure 5.3: Schematic representation of the SLS model. (a) Maxwell representation; (b) Kelvin representation.

As discussed above, the Maxwell model has limitations in describing creep and recovery, and the Voigt model is short of capabilities to predict stress relax-

ation behaviour accurately. Standard linear solid (SLS) model addresses both of the limitations by using two elastic spring element and one viscous damper arranged in both serial and parallel. There are two different representations of the SLS model. Maxwell representation contains an 'arm' resembling the Maxwell model, while Kelvin representation (*i.e.* Kelvin model) contains a component resembling the configuration of a Voigt model. Although there are added complexities in comparison to the two models introduced above, the elements in the SLS model have physical relations as follow:

$$\text{For series elements: } \sigma_{\text{total}} = \sigma_1 = \sigma_2 \text{ and } \varepsilon_{\text{total}} = \varepsilon_1 + \varepsilon_2$$

$$\text{For parallel elements: } \sigma_{\text{total}} = \sigma_1 + \sigma_2 \text{ and } \varepsilon_{\text{total}} = \varepsilon_1 = \varepsilon_2$$

where, σ and ε are stress and strain, respectively, and subscript represents the total and each component. In the SLS model, stress (σ), strain (ε) and their rates of changes with respect to time t are described as follow:

In Maxwell representation:

$$\sigma(t) + \frac{\eta}{E_2} \cdot \frac{\mathrm{d}\sigma(t)}{\mathrm{d}t} = E_1\varepsilon(t) + \frac{\eta(E_1 + E_2)}{E_2} \cdot \frac{\mathrm{d}\varepsilon(t)}{\mathrm{d}t} \tag{5.7}$$

$$\text{with relaxation time } \tau = \frac{\eta}{E_2}$$

In Kelvin model:

$$\sigma(t) + \frac{\eta}{E_1 + E_2} \cdot \frac{\mathrm{d}\sigma(t)}{\mathrm{d}t} = \frac{E_1 E_2}{E_1 + E_2}\varepsilon(t) + \frac{E_1\eta}{E_1 + E_2} \cdot \frac{\mathrm{d}\varepsilon(t)}{\mathrm{d}t} \tag{5.8}$$

$$\text{with relaxation time } \tau = \frac{\eta}{E_2}$$

The SLS model combines the advantages of both Maxwell and Voigt models in accurately describing the material behaviour in various loading scenarios. The application of SLS model is suitable for both creep and stress relaxation analysis, which made it one of the most common viscoelastic models in studying soft and highly hydrated biomaterials [225]. Also, a more general form of the linear viscoelastic model is available by addition of 'Maxwell arms' to the model, enabling it to distribute relaxation times in the model to achieve more realistic relaxation modelling. A study has shown a generalised SLS model (*i.e.* Maxwell-Weichert model) can provide a more accurate representation of the relaxation response than SLS model [2]. However, more calculations are needed to be performed with more unknown parameters, which outweighs the gain of accuracy in characterising viscoelastic properties of collagen hydrogels.

5.1.2 Experimental methods

As one of the aims for characterising the viscoelastic properties of collagen hydrogel is to help improve and calibrate the theoretical model used in the hydrogel-based contraction force measurement technique. The construction of the hydrogel mostly follows the technique described in the previous chapter, where the technique for hydrogel-based contraction force measurement was introduced. Collagen hydrogels were constructed using rat-tail type I collagen (Corning, USA). All components were kept on ice to avoid premature collagen polymerisation. A 1.5 $\mathrm{mg\,ml^{-1}}$ collagen solution was formed by adding the corresponding volume of phosphate buffer saline (PBS) (Sigma, UK) into concentrated collagen solution at 9.33 $\mathrm{mg\,ml^{-1}}$. Subsequently, the collagen solution is neutralised with 1M NaOH solution with the help of phenol red solution as an acid-alkaline indicator. 2 ml of collagen solutions were then transferred into non-culture-coated Petri dish of 35 mm diameter (Eppendorf, Germany) and allowed to polymerise in air incubator at 37 ℃ for 30 mins. Once the

gels are formed, 2 ml of PBS is added to each Petri dish to prevent dehydration of collagen hydrogel and placed back into the incubator for a further 90 mins. Gels were dislodged from the bottom of the Petri dish with a sterile spatula and suspended in the culture medium. The dislodge process allows the hydrogel to swell as well as dissipating the internal stress accumulated during the polymerisation process. Moreover, such process subjects the collagen hydrogel used in the characterisation of viscoelasticity to the same condition as the ones used in the measurement of contraction force.

5.1.3 Analysis

The stress relaxation test is conducted on the nano-biomechanical tester, and the general testing conditions are as previously described in Chapter 4. Several trial experiments were conducted to determine the best testing parameters. The strain of the indentation was set to 0.6 to keep the deformation within the linear viscoelastic regime as well as reducing the accidental puncture of the hydrogel due to high initial strain rate. The relaxation time is set to be 60 seconds, at which point rate of force/stress change, respect to time is negligible as the relaxation approaches a steady state.

The three-parameter standard linear model (*i.e.* SLS model) is used to examine the viscoelastic relaxation response under the constant strain. As described previously, the SLS model consists of a single spring and a Maxwell element in parallel, where the total stress in the model, σ_{total} has the following relation:

$$\sigma_{\text{total}} = \sigma_0 + \sigma_1 \tag{5.9}$$

where σ_0 and σ_1 are the stresses applied to the spring and Maxwell element, respec-

tively. The value of the stresses can also be described as:

$$\sigma_0 = \varepsilon E_0 \tag{5.10}$$

$$\sigma_1 = \varepsilon E_1 exp(\frac{-E_1 t}{\eta}) \tag{5.11}$$

where η is the viscosity of the damper unit. Stress relaxation function $g(t)$ is defined as the ratio between stress at a given time point (σ_t) and the initial stress (σ_0). It is a useful parameter to determine and describe the relaxation properties. By substituting σ_0 and σ_1 into the stress relaxation function, it can be written as:

$$g(t) = A_0 + A_1 exp(\frac{-t}{\tau_1}) \tag{5.12}$$

where the strain-dependent time constant $\tau_1 = \eta/E_1$, describing the time-dependent relationship between the spring and the damper in the Maxwell arm of the SLS model under loads. And A_0 and A_1 are strain-dependent amplitudes, which describes the connections between the two parallel arms of the SLS model. There are no straightforward physical meanings associated with there parameters; however, collectively determines the viscoelastic properties of the material. The connections between these parameters are shown as follows:

$$A_0 = \frac{E_0}{(E_0 + E_1)} \tag{5.13}$$

$$A_1 = \frac{E_1}{(E_0 + E_1)} \tag{5.14}$$

The values of A_0, A_1 and τ_1 are determined using nonlinear regression three-parameter fitting on MatLab (MathsWorks, USA) [2].

5.1.4 Results and discussion

Three parameter fitting

The relations of stresses in different elements of the Maxwell representation of the standard linear solid model can be written as:

$$\sigma(t) = \varepsilon E_0 + \varepsilon E_1 exp(-\frac{tE_1}{\eta}) \tag{5.15}$$

which can be rearranged as:

$$\frac{\sigma(t)}{\varepsilon} = E_0 + E_1 exp(-\frac{tE_1}{\eta}) \tag{5.16}$$

Let $y = \frac{\sigma(t)}{\varepsilon}$; $x = exp(-t)$; $A = E_0$; $B = E_1$; $C = \frac{E_1}{\eta_1}$, the constitutive equation of the model can be described as a power function of $y = A + Bx^C$. The value of A, B and C are determined through nonlinear least-squares of stress relaxation data achieving $R^2 \geq 0.995$, as shown in Figure 5.4.

Stress relaxation of collagen hydrogels

Through nonlinear regression fitting of the standard linear data to the stress relaxation data, the parameters in stress relaxation function for this study is A_0= 0.6411±0.008, A_1= 0.3589±0.008 and τ_1= 3.5224±0.249. Stress relaxation data were normalised for the assessment of the obtained stress relaxation function, as

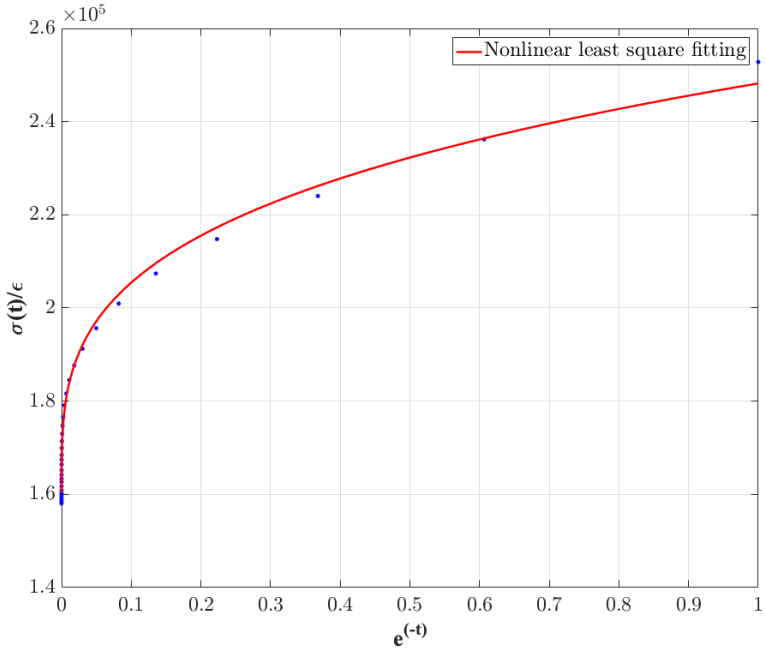

Figure 5.4: Nonlinear least square fitting of the stress relaxation data with constitutive equation in SLS model.

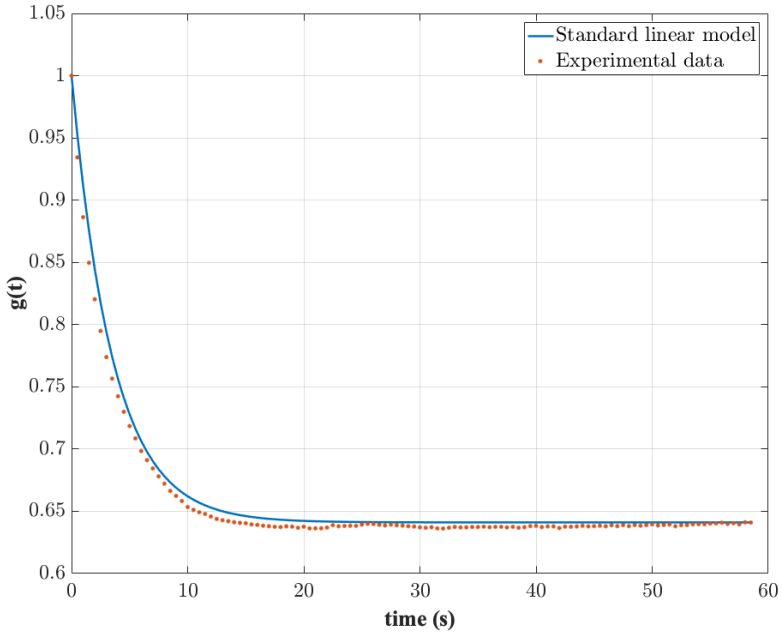

Figure 5.5: Normalised experimental stress-relaxation data fitted by SLS model for 1.5 mg ml^{-1} collagen gel.

demonstrated in Figure 5.5. Collagen hydrogel appeared to exhibit relaxation behaviour consistent with that of viscoelastic materials. The normalised force decreased rapidly but slowly converges and reaching towards a steady state. There is a high degree of correlation between the experimental data and the theoretical prediction, suggesting that the standard linear solid model is adequate in modelling viscoelastic behaviours of collagen hydrogels. In contrast, applications of generalised Maxwell-Weichert model requires more information about the parameters, which are often difficult to be determined. Moreover, it is worth noting that as the cells only take up a negligible volume of the cell-embedded collagen hydrogel, neither contribute nor affect the viscoelastic properties of the hydrogel. Therefore, despite the fact that the characterisation of viscoelastic properties of collagen hydrogel was conducted without the presence of cells, the stress relaxation function, and its parameters remain valid and indicative in help to assess and improve the theoretical model and techniques used in hydrogel-based contraction force measurement.

5.2 Parameter analysis through ABAQUS finite element modelling of Nano-indentation

Introduction

Finite element method is a numerical scheme for modelling and simulating many engineering and scientific problems. It has an extensive range of applications in resolving models aiming to study areas such as engineering structures, contact mechanics, fluid flow, mass transport, and electromagnetic properties. The core concept of FEM is discretisation, where the method divides a subject or a system into a finite number of smaller and simpler parts, hence the name 'finite element'. Such a process is achieved by setting up a mesh of the subject in the finite element

model, specifying a particular discretisation of a system in the spatial domain. The laws of physics related to the spatial and temporal domains of individual elements and their relations with neighbouring elements are usually expressed as partial differential equations (PDEs). The simple equations that govern these elements are assembled mathematically into an augmented matrix of equations that represent the entire system for model solving, with local effects captured and preserved.

Very often, the PDEs applied in the finite elements can not be solved through simple analytical approaches due to the complex nature of the problems and the geometries of the modelling subject. Instead, approximations to these PDEs are created through various discretisation methods. Such methods substitute the PDEs with approximated numerical model equations, which can be solved by numerical means. The solutions to these numerical model equations are a representation of the results of the PDEs. The FEM compute such approximations and employs a variation based methods to output a solution where associated error function in the model is minimised.

Studying or analysing a system, and the practical application of FEM is known as finite element analysis (FEA). Although the finite element methods first came to light in the 1920s, it was not fully applied for practical work until the late 1950s with the development of modern computers. With the ever-increasing computational capabilities, FEA has become an important computational tool for performing engineering analysis. Complex engineering problem can often be categorised into several fundamental physics principles such as Navier-Stokes equation for fluid flow, and Euler-Bernoulli beam equation for solid mechanics, which can be expressed in differential equations, providing the basis of performing FEA. Also, the concept of discretisation of the spatial domain can help in capturing local effects.

Since its first application in bioengineering and biomedical fields in the early

1970s, FEA has been popular in the study of biomedical engineering. In the area of hydrogel biomaterials, FEA has been applied in studies such as manipulating hydrogel swelling [21, 81], hyperelastic deformation [164, 230] and solvent diffusion [28]. The application of FEA is especially suited to the study of hydrogel properties as it offers the ability to predict spatial and temporal variations in stress, strain, and contact area or contact forces. Firstly, it allows evaluation of the changes in designs through model modifications and simulations, which are not easily achieved through ordinary experimental works. Secondly, as a biphasic material, hydrogels have complex structures, which make the determination of the effect of a single isolated physical parameter on the system difficult. In contrast, such objective can be easily achieved by FEA. Thirdly, FEA permits the definition and output of the analyses to be presented in engineer-friendly physical terms (*e.g.* dimensions, various moduli, stresses), which can be directly used in further analysis. Lastly, there are many readily available powerful software packages for 'off the shelf' use, while conducting experiments on hydrogels can lead to extensive material and time costs. The cost effectiveness of the FEA is especially prominent when cell culture is required for studying cell-hydrogel interactions. Although there are many advantages of adopting FEA in studying hydrogel properties, limitations also present. Often, the exercise of engineering judgements is required to interpret the results as FEA is based on seeking the mathematical solution, which does not always lead to the results being physically plausible and feasible. The model building can be labour intensive, especially for the case of modelling super soft hydrogels materials, required many adjustments for yielding a good result. Moreover, nonlinear elastic nature of hydrogel is challeging to model due to the need of applying a suitable hyperelastic material model as well as the amount of constraints and load cases required for the model setup. The added complexity ultimately renders the model unsolvable and lead to non-convergence of the model simulation.

FEA modelling of nano-indentation with a cylindrical flat punch

The study aims to varify the theoretical model developed to determine Young's modulus of the cell embedded hydrogel. Parametric analysis is conducted to determine how each parameter affects the modelling accuracy, as well as testing the validity of the assumptions made on the material properties of the hydrogel (*e.g.* homogeneity, Poisson's ratio) for simplifying the theoretical model.

ABAQUS FEA (Dassault Systemes, France) is used to stimulate the nano-indentation of the collagen hydrogel with a rigid indenter in a 2D axisymmetrical manner. The choice of a axisymmetrical model aims to achieve dimensionality reduction of the model, allowing the contact to be model in 2D, which is comparatively computationally inexpensive. The geometry of the collagen hydrogel and the indenter in the FEA closely represents that used in the measurement of cell contraction force with collagen hydrogels. Thus is it possible to form direct comparisons between the model output and the empirical data acquired from the nano-indentation experiments. The nano-indentation was simulated as linear elastic contact between a rigid cylindrical flat punch ($r = 0.5$mm) and a soft hydrogel disk (35 mm diameter, 2 mm thick) with Young's modulus of 200 Pa and Poisson's ratio ranging from 0.45 to 0.499. Models were executed for up to 0.5 mm displacement (0.25 strain) at uniform rate of 40 μm s^{-1}. The extent and the rate of displacement were chosen to be comparable and inclusive of the pseudo-elastic regime of the force-displacement curve in the empirical studies. At this rate, the effect of the stress relaxation due to the viscoelastic properties of collagen hydrogel is minimised, where the feasibility of indentation testing in respect to experimental time is largely preserved.

The bottom of the gel is fixed in space and the load is applied along the central axis of the rigid indenter, where contact point between the indenter and the gel is set to be on the centre of the gel (shown in Figure 5.6). The geometrical constraint

only allows the top surface of the hydrogel to flex during nano-indentation as well as restricting the movement of the indenter within the vertical direction. The explicit dynamic contract algorism is used in the simulation for computational efficiency and short dynamic response time. Nlgeom (nonlinear geometry) setting was enabled to account for geometric nonlinearity in the simulation. As gel undergoes large deformation to maintain force equilibrium during the nano-indentation process, causing potential nonlinearity in geometry. The reacrion force and contract stress in relation to the indentation depth were extracted for comparison. The density of the FEA mesh was designed to increase with proximity to the contact site in order to capture more localised deformation and stress distribution while minimising the model run time by adapting a coarser mesh in area of less interest (shown in Figure 5.7).

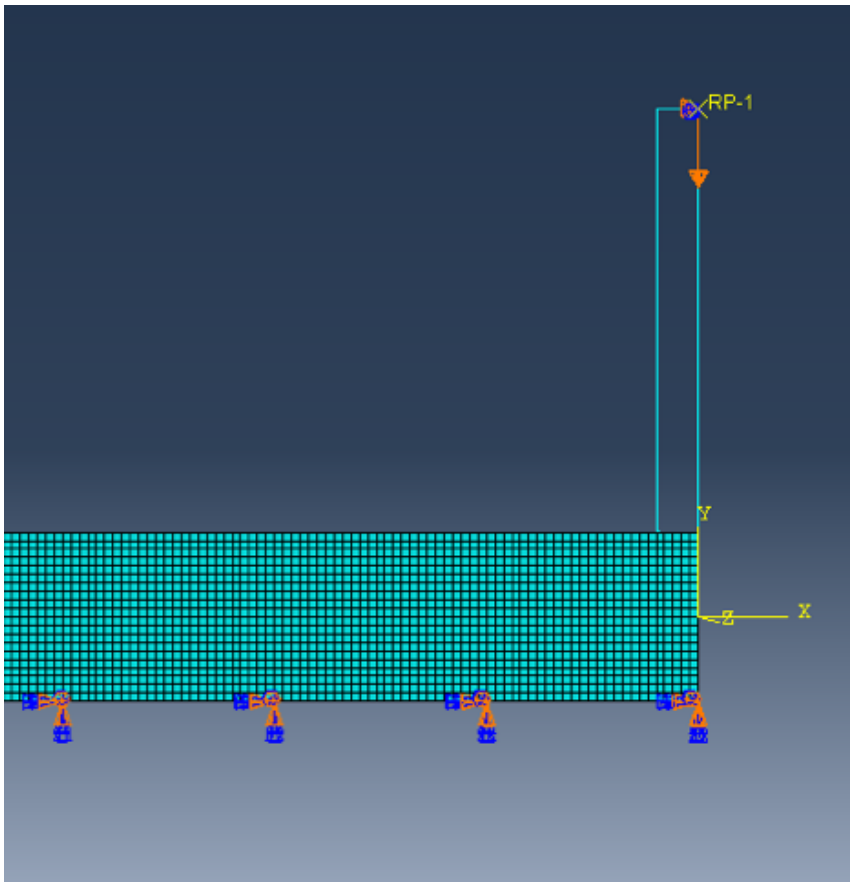

Figure 5.6: Model setup on boundary conditions and force application in FEA.

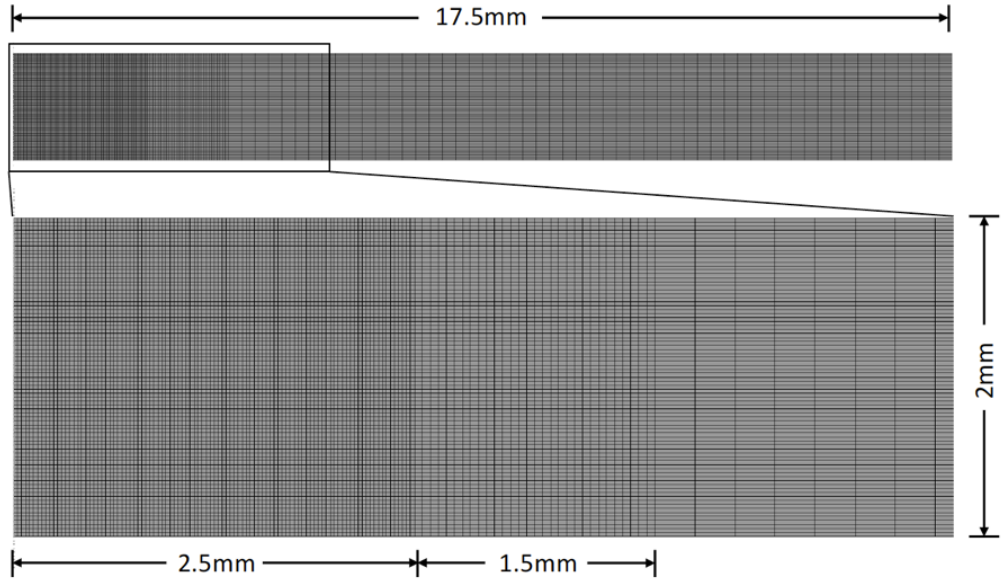

Figure 5.7: Details of the FEA mesh of collagen hydrogel for simulations of nano-indentation. The hydrogel is modelled as a disk such that the entire model has rotational symmetry around the left boundary of the mesh.

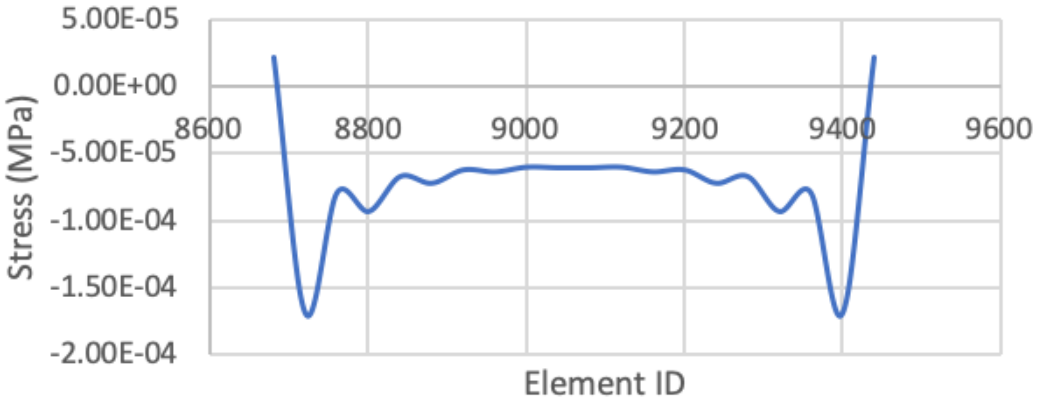

Figure 5.8: FEA simulated contact stress distribution.

Firstly, the distribution of the extracted contact stress on gel elements that are in contact with the indenter, which shown in Figure 5.8. Symmetrical distribution of stress can be observed with concentrated stress at the edge of the indenter. The stress distribution shown in the simulation is inline with the theory of non-adhesive elastic contact between a rigid cylinder with a flat end and an elastic half-space, which pressure distribution is described by Sneddon *et al* [207] as:

$$p(r) = \frac{1}{\pi} E^* \frac{d}{R} (1 - \frac{r^2}{R^2})^{-\frac{1}{2}} \tag{5.17}$$

and the reaction force is described as:

$$F = 2RE^* d \tag{5.18}$$

where, E^* is the reduced modulus of the elastic half-space, R is the radius of the cylinder, r is the radius of the circle which passes a give location on the contact surface, and d is the indentation depth.

Based on the extracted stress distribution and the size of the mesh element, the reaction force is calculated to be 0.05712 mN at the indentation depth of 0.25 mm, where empirical data suggest an average reaction force of 0.05388 mN at same indentation depth. The percentage difference between the FEA result and empirical data is approximately 6%, which suggests that the mesh size and arrangements selected for the FEA simulation fulfil the purpose of representing the nano-indentation testing of the hydrogel.

Also, the simulated changes of reaction force with the increase in the indentation depth is calculated and compared with that suggested by the Hertz contact theory, as shown in Figure 5.9 it can be observed that with small displacements

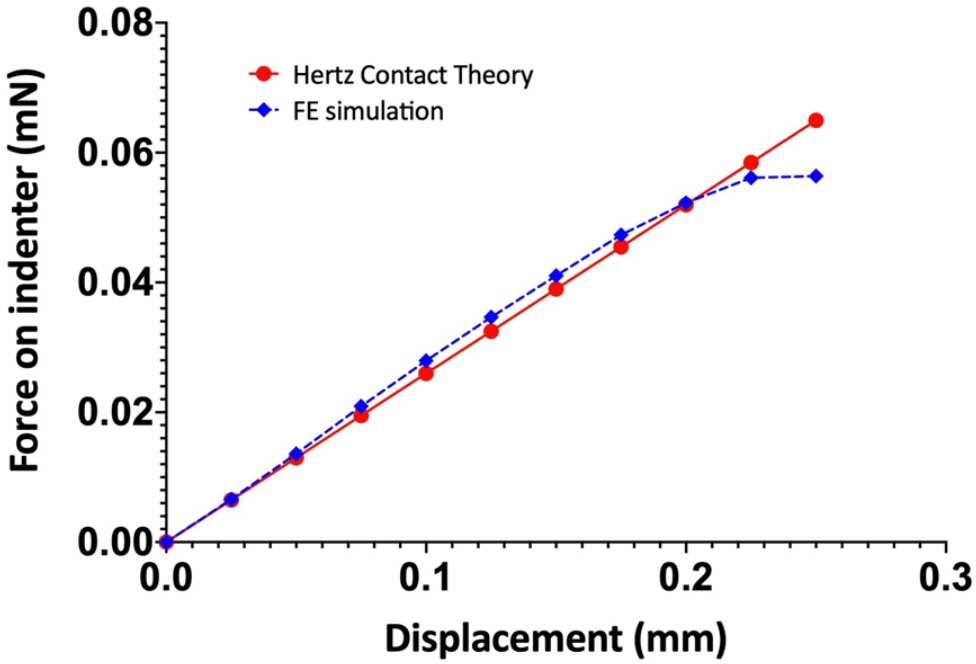

Figure 5.9: The comparison of *F-D* curves between FEA simulation (Poisson's ratio = 0.499) and the Hertz theory.

(strain < 0.1), the stress-strain response from the simulation matches closely (*ca.* 5% difference) with the linear curve predicted by the Hertz contact theory, while as the strain increases beyond 0.1, the curve with simulated results deviates away from linearity and no longer precisely follow the prediction of the Hertz contact theory. The simulation results suggest that, despite the common belief that many hydrogel materials often exhibit nonlinear stress-strain responses, the nano-indentation of the collagen hydrogel is primarily governed by linear deformation at small displacements. Thus, the nano-indentation of the soft hydrogel by using a rigid cylindrical flat punch can be modelled as linearly elastic for a more straightforward calculation in the future. However, a further increase in the displacement will lead to a nonlinear regime of the indentation, where the material nonlinearity must be taken into consideration.

Lastly, several models with varying Poisson's ratios were simulated, and con-

tact stress was extracted, and the reaction force was then calculated. In the displacement range adopted in FEA simulation, the reaction force variation is less than 0.5% between the Poisson's ratio of 0.45 and 0.499, suggesting that it is suitable to model the hydrogel as an incompressible material with a Poisson's ratio of 0.5.

5.3 Influence of different indenter shape on force measurements

As introduced in Chapter 4, the tip of the indenter probe of the bio-nano-indentation tester can adopt various shapes and indeed the shape of the indenter plays an integral part in the measurement of cell contraction force through nano-indentation of cell embedded hydrogel. The current modification of the probe tip as a cylindrical flat punch allows easier modelling of the contact between the probe and the gel sample as the contact area is kept constant throughout the nano-indentation (see Figure 5.10(a)). However, the current indenter shape can lead to concentrated stress on the contact bodies (see Figure 5.8), which is a potential cause of sample rupture, consequently invalid the results and resulting in inaccuracy in estimating the cell contraction force by the novel nano-biomechanical technique. Out of various indenter shapes, spherical indenters (see Figure 5.10(b)) are favoured in the study of material properties of soft biomaterials as many suggested that spherical indenter is more 'friendly' to hydrogel materials especially when cells are embedded, yet the variable contact geometry during the indentation process inevitably lead to greater difficulties in the analysis.

ABAQUS model used in modelling cylindrical flat indenter described in the previous section was modified for the spherical indenter. The rigid cylindrical flat punch is replaced with a rigid shell structure representing a sphere indenter, which has a radius of 0.5 mm. The sphere indenter is fixed in such a way that only verticle

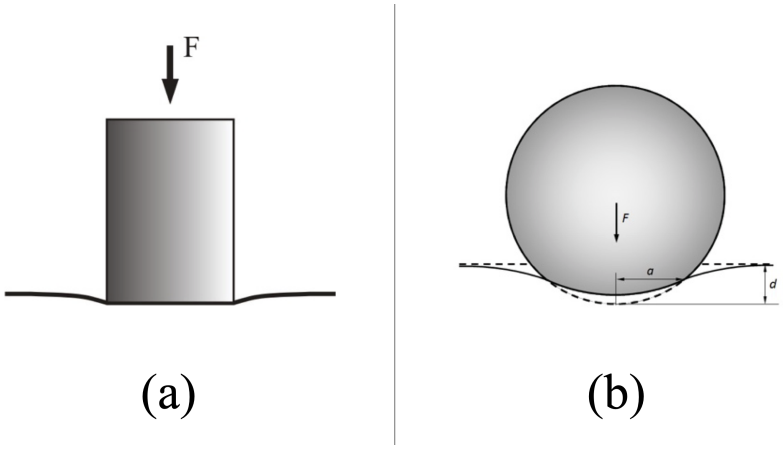

Figure 5.10: (a) Cylindrical flat indenter on elastic half-space. (b) Spherical indenter on elastic half-space.

translation is allowed. The displacement is modelled to be 0.5 mm at the rate of 40 μm s^{-1}, consistent with the simulation parameters specified for that of the cylindrical indenter. All other parameters remain the same to form a comparison between two different types of indenters.

Sample number	**Young's modulus measured (Pa)**	
	Flat punch	**Sphere indenter**
1	65.5834	51.4864
2	76.9889	70.7890
3	78.9091	89.6252
Average	73.8271	70.6335
Standard deviation	7.2	19.07
Difference (%)	4.52%	

Table 5.1: Table showing Young's moduli measured on three different samples with the flat punch and spherical indenter.

As shown, in comparison, cylindrical flat indenter showed a more linear correlation between the reaction force and the displacement. Also, the nonlinear increase observed in the case of spherical indenter corresponds to the increase of the contact area with the displacement. Moreover, the correlation between the reaction force and displacement is preserved to a greater extent in the case of the spherical indenter.

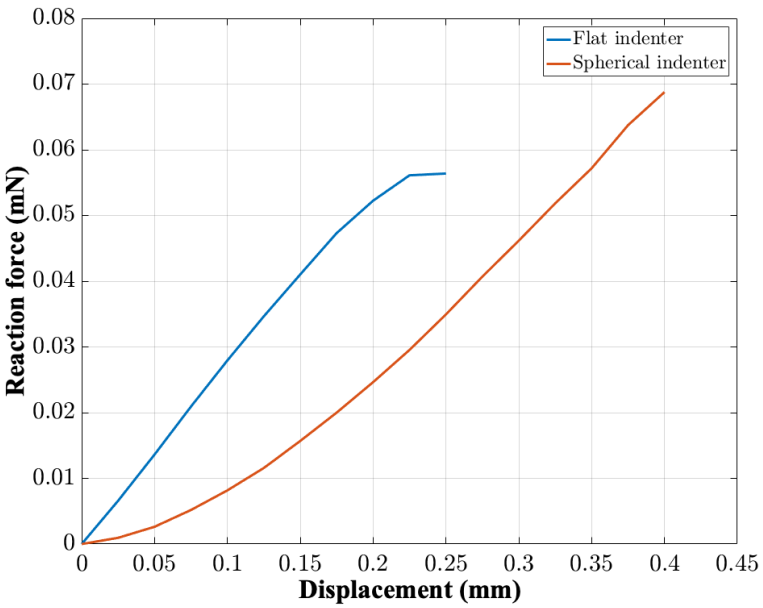

Figure 5.11: Comparison of simulation *F-D* curve between spherical and cylindrical flat indenter.

To verify the difference seen between the cylindrical flat indenter and spherical indenter in the FEA simulation, experiments were conducted with both indenters. Collagen hydrogels with 1.5 $\mathrm{mg\,ml^{-1}}$ concentration were fabricated without embedded cells and indentation rate was set to be 40 $\mu\mathrm{m\,s^{-1}}$, consistent with that adopted in hydrogel-based contraction force measurement technique and Young's modulus was calculated.

It can be seen from Table 5.1 that the variation of Young's moduli of the collagen hydrogel obtained by flat punch and spherical indenter have slight difference yet within the acceptable error margin. Although as suggested by the FEA simulation results that spherical indenter may generate more reliable results in the large deformation regime, the calculation of Young's modulus will become increasingly difficult at large deformation. It becomes especially complicated when taking into consideration of nonlinear elastic effect, which requires alternative constitutive laws to be applied, which adds a certain degree of complexity. In summary, it can be

seen from the results that the flat punch indenter tip is suitable for current methodology of the indentation testing dedicated for measuring the Young's modulus of cell-embedded collagen gel.

Chapter 6

Ageing modulates human dermal fibroblast contractility

Thanks to the development of high precision depth-sensing bio-nano-indentation tester system (see Chapter 4), the material properties (*e.g.* Young's modulus) of soft biomaterials, such as cell-embedded collagen hydrogel can be measured. Also, considering the mechanical behaviours of collagen hydrogel (see Chapter 5), a theoretical model for measuring cell contraction force on cell-embedded collagen hydrogels based on gel elasticity, thickness and radius is established. The contraction forces of normal human dermal fibroblasts (NHDF) derived from young (< 30 years old) and aged (> 60 years old) donors were measured. Transforming growth factor $\beta 1$ (TGF-$\beta 1$) was used to stimulate the fibroblasts to assess their contractile potential. Figure 6.1 shows the graphical summary of the study underwent and the observations made on young and aged fibroblasts in the study through the developed cell contraction measurement technique. The study demonstrates that aged human dermal fibroblasts are more contractile than young cells without stimulation, while young cells are more responsive to the stimulation of TGF-$\beta 1$. Moreover, the study

has shown optimal dermal fibroblast seeding density for adopting the technique in measuring cell contraction force, giving guidance to future studies.

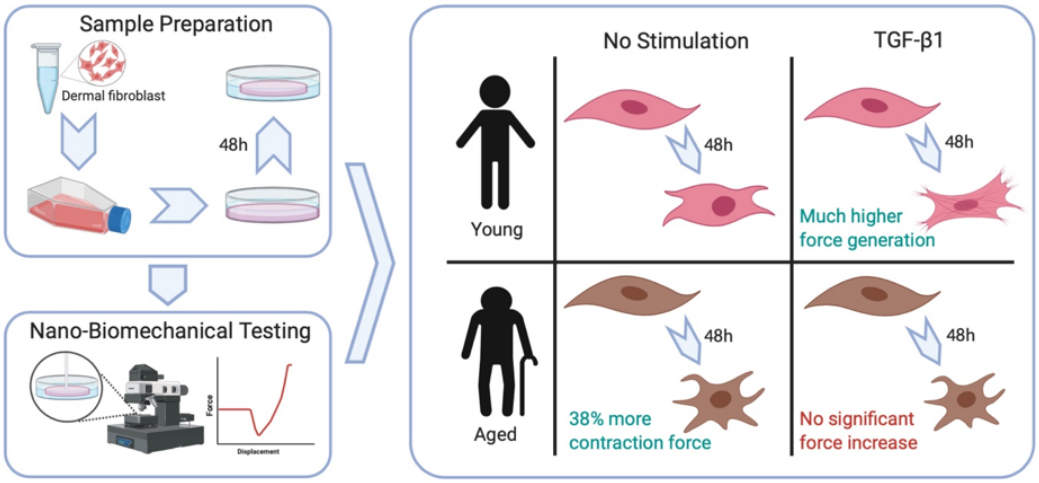

Figure 6.1: Graphical summary of the study on ageing modulated NHDF contractility change.

6.1 Introduction

As introduced in Chapter 2, the skin has a layered structure, within which the dermis provides the majority of structural and mechanical strength to the tissue. Dermal fibroblasts play a vital role in the function of the dermis due to their strong link in ECM function as well as their abilities to proliferate, migrate and respond to cytokines such as TGF-β for myofibroblast differentiation and contraction [31, 233]. Dermal fibroblasts are also at an interest in the study of ageing as the post-mitotic nature dictates the they rarely regenerate, thus accumulate damages and adapt to environmental stresses associated with extrinsic ageing [171].

Dermal fibroblasts contraction is closely related to physiological processes such as wound healing, wrinkling, response to inflammation, angiogenesis and metastasis [131, 182]. Thus, investigating the changes in contractility of dermal fibroblasts

will provide novel insights for skin ageing from biomechanical perspectives and clinical applications of monitoring the impact of ageing.

Several techniques have been developed for *in vitro* studies of cell contraction, which can be briefly categorised based on whether contraction force is measured on a single cell basis or populations of cells. Out of many cell contraction force sensing techniques introduced in Chapter 3, TFM and EMP technique are two well-known single-cell-based approaches [178]. They share the working principle of measuring the deformation of the substrate with known elasticity due to cell contraction. TFM utilises cells cultured on the surface of a 2D substrate and tracks substrate deformation through displacements of embedded fluorescent microbeads (see Section 3.3.2. EMP requires cells to be placed on the tips of microfabricated elastomeric beam array, which degree of pillar deflection will reflect the magnitude of contraction force (see Section 3.3.3). Both techniques are highly quantitative yet inherently neither cell-friendly nor physiological as the contraction is assessed on a 2D surface instead of a 3D biomimetic matrix. The recent introduction of 3D-TFM technique embeds both cells and beads into a deformable matrix and tracks bead movements in 3D with confocal microscopy and optical coherence microscopy [144, 160]. However, such a technique still has shortfalls in resembling *in vivo* conditions as the cell seeding density is usually kept at a very low level to avoid interferences between traction fields of cells, which may hinder their mechanosensing process(see Section 3.3.2).

Techniques for contraction force measurement in populations of cells can mostly provide cells with a biomimetic environment. Among these, collagen gel-based contraction assay (CGCA) is the most prevailing technique as it provides cells with a physiologically relevant 3D matrix environment. However, as indicated in Section 3.3.4, CGCA technique only assesses contractility through gel diameter change without considering the changes in the gel's thickness and stiffness during

contraction. To improve the CGCA technique's quantitativeness, CFM technique was developed by attaching strain gauges on the edge of cell-embedded collagen gel [53]. CFM achieves continuous and direct measurement of cellular contraction force without the influence of varying elasticity of collagen gel. However, the measurement is limited to uniaxial stress as the strain gauges are only capable of measuring contraction force in single directions. Moreover, the attachment of strain gauges to the gel unavoidably compromises cell-friendliness to some extent (see Section 3.3.5).

The novel nano-biomechanical technique based on cell-embedded collagen hydrogel developed in this project offers both quantitativeness and cell-friendliness. The technique accurately measures cell-embedded hydrogels' elasticity through nano-indentation testing on the tailored bio-nano-indentation tester (see Chapter 4) in combination with mathematical modelling [108]. In comparison to TFM and EMP, the technique excels in cell-friendliness and resolved the unidirectional measurement issue associated with CFM, while causing minimal disturbance to the cells.

Moreover, this study investigates the influence of ageing on the contractility of NHDF isolated from young and aged donors' skin. The vast majority of the studies aimed at characterising behavioural change of dermal fibroblasts during ageing have adopted '*in vitro*' models, which have used early and late passage cells as a surrogate for young and aged cells respectively [182]. Such models have yielded insights into the ageing process, however, do not accurately recapitulate chronological ageing and cannot replace studies using cells isolated from young and aged human donors [25], especially in the light of complex ageing mechanisms in the skin arising from both intrinsic physiological and extrinsic environment-related ageing. Employing our novel nano-biomechanical technique, we have studied the contractility of cultured NHDF. The results provide new insights into the baseline contractility of cells from both young and aged individuals, as well as showing the potential decline in responsiveness to human TGF-β1 by the aged NHDF. it has

been demonstrated that the novel technique can differentiate and quantify the altered contractility between the young and aged dermal fibroblasts.

6.2 Materials and methods

6.2.1 Cell culture and preparation for seeding

NHDF cell lines derived from skin biopsies on healthy female individuals with respective age of 20, 26, 29, 62, 68 and 75 were purchased from commercial sources; Caltag Medsystems (Buckingham, UK), Axol Bioscience (Cambridge, UK) and Lonza (Basel, Switzerland). Cells were expanded in low glucose phenol red-free Dulbecco's modified Eagle's medium (DMEM) (Merk, USA) with 10% foetal bovine serum (FBS) (Merk, USA), 2 mM L-glutamine and 1% penicillin/streptomycin at 5% CO_2 and 37 ℃. For all experiments, cells between passage 3 to 5 were used. For comparing contractility at a different age, cell lines were grouped into 'young' ($<$ 30 years old) and 'aged' ($>$ 60 years old) groups resulting in 3 donors per group.

6.2.2 Cell-embedded collagen hydrogel preparation

NHDF were washed with PBS and exposed to 0.05% Trypsin/EDTA for 4 mins and detached from the bottom of culture flasks, quenched with complete media, centrifuged at 1,000 rpm for 5 mins, resuspended with PBS and counted on a haemocytometer.

Hydrogels were made using rat-tail type I collagen (Corning, USA). All materials were kept on ice to avoid premature collagen polymerisation. A hydrogel solution was first made containing 1-part DMEM (10×) (Sigma, USA) and 8-parts collagen with double distilled water. This solution was then neutralised with NaOH

solution before adding 1-part cell suspension in the PBS to give a final collagen concentration of 1.5 mg ml^{-1}. The solution was then transferred into non-culture-coated Petri dishes of 35 mm diameter (Corning, USA) (1.5 ml per dish) and allowed to polymerise in an air incubator at 37 ℃ for 30 mins. Subsequently, 2 ml DMEM containing 1% FBS was added to each dish and then transferred to 5% CO_2 incubators at 37 ℃ for a further polymerisation and swelling of 90 mins. Some dishes were stimulated with the agonist recombinant human TGF-β1 (eBioscience, UK), supplemented into the DMEM at the concentration of 5 ng ml^{-1} [154, 173]. Gels were dislodged from the bottom of the Petri dish with a sterile spatula and suspended in the culture medium, allowing the free contraction of the gel for a further 48 h. Different time protocols were previously trialled for determining the optimal gel incubation time. It was found that 48 h yielded the highest contraction force in comparison, where lower contraction forces were measured with protocols associated with a longer incubation time, as the gel experienced excessive shrinkage. In order to assess the most suitable cell seeding density to measure the cell-embedded gel contraction, densities of 50,000; 100,000 and 200,000 cells ml^{-1} were initially chosen for comparison. Based on the preliminary results, the seeding density of 50,000 cells ml^{-1} was selected for further studies comparing the contractility difference between young and aged dermal fibroblasts.

6.2.3 Measuring Young's modulus and radius change of the cell-embedded hydrogel

The measurement gel's Young's modulus and radius change is achieved by utilising the novel bio-nano-indentation tester as introduced in Chapter 4. Disk-shaped collagen gels were indented at the rate of 40 μm s^{-1} for the entire thickness of the gel, during which, force and displacement data were simultaneously recorded. Collagen gel was removed from the liquid medium and placed in a separate Petri dish.

Samples were kept at 37 ℃ to preserve the functionality of the embedded cells and structural integrity of the gels. Seven evenly spaced diametrical points on the gel were selected for the measurements to be representative to the entire sample. The Young's modulus of the gel is determined by extracting the first 10% of the *F-D* curve and fitting a non-linear strain dependent elasticity model (see Section 6.3). The thickness of the gel was obtained by the differences in the displacements measured between the top surface of the gel and the surface of the Petri dish.

6.3 Theoretical analysis

6.3.1 Young's modulus of cell-embedded hydrogel

As the indenter probe tip has a flat HDPE disk (see Section 4.2.1), the nature of the nano-indentation test is a rigid cylindrical punch indenting a gel which is a flat, incompressible elastic substrate. Hydrogels are generally recognised as hyperelastic materials, which exhibit nonlinear elastic behaviours under large deformation. However, at very low strain, it is predominantly linearly elastic. Thus, we can correlate the modulus with the first 10% of the *F-D* curve based on the following expression derived from the Hertz contract theory [90].

$$E^* = \frac{F}{2rD} \tag{6.1}$$

where E^* is the reduced modulus of the gel, F is the measured force on the force transducer, D is the displacement of the indenter in relative to the gel top surface, and r is the radius of the indenter tip. Also, the Hertz contact model described the reduced modulus in the contract of two elastic bodies as:

$$\frac{1}{E^*} = \frac{1-\nu_g^2}{E_g} + \frac{1-\nu_i^2}{E_i} \tag{6.2}$$

where E is the Young's modulus, and ν is the Poisson's ratio of the contract bodies. The subscripts 'g' and 'i' denote the properties of the gel and indenter, respectively. As the hydrogel is modelled as an incompressible material (*i.e.* Poisson's ratio ν=0.5) and indenter is rigid compared with gel (*i.e.* $E_i \gg E_g$), Equation (6.2) can be simplified as:

$$E^* = \frac{4E_g}{3} \tag{6.3}$$

Furthermore, the gel can exhibit up to 50% diameter reduction during the contraction, where nonlinear elastic behaviour manifests; therefore, the strain-dependent elasticity [219] is employed to describe the nonlinear behaviour:

$$E_g = E_0 \cdot \frac{(1-\bar{\epsilon})^2}{\bar{\epsilon} - \bar{\epsilon}^2 + \frac{\bar{\epsilon}^3}{3}} = F \cdot \frac{3}{8rD} \cdot \frac{(1-\bar{\epsilon})^2}{\bar{\epsilon} - \bar{\epsilon}^2 + \frac{\bar{\epsilon}^3}{3}} \tag{6.4}$$

where $\bar{\epsilon} = D/h_0$ (see the definition of h_0 later) is the engineering strain, and E_0 is Young's modulus of the gel at $\bar{\epsilon} \approx 0$.

It is worth mentioning that the measured Young's modulus of the hydrogel will not be affected by the cross-sectional diameter of the cylindrical indenter as can be seen from Equation (6.1), which shows a linear correlation between the radius of the indenter (r) and the measured reaction force (F). Also, as Young's modulus is a material property, it is independent of the probe size. However, in the very extreme case where an indenter of micro-/nanoscale is used, the intermolecular forces or adhesion may manifest in the measurement. However, such microscopic effects are

beyond the scope of this project.

6.3.2 Measuring contraction force

Due the disk shape of the gel, the contraction force generated by the embedded cells predominantly acts perpendicularly on the circumference surface of the gel and causing the reduction in the gel radius. Based on this a simple model for estimating total contraction force generated by the embedded cells (F_{total}) is developed. As the gel radius reduction is a result of the contraction force generated by the cells, at any given point, the following elastic correlation applies:

$$E = \frac{\mathrm{d}\sigma}{\mathrm{d}\varepsilon} \tag{6.5}$$

where E represents the Young's modulus of the hydrogel, $\mathrm{d}\sigma$ and $\mathrm{d}\varepsilon$ represent the stress and strain caused by the contraction force, respectively. As the contraction force is subjected to the circumference surface of the gel, the following expression on the stress and strain can be obtained:

$$\mathrm{d}\sigma = \frac{\mathrm{d}F_{total}}{2\pi r \cdot h} \tag{6.6}$$

and

$$\mathrm{d}\varepsilon = \frac{\mathrm{d}r}{r} \tag{6.7}$$

where r and h are the radius and thickness of the cell-embedded hydrogel respectively.

Combining equation (6.5), (6.6) and (6.7) we can express the gel Young's modulus at a given stage of the cell contraction as:

$$E = \frac{\mathrm{d}F_{total}}{2\pi \cdot h \cdot \mathrm{d}r} \tag{6.8}$$

Despite the contraction of the gel is predominantly reflected in the reduction of the gel radius, to account for the variations of thickness during the contraction, the average thickness of the gel during the process is used. Rearranging Equation (6.8) and turn into the integration format the total contraction force generated by the embedded cells can be expressed as:

$$F_{total} = \int_{r_1}^{r_0} E \cdot 2\pi \cdot (\frac{h_0 + h_1}{2}) \cdot \mathrm{d}r = \pi \cdot E_g \cdot (h_0 + h_1) \cdot (r_0 - r_1) \tag{6.9}$$

where E_g is measured through fitting the experimental data from bio-nano-indentation testing, as described in Equation (6.4). Subscripts '*0*' and '*1*' denoting their values before and after contraction, where both radius and thickness of the gel is experimentally measured (see Section 4.5). Furthermore, the single-cell contraction force can be calculated as an average of overall contraction force using the cell number (n), shown below:

$$F_{single} = \frac{F_{total}}{n} \tag{6.10}$$

6.4 Results

6.4.1 NHDF contraction force influenced by cell density

The overall and corresponding single-cell contraction forces generated by fibroblasts with seeding densities of 50,000, 100,000 and 200,000 cell ml^{-1} are shown in Figure 6.2. The total contraction forces exhibit a positively correlated increase with cell density. For single-cell contraction forces, two lower seeding densities presented similar values, while statistically significant reduction (*ca.* 26%) was observed in the gels with a high cell seeding density. The results demonstrated a consistent single-cell contraction force value between the samples of two lower cell densities. Such consistency suggests that at a relatively low cell seeding density range ($\leq$ 100,000 cells ml^{-1}), all cells are sufficiently contributing to the overall contraction of the gel. This result also leads to the adaptation of 50,000 cells ml^{-1} seeding density for the study on the contractility of young and aged NHDF. The selected seeding density is also in line with the previous research on the ideal cell seeding density for the study on long-term (more than 24h) contraction force measurement [108].

6.4.2 Contractility difference between young and aged NHDF

Shown in Figure 6.3, in the absence of TGF-β1 treatment, NHDF from young donors shown statistically significant less contractility of approximately 38% compared to those from the aged donors. However, under TGF-β1 (5 ng ml^{-1}) stimulations, higher responses to the agonist treatments have shown by young NHDF. The increased responses are reflected in the significant increase in contraction force. The single-cell contraction force by the TGF-β1 treated young NHDF has shown an increase of 78% while aged counterparts did not significantly change.

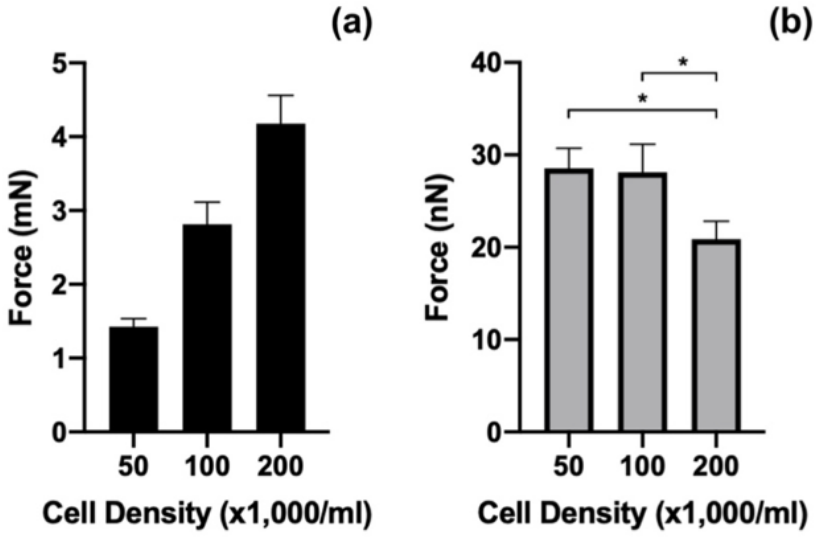

Figure 6.2: Contraction forces generated without TGF-β1 treatment at 10% FBS for three different cell densities. (a) total contraction forces; (b) single-cell contraction forces. Data denote mean ± s.e.m, n = 3 donors, $^{*}P < 0.05$ (one-way ANOVA with Tukeys post-hoc test).

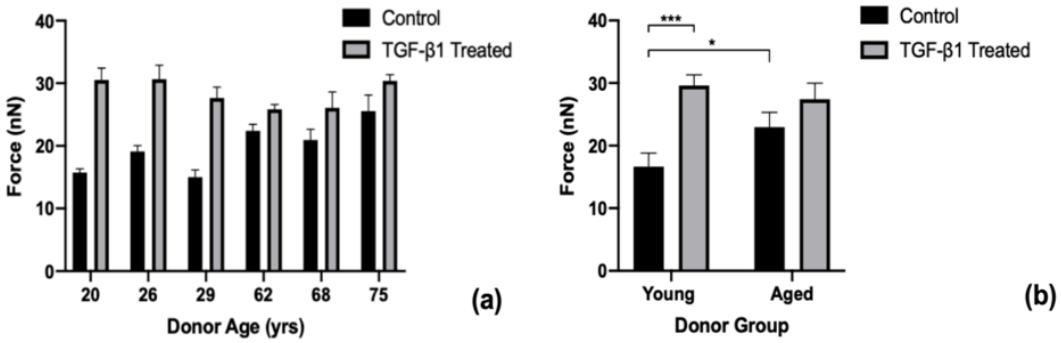

Figure 6.3: Single-cell contraction forces of NHDF from donors of different age with/ without TGF-β1 treatments. (a) forces shown by individual donor; (b) forces grouped by donor age. Data denote mean ± s.e.m, n = 3 donors, $^{*}P < 0.05$, $^{***}P < 0.001$ (two-way ANOVA with Tukeys post-hoc test).

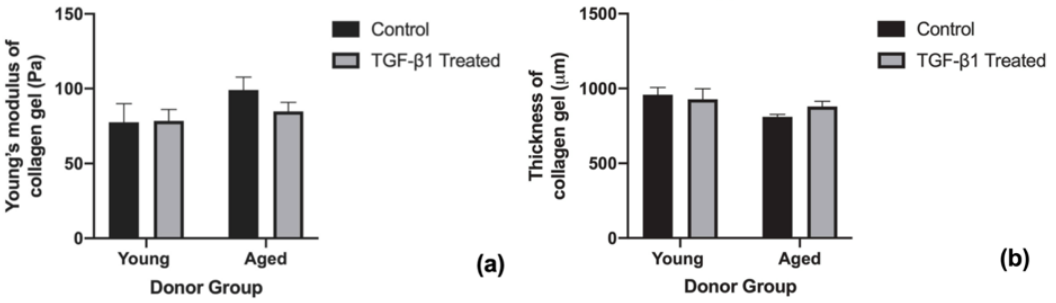

Figure 6.4: Post-contraction hydrogel parameters grouped by donor age. (a) Young's moduli; (b) thickness. Data denotes mean ± s.e.m, n = 3.

6.4.3 Young's modulus and the thickness difference between gels embedded with young and aged NHDF

The Young's moduli and the thickness of the sample gels of different age groups after contraction are shown in Figure 6.4. Young's moduli for the young group were observed slightly lower than those of the aged group (Figure 6.4(a)), although not statistically significant. Meanwhile, thicknesses of the gels are uniform across two age groups (Figure 6.4(b)). The lower Young's moduli of the young donor group suggest higher collagen digestion and matrix remodelling activity undergone by young NHDF. Also, a decrease in Young's moduli in the aged group under TGF-β1 treatment suggests that TGF-β1 may also stimulate collagen digestion in aged NHDF.

6.5 Discussion

The proportionality of the total contraction force shown in Figure 6.2(a) demonstrated the effectiveness of the nano-biomechanical technique in measuring the contraction force of populated cells through the cell-mediated contraction of collagen hydrogel. Also, the similar single-cell contraction force in 50,000 and 100,000 cells ml^{-1} as shown in Figure 6.2(b) suggests that embedded cells underwent minimal prolifer-

ation during the culturing time, providing confidence in adopting initial cell seeding density in the calculating single-cell contraction force (see Equation (6.10)). As outlined in Chapter 1, focal adhesions need to be formed for cells to exert forces onto the collagen matrix, where at high cell seeding density the binding site becomes saturated, resulting in less contraction force generation. Hence, contrary to intuition, single-cell contraction force has shown a reduction at cell seeding density of 200,000 cells ml^{-1}. Brightfield images shown in Figure 6.5 demonstrates the cell's interaction within the gel at different cell seeding densities. Images show that cells had enough space to spread and separate from each other at low and medium seeding densities (50,000 and 100,000 cells ml^{-1}). However, at high density (200,000 cells ml^{-1}), cells are generally aggregated and attached with neighbouring cells, which led to the belief that a significant portion of the contraction force generated by the cells is dissipated through cell-cell adhesion and subsequent cell aggregation. Observations support the near-equal single-cell contraction forces at low and medium densities as the interaction conditions are similar.

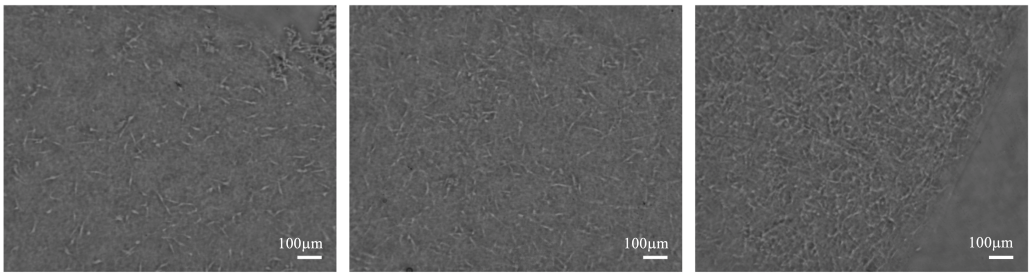

Figure 6.5: Brightfield microscopy images of cell embedded collagen hydrogel at different cell seeing densities.

TGF-β1 is a cytokine associated with wound healing and ageing that can impact on dermal fibroblast function. The effect of TGF-β1 is especially prominent in fibroblast contraction as it initiates fibroblast differentiation towards a myofibroblast phenotype by inducing alpha smooth muscle actin (αSMA) expression [54].

The contractility of fibroblasts under TGF-β1 stimulation is thus an indication of the ability of fibroblasts to engage in normal skin homeostasis.

Previous studies have demonstrated the aged-related decline of fibroblast functions in various aspects related to contractility such as ECM remodelling, migration and protein synthesis, amongst others [71, 138]. The cell contraction force measured (shown in Figure 6.3)) suggest lower basal contractility of young NHDF without agonist stimulation, which would give it a greater ability to respond to agonist before a saturation threshold is reached. Moreover, such findings may suggest the lower tendency of myofibroblast transition in the NHDF population derived from young donors.

Such a transition could result in the reduction of their contribution towards other functions in normal skin maintenance, giving rise to some of the deteriorations observed in ageing skin [15]. Also, the differences between young and aged dermal fibroblasts in the basal contractility and responsiveness of TGF-β1 indicate that young cells are far more adaptive to agonist stimulations and thus possess a higher tissue regeneration capability in comparison to the aged cells. TGF-β1 will increase contraction force generation by increasing the synthesis of actin, fibronectin and matrix receptors [154]. The TGF-β family of molecules have been shown to mediate functional changes in ageing and disease processes [120]. During skin ageing, the ECM undergoes progressive deterioration and fragmentation due to reduced MMP and collagen transcription resulting from diminished TGF-β receptor expression and attenuated TGFβ-1/Smad signalling as previously shown in cultured human dermal fibroblasts [65, 114, 153]. The loss of collagen expression and degradation of ECM can impair the attachment of dermal fibroblasts within the dermis which results in a change in cellular morphology, resulting in smaller cells with less mechanical force [232]. The reduction in TGF-β stimulated contraction force in dermal fibroblasts from aged donors observed in our study is consistent with the literature reports

on ageing-related perturbations in TGF-β receptor-mediated signalling events in the skin [202]. In other words, the TGF-β receptor and the associated signalling pathways will influence the mechanical parameters of fibroblast cells during ageing through affecting the ECM. Yet, no evidence suggests a direct role of the TGF-β receptors dictating the mechanical properties of cells during ageing.

Fibroblasts undergo constant matrix remodelling involving generation and digestion of collagen within the hydrogel. The lower Young's moduli exhibited by gels within the young donor group suggests a lower collagen concentration. Thus, it is evident that young NHDF has shown a higher level of remodelling activities. Comparing the corresponding gel's Young's moduli with or without the presence of TGF-β1 within each group, a trend of Young's moduli reduction can be seen in the aged group after treatment. This observation suggests that TGF-β1 may also stimulate the remodelling behaviour of aged fibroblasts, yet the remodelling activities are still less than the young group.

Comparing the gel thickness between control and TGF-β1 treated samples in each group (Figure 6.4(b)), a slight difference can be seen. However, the difference is small and has minimal effects on contraction force calculations. The fact that hydrogels are disk-shaped (with large diameter/thickness ratio), dislodged and suspended at the first instance after polymerisation, results in the majority of the contraction of hydrogel occurring along the diameter of the gel. In other words, gel radius reduction plays a major role in cell-mediated gel contraction rather than the thickness change. For example, the post-contraction gel thickness (h_1) observed for the treated group is 3% lower than the control group. As can be seen from Equation (6.9), the single-cell contraction force is linearly proportional to the product of the sum of gel thicknesses before and after contraction ($h_0 + h_1$) and the radius reduction ($r_0 - r_1$). The 3% difference in h_1 leads to less than a 1.5% difference in the value of the ($h_0 + h_1$), which is trivial compared to the more than 70% difference in

$(r_0 - r_1)$ as a result of the significant reduction of gel radius.

6.6 Summary

This chapter describes a study that utilises the novel nano-biomechanical technique on cell-embedded collagen hydrogels in combination with mathematical modelling, which can differentiate the contractility of young and aged dermal fibroblasts. The findings validate the novel bio-nano-indentation tester and the developed contraction force measurement technique in accurately measure cell contraction force. The findings also suggest that 50,000 cells ml^{-1} is an optimal seeding density to achieve effective and accurate measurements on dermal fibroblasts through this technique. Lastly, the contractility differences between young and aged dermal fibroblasts identified in this study may represent a potential biomarker of akin ageing.

Chapter 7

Summaries and future work

The contraction force of dermal fibroblasts can be accurately measured using a novel force measurement technique, and the difference in contractility exhibited by young and aged cells was well categorised. The design of the depth-sensing bio-nano-indentation tester and the measurement procedures were described in detail. Moreover, this thesis presented the mathematical models associated with the techniques and their validation through FE simulation. This chapter summarises the key aspects of the project and outlines the advancements made through the developed technique and points out the limitations of the techniques, and recommend future works that can be undertaken to further extend the work in the project.

7.1 Research highlight

In this project, human dermal fibroblast contraction force was measured by applying a novel nano-biomechanical technique on cell-embedded collagen hydrogel in combination with mathematical modelling and numerical simulation. The advancements made in the project can be categorised into the following parts; (1) differentiation of

HNDF contractility isolated from donors with different age, (2) adopting a collagen-based 3D matrix *in vitro* biomimetic contraction model and (3) development of a versatile bio-nano-indentation tester and mathematical model for characterising hydrogel mechanics. They are summarised in the following sections.

7.1.1 Differentiation of contractility of NHDF from donors with different age

The majority of the studies on alterations of cell behaviours in relation to ageing adopt '*in vitro*' ageing models, which assumes the low passage cells as young ones while using high passage cells as a surrogate for aged cells. In this project, NHDFs isolated from dermal tissues of donors of respective ages were used to recapitulate the effects associated with chronological ageing accurately. The study demonstrated that aged HNDF is 38% more contractile than young counterparts in the absence of agonists; however, not significantly responsive to TGF-β1 stimulations as opposed to the 78% increase in contractility for the young NHDF. The diminished contraction force generation following TGF-β1 treatment observed in the aged NHDFs is in line with the overall ageing process of the skin as diminished TGF-β receptor expression and attenuated TGF-β1/Smad signalling is largely related to dermal fibroblasts' function in ECM regulation. Also, the higher contraction force exhibited by aged cells without treatment suggests a higher tendency of myofibroblasts transition within aged dermal tissues. This observation further highlights the advantages of using cells isolated from donors with of different ages instead of adopting conventional '*in vitro*' models. Furthermore, the results demonstrated the possibilities of using dermal fibroblasts contractility as a hallmark of skin ageing.

7.1.2 Adopting a collagen-based 3D matrix *in vitro* biomimetic contraction model

The novel technique developed in the project adopts a contraction model based on a cell embedded 3D collagen matrix, which provides cells with a physiological and biomimetic 3D matrix. As described in Chapter 2, the ageing of dermal fibroblast is often accompanied by the overall deterioration of the dermal structure, resulting in changes in dermal fibroblast functions associated with ageing. Such change is mainly reflected in the generation of matrix proteins and ECM remodelling capabilities, which is not necessarily related to contractility change, yet it is worth considering when constructing an *in vitro* model for contractility study. In other words, collagen hydrogels are advantageous over 3D matrix constructed with other materials (*e.g.* PEG used in 3D TFM) (see Chapter 3), since embedded young and aged dermal fibroblasts can modify the matrix to best mimic the state of their native tissues for exhibiting corresponding levels of focal adhesion and inducing appropriate mechanotransduction. Moreover, the collagen matrix concentration and the cell seeding density most appropriate for mimicking the dermal tissue were studied in the project, upon which 1.5 $\mathrm{mg\,ml^{-1}}$ and 50,000 $\mathrm{cells\,ml^{-1}}$ were adopted as the matrix concentration and cell seeding density for the contraction model, respectively. With a 3D collagen matrix, native behaviours of both young and aged dermal fibroblasts are promoted, hence adding credibility in the study of age modulated contractility change.

7.1.3 Development of versatile bio-nano-indentation tester and mathematical model for characterising hydrogel mechanics

A depth-sensing bio-nano-indentation tester was designed to conduct indentation testing at preprogrammed locations of the gel sample. The tester developed in the

project is advantageous in conducting nano-indentation testing on soft biomaterials (*e.g.* hydrogel) and record their force-displacement response, thanks to its ultra-high resolutions and the ability to systematically characterise the sample (see Chapter 4). To determine the Young's modulus of the hydrogel sample, *F-D* data from the testing is fitted with a mathematical model. It incorporated a nonlinear strain-dependent elasticity model to address the large deformation of the hydrogel during cellular contraction. A Hertz contact model was also factored in for resolving the relations between the displacement of indenter and the measured force during the initial pseudo-linear stage (*i.e.* strain < 0.1) of the indentation for the simplicity of the model. FE analysis on the nano-indentation testing was conducted to validate the assumptions and parameters adopted in formulating the model, which showed that the Hertz contact theory is valid up to 10% strain and the Poisson's ratio can be safely assumed as 0.5 for the collagen matrix used in the technique. Moreover, through further FE simulation of nano-indentation testing with different indenter shape, it was verified that the measured Young's modulus of the hydrogel is independent of the indenter shape. Also, the experiments aimed at characterising the hydrogel's viscoelastic behaviours showed that the parameters used for the testing (*e.g.* indentation speed) are appropriate for the material, giving confidence in the capability of the tester alongside with the mathematical model in characterising hydrogel mechanics.

7.2 Technique limitations

The bio-nano-indentation tester and the mathematical model developed for measuring contraction force offer excellent accuracy and physiologically relevant conclusions to age modulated human dermal fibroblasts contractility change. However, several limitations have been identified to further applying the nano-biomechanical

technique, as listed below:

- Although the tester developed is excellent in many aspects, it cannot be easily reproduced as the tester system's components are from different manufacturers and require extensive instrument testing to coordinate various equipment to achieve the best responsiveness and robustness of the system. However, the tailored bio-nano-indentation tester demonstrated the system's capability and provided a viable design, while is easily transferrable to a specifically designed commercially available model, where functioning components are well-integrated at the hardware level.

- At the current stage, the applications of the tester are limited to soft biomaterials and biological tissues. Although the tester system's force and displacement sensitivity suggest that it can undertake indentation testing at single-cell scale, it is very challenging to modify the current indenter probe tip to suit the needs.

- The current system is unable to conduct prolonged tests ($i.e. > 10$ mins) as the hydrogel samples would be exposed to ambient air during the process, hence, unable to achieve control over humidity and gas content ($e.g.$ CO_2). The current limitation in testing time renders it impossible to adopt significantly lower indentation speed or more testing locations on a single sample without raising reasonable concerns over the change of the gel sample's mechanical properties during testing.

- The model used for calculating cell contraction force in the technique assumes gels to have a perfect concentric contraction. However, as the state of gel contraction results from both the cellular contraction force acting on the matrix and the ability of the matrix to resist deformations, irregular non-concentric contraction of the gel can be seen, though as a rare occurrence. The irregular-

ity in gel contraction invalidates the mathematical model, and the sample can no longer be used to determine contraction force. This limitation may become very pronounced when the number of replications is small.

7.3 Future application and recommendation

In the experimental aspects, the following works can be undertaken:

- The current bio-nano-indentation tester can be further improved. Humidity and gas controlled enclosures are commercially available to be integrated into the current tester system, which allows the testing time to be extended while maintaining the appropriate environmental conditions to preserve the mechanical properties of the hydrogel samples. Also, there is a possibility of substituting the current indentation tester probe with a micromanipulator used in microinjection to achieve indentation testing at the single-cell level, yet such modification envisaged extremely challenging.

- The bio-nano-indentation tester is based on an inverted fluorescence microscope and a CCD camera. This setup gives the possibility of staining the embedded cells and studying mechanotransduction during the contraction by taking time-lapse videos of the process. The force transducer within the tester can be extended from purely sensing the force to applying forces to the sample as a mechanical cue for cell functions, providing an alternative route for the study of cell mechanics in future.

- Laser-confocal microscopy can be utilised to investigate the cell-cell and cell-matrix interactions within the cell-embedded collagen hydrogel and gather visual evidence in the variation of contractility possessed by different cell types through observing aggregation of the cytoskeleton.

- The collagen cell contraction assay can be fabricated through 3D Bio-printing, capable of producing tailored structures within the biomimetic 3D matrix with appropriate cell populations. Compared to the current collagen assay, the 3D printed tissue-equivalent will be a significant leap in advancing the technique as it will ultimately represent the conditions of native tissues and promotes cellular behaviours the closest to *in vivo* conditions. Moreover, the customizability of 3D bioprinting has the potential of replicating pathological tissues, which could be the next advancement in study cell contractility in aged tissues.

- Soft hydrogel is an attractive material for mimicking natural ECM. However, the methodology can be further improved with bioactive modification to better address the biochemical composition of various tissue at different physiological and pathological states. As reviewed by Zhu *et al* [255], short peptide chains derived from ECM proteins such as laminin and fibronectin are among the popular choices. A broad range of potential studies can be conducted by combining bioactive modification of the soft hydrogel matrix with the technique developed in this project. For example, the cell-embedded hydrogel can be bio-actively modified to change the state of cross-linking according to the morphology or the physiological state of the embedded cells. The change of cross-linking form of the hydrogel will inherently alter the mechanical properties of the hydrogel, which is measurable with the bio-nano-indentation tester. Through such an approach, qualitative changes (*e.g.* morphological or physiological changes) can be quantified.

In the aspect of theoretical analysis and mathematical modelling of the nano-indentation testing of soft biomaterials, the potential future work is as following:

- A new model for describing the cell-mediated gel contraction addressing the

collagen matrix's irregular contraction can be formulated. The new, improved model shall adopt a concept of 'discrete element' and divide the hydrogel into different elements with a smaller volume. With fluorescent markers placed on the gel, it is possible to resolve the geometrical change in individual gel elements. Through the geometrical change and the spatial relations between each gel element, combined with Young's moduli measured, the improved model can better recapitulate the variation of the hydrogel contraction and estimating contraction force in the scenario where the gel contraction is irregular.

- The current FE analysis on the nano-indentation testing on collagen hydrogel is based on a linear elastic model, as the strain does not exceed the pseudo-elastic regime for the given material. However, soft biomaterials often exhibit nonlinearly elastic behaviours, where hyperelasticity manifests. To add technique's versatility in estimating mechanical properties of other soft biomaterial, finite element analysis of hyperelastic materials can be conducted. The soft biomaterial can be modelled by applying an incompressive hyperelastic constitutive model such as the Mooney-Rivlin model [187] or the Arruda-Boyce model [6].

Bibliography

[1] Ahearne, M. Introduction to cell-hydrogel mechanosensing. *Interface focus 4* (2014), 20130038.

[2] Ahearne, M., Siamantouras, E., Yang, Y., and Liu, K.-K. Mechanical characterization of biomimetic membranes by micro-shaft poking. *Journal of the Royal Society, Interface*, 6 (2009), 471–478.

[3] Ahearne, M., Wilson, S. L., Liu, K.-K., Rauz, S., El Haj, A. J., and Yang, Y. Influence of cell and collagen concentration on the cell-matrix mechanical relationship in a corneal stroma wound healing model. *Experimental Eye Research 91*, 5 (2010), 584–591.

[4] Ahearne, M., Yang, Y., El Haj, A. J., Then, K. Y., and Liu, K.-K. Characterizing the viscoelastic properties of thin hydrogel-based constructs for tissue engineering applications. *Journal of the Royal Society, Interface 2*, 5 (2005), 455–463.

[5] Al Anouti, F., Taha, Z., Shamim, S., Khalaf, K., Al Kaabi, L., and Alsafar, H. An insight into the paradigms of osteoporosis: From genetics to biomechanics. *Bone Reports 11* (2019), 100216.

[6] Arruda, E. M., and Boyce, M. C. A three-dimensional constitutive model for the large stretch behavior of rubber elastic materials. *Journal of the Mechanics and Physics of Solids 41*, 2 (1993), 389–412.

[7] Asgari, M., Latifi, N., Heris, H. K., Vali, H., and Mongeau, L. In vitro fibrillogenesis of tropocollagen type III in collagen type i affects its relative fibrillar topology and mechanics. *Scientific Reports 7*, 1 (2017), 1392.

[8] Ashkin, A., and Dziedzic, J. M. Optical trapping and manipulation of viruses and bacteria. *Science 235*, 4795 (1987), 1517–1520.

[9] Aunan, J. R., Watson, M. M., Hagland, H. R., and Søreide, K. Molecular and biological hallmarks of ageing. *British Journal of Surgery 103*, 2 (2016), 29–46.

[10] Aurora Scientific. Instruction Manual Model 400A, 402A, 403A, 404A, 405A, 406A, 407A Force Transducer Systems, 2004.

[11] Banerjee, A., Arha, M., Choudhary, S., Ashton, R. S., Bhatia, S. R., Schaffer, D. V., and Kane, R. S. The influence of hydrogel modulus on the proliferation and differentiation of encapsulated neural stem cells. *Biomaterials 30*, 27 (2009), 4695–4699.

[12] Bansal, N. P., and Doremus, R. H. *Handbook of Glass Properties*. Academic Press handbook series Handbook of glass properties. Elsevier Science, 2013.

[13] Bao, G., and Suresh, S. Cell and molecular mechanics of biological materials. *Nature materials 2*, 11 (2003), 715–725.

[14] Bárány, M. ATPase activity of myosin correlated with speed of muscle shortening. *The Journal of general physiology 50*, 6 (1967), 197–218.

[15] Baum, J., and Duffy, H. S. Fibroblasts and myofibroblasts: What are we talking about? *Jounal of Cardiovascular Pharmacology 57*, 4 (2011), 376–379.

[16] Baylis, D., Bartlett, D. B., Patel, H. P., and Roberts, H. C. Understanding how we age: insights into inflammaging. *Longevity & Healthspan 2*, 8 (2013).

[17] Behring, J., Junker, R., Walboomers, X. F., Chessnut, B., and Jansen, J. A. Toward guided tissue and bone regeneration: Morphology, attachment, proliferation, and migration of cells cultured on collagen barrier membranes. A systematic review. *Odontology 96*, 1 (2008), 1–11.

[18] Bell, E., Ivarsson, B., and Merrill, C. Production of a tissue-like structure by contraction of collagen lattices by human fibroblasts of different proliferative potential in vitro. *Proceedings of the National Academy of Sciences of the United States of America 76*, 3 (1979), 1274–1278.

[19] Beningo, K. A., Dembo, M., Kaverina, I., Small, J. V., and Wang, Y. L. Nascent focal adhesions are responsible for the generation of strong propulsive forces in migrating fibroblasts. *Journal of Cell Biology 153*, 4 (2001), 881–888.

[20] Binnig, G., Quate, C. F., and Gerber, C. Atomic force microscope. *Physical Review Letters 56*, 9 (1986), 930–933.

[21] Blanco, A., González, G., Casanova, E., Pirela, M. E., and Briceño, A. Mathematical modeling of hydrogels swelling based on the finite element method. *Applied Mathematics 4*, 8 (2013), 161–170.

[22] Block, S. M., Asbury, C. L., Shaevitz, J. W., and Lang, M. J. Probing the kinesin reaction cycle with a 2D optical force clamp. *Proceedings of the National Academy of Sciences of the United States of America 100*, 5 (2003), 2351–2356.

[23] Bloom, R. J., George, J. P., Celedon, A., Sun, S. X., and Wirtz, D. Mapping local matrix remodeling induced by a migrating tumor cell using three-dimensional multiple-particle tracking. *Biophysical journal 95*, 8 (2008), 4077–4088.

[24] Bonnans, C., Chou, J., and Werb, Z. Remodelling the extracellular matrix in development and disease. *Nature Reviews Molecular Cell Biology 15* (2014), 786–801.

[25] Boraldi, F., Annovi, G., Tiozzo, R., Sommer, P., and Quaglino, D. Comparison of ex vivo and in vitro human fibroblast ageing models. *Mechanisms of Ageing and Development 131*, 10 (2010), 625–635.

[26] Boraldi, F., Bini, L., Liberatori, S., Armini, A., Pallini, V., Tiozzo, R., Pasquali-Ronchetti, I., and Quaglino, D. Proteome analysis of dermal fibroblasts cultured in vitro from human healthy subjects of different ages. *Proteomics 3*, 6 (2003), 917–929.

[27] Boudou, T., Legant, W. R., Mu, A., Borochin, M. A., Thavandiran, N., Radisic, M., Zandstra, P. W., Epstein, J. A., Margulies, K. B., and Chen, C. S. A microfabricated platform to measure and manipulate the mechanics of engineered cardiac microtissues. *Tissue Engineering - Part A 18*, 19-10 (2012), 910–919.

[28] Bouklas, N., Landis, C. M., and Huang, R. A nonlinear, transient finite element method for coupled solvent diffusion and large deformation of hydrogels. *Journal of the Mechanics and Physics of Solids 79*, 1 (2015), 21–43.

[29] Breitenbach, J. S., Rinnerthaler, M., Trost, A., Weber, M., Klausegger, A., Gruber, C., Bruckner, D., Reitsamer, H. A., Bauer, J. W., and Breitenbach, M. Transcriptome and ultrastructural

changes in dystrophic Epidermolysis bullosa resemble skin aging. *Aging 7*, 6 (2015), 389–411.

[30] Brennan, M., Bhatti, H., Nerusu, K. C., Bhagavathula, N., Kang, S., Fisher, G. J., Varani, J., and Voorhees, J. J. Matrix metalloproteinase-1 is the major collagenolytic enzyme responsible for collagen damage in UV-irradiated human skin. *Photochemistry and Photobiology 78*, 1 (2003), 43–48.

[31] Brun, C., Jean-Louis, F., Oddos, T., Bagot, M., Bensussan, A., and Michel, L. Phenotypic and functional changes in dermal primary fibroblasts isolated from intrinsically aged human skin. *Experimental Dermatology 25*, 2 (2016), 113–119.

[32] Buehler, M. J. Mechanical players - The role of intermediate filaments in cell mechanics and organization. *Biophysical Journal 105*, 8 (2013), 1733–1734.

[33] Burgeson, R. E., and Christiano, A. M. The dermal-epidermal junction. *Current Opinion in Cell Biology 9*, 5 (1997), 651–658.

[34] Burridge, K., and Wittchen, E. S. The tension mounts: Stress fibers as force-generating mechanotransducers. *Journal of Cell Biology 200*, 1 (2013), 9–19.

[35] Butt, H. J., Cappella, B., and Kappl, M. Force measurements with the atomic force microscope: Technique, interpretation and applications. *Surface Science Reports 59*, 1-6 (2005), 1–152.

[36] Campbell, B. H., Clark, W. W., and Wang, J. H. A multi-station culture force monitor system to study cellular contractility. *Journal of Biomechanics 36*, 1 (2003), 137–140.

[37] Chandeck, C., and Mooi, W. J. Oncogene-induced cellular senescence. *Advances in Anatomic Pathology 17*, 1 (2010), 42–48.

[38] Chen, J. L., Duan, L., Zhu, W., Xiong, J., and Wang, D. Extracellular matrix production in vitro in cartilage tissue engineering. *Journal of Translational Medicine 12*, 88 (2014).

[39] Chen, X., Li, Z., Feng, Z., Wang, J., Ouyang, C., Liu, W., Fu, B., Cai, G., Wu, C., Wei, R., Wu, D., and Hong, Q. Integrin-linked kinase induces both senescence-associated alterations and extracellular fibronectin assembly in aging cardiac fibroblasts. *Journals of Gerontology - Series A Biological Sciences and Medical Sciences 61*, 12 (2006), 1232–1245.

[40] Chen, X. Y., Huang, Y. X., jing Liu, W., and jian Yuan, Z. Membrane surface charge and morphological and mechanical properties of young and old erythrocytes. *Current Applied Physics 7*, Supplement 1 (2007), e94–e96.

[41] Cheng, L., Xia, X., Scriven, L. E., and Gerberich, W. W. Spherical-tip indentation of viscoelastic material. *Mechanics of Materials 37*, 1 (2005), 213–226.

[42] Childs, B. G., Durik, M., Baker, D. J., and Van Deursen, J. M. Cellular senescence in aging and age-related disease: From mechanisms to therapy. *Nature Medicine 21*, 12 (2015), 1424–1435.

[43] Cohen, Y., Ramon, O., Kopelman, I. J., and Mizrahi, S. Characterization of inhomogeneous polyacrylamide hydrogels. *Journal of Polymer Science Part B: Polymer Physics 30*, 9 (1992), 1055–1067.

[44] Cole, M. A., Quan, T., Voorhees, J. J., and Fisher, G. J. Extracellular matrix regulation of fibroblast function: redefining our perspective on skin aging. *Journal of Cell Communication and Signaling 12*, 1 (2018), 35–43.

[45] Collinsworth, A. M., Zhang, S., Kraus, W. E., and Truskey, G. A. Apparent elastic modulus and hysteresis of skeletal muscle cells throughout differentiation. *American Journal of Physiology - Cell Physiology 283*, 4 (2002), C1219–1227.

[46] Coppé, J. P., Desprez, P. Y., Krtolica, A., and Campisi, J. The senescence-associated secretory phenotype: The dark side of tumor suppression. *Annual Review of Pathology: Mechanisms of Disease 5*, 1 (2010), 99–118.

[47] Cukierman, E., Pankov, R., Stevens, D. R., and Yamada, K. M. Taking cell-matrix adhesions to the third dimension. *Science 294*, 5547 (2001), 1708–1712.

[48] Curtze, S., Dembo, M., Miron, M., and Jones, D. B. Dynamic changes in traction forces with DC electric field in osteoblast-like cells. *Journal of Cell Science 117*, 1 (2004), 2721–2729.

[49] Davalli, P., Mitic, T., Caporali, A., Lauriola, A., and D'Arca, D. ROS, cell senescence, and novel molecular mechanisms in aging and age-related diseases. *Oxidative Medicine and Cellular Longevity 2016* (2016), 3565127.

[50] De Cecco, M., Criscione, S. W., Peckham, E. J., Hillenmeyer, S., Hamm, E. A., Manivannan, J., Peterson, A. L., Kreiling, J. A., Neretti, N., and Sedivy, J. M. Genomes of replicatively senescent cells undergo global epigenetic changes leading to gene silencing and activation of transposable elements. *Aging Cell 12*, 2 (2013), 247–256.

[51] De Forges, H., Bouissou, A., and Perez, F. Interplay between microtubule dynamics and intracellular organization. *International Journal of Biochemistry and Cell Biology 44*, 2 (2012), 266–274.

[52] De La Cruz, E. M., and Gardel, M. L. Actin mechanics and fragmentation. *Journal of Biological Chemistry 290*, 28 (2015), 17137–17144.

[53] Delvoye, P., Wiliquet, P., Levêque, J. L., Nusgens, B. V., and Lapière, C. M. Measurement of mechanical forces generated by skin fibroblasts embedded in a three-dimensional collagen gel. *Journal of Investigative Dermatology 97*, 5 (1991), 898–902.

[54] Desmoulière, A., Geinoz, A., Gabbiani, F., and Gabbiani, G. Transforming growth factor-beta 1 induces alpha-smooth muscle actin expression in granulation tissue myofibroblasts and in quiescent and growing cultured fibroblasts. *The Journal of cell biology 122*, 1 (1993), 103–111.

[55] Discher, D. E., Janmey, P., and Wang, Y. L. Tissue cells feel and respond to the stiffness of their substrate. *Science 310*, 5751 (2005), 1139–1143.

[56] Doyle, A. D., and Lee, J. Cyclic changes in keratocyte speed and traction stress arise from Ca2+-dependent regulation of cell adhesiveness. *Journal of Cell Science 118*, 2 (2005), 369–379.

[57] Du Roure, O., Saez, A., Buguin, A., Austin, R. H., Chavrier, P., Siberzan, P., and Ladoux, B. Force mapping in epithelial cell migration. *Proceedings of the National Academy of Sciences of the United States of America 102*, 7 (2005), 2390–2395.

[58] Dufrêne, Y. F., and Pelling, A. E. Force nanoscopy of cell mechanics and cell adhesion. *Nanoscale 5*, 10 (2013), 4094–4104.

[59] Dulińska-Molak, I., Pasikowska, M., Pogoda, K., Lewandowska, M., Eris, I., and Lekka, M. Age-related changes in the mechanical properties of human fibroblasts and its prospective reversal after anti-wrinkle tripeptide treatment. *International Journal of Peptide Research and Therapeutics 20*, 1 (2014), 77–85.

[60] Eastwood, M., McGrouther, D. A., and Brown, R. A. A culture force monitor for measurement of contraction forces generated in human dermal fibroblast cultures: evidence for cell-matrix mechanical signalling. *BBA - General Subjects 1201*, 2 (1994), 186–192.

[61] Ehrlich, H. P., and Rajaratnam, J. B. Cell locomotion forces versus cell contraction forces for collagen lattice contraction: An in vitro model of wound contraction. *Tissue and Cell 22*, 4 (1990), 407–417.

[62] Ewoldt, R. H., Hosoi, A. E., and McKinley, G. H. Nonlinear viscoelastic biomaterials: Meaningful characterization and engineering inspiration. *Integrative and Comparative Biology 49*, 1 (2009), 40–50.

[63] Farage, M. A., Miller, K. W., and Maibach, H. I. *Textbook of aging skin*. Springer Berlin Heidelberg, 2010.

[64] Fenix, A. M., Taneja, N., Buttler, C. A., Lewis, J., Van Engelenburg, S. B., Ohi, R., and Burnette, D. T. Expansion and concatenation of nonmuscle myosin IIA filaments drive cellular contractile system formation during interphase and mitosis. *Molecular Biology of the Cell 27*, 9 (2016), 1465–1478.

[65] Feru, J., Delobbe, E., Ramont, L., Brassart, B., Terryn, C., Dupont-Deshorgue, A., Garbar, C., Monboisse, J. C., Maquart, F. X., and Brassart-Pasco, S. Aging decreases collagen IV expression in vivo in the dermo-epidermal junction and in vitro in dermal fibroblasts: Possible involvement of TGF-β1. *European Journal of Dermatology 26*, 4 (2016), 350–360.

[66] Fisher, G. J., Datta, S. C., Talwar, H. S., Wang, Z. Q., Varani, J., Kang, S., and Voorhees, J. J. Molecular basis of sun-induced premature skin ageing and retinoid antagonism. *Nature 379*, 6563 (1996), 335–339.

[67] Fitts, R. H. The cross-bridge cycle and skeletal muscle fatigue. *Journal of Applied Physiology 104*, 2 (2008), 551–558.

[68] Fletcher, D. A., and Mullins, R. D. Cell mechanics and the cytoskeleton. *Nature 463*, 1 (2010), 485–492.

[69] Franceschi, C., Bonafè, M., Valensin, S., Olivieri, F., De Luca, M., Ottaviani, E., and De Benedictis, G. Inflamm-aging. An evolutionary perspective on immunosenescence. *Annals of the New York Academy of Sciences 908* (2000), 244–254.

[70] Fratzl, P. *Collagen: Structure and mechanics*. Springer US, 2008.

[71] Fujimura, T., Hotta, M., Kitahara, T., and Takema, Y. Loss of contraction force in dermal fibroblasts with aging due to decreases in myosin light chain phosphorylation enzymes. *Archives of Pharmacal Research 34*, 6 (2011), 1015–1022.

[72] Ghassemi, S., Meacci, G., Liu, S., Gondarenko, A. A., Mathur, A., Roca-Cusachs, P., Sheetz, M. P., and Hone, J. Cells test substrate rigidity by local contractions on submicrometer pillars. *Proceedings of the National Academy of Sciences of the United States of America 109*, 14 (2012), 5328–5333.

[73] Gieni, R. S., and Hendzel, M. J. Mechanotransduction from the ECM to the genome: Are the pieces now in place? *Journal of Cellular Biochemistry 104*, 6 (2008), 1964–1987.

[74] Gimbrone, M. A., Topper, J. N., Nagel, T., Anderson, K. R., and Garcia-Cardena, G. Endothelial dysfunction, hemodynamic forces, and atherogenesisa. *Annals of the New York Academy of Sciences 902* (2006), 230–239.

[75] Goldman, R. D., Goldman, A. E., Green, K. J., Jones, J. C., Jones, S. M., and Yang, H. Y. Intermediate filament networks: organization and possible functions of a diverse group of cytoskeletal elements. *Journal of cell science. Supplement 1986* (1986), 69–97.

[76] Greco, M., Villani, G., Mazzucchelli, F., Bresolin, N., Papa, S., and Attardi, G. Marked aging-related decline in efficiency of oxidative phosphorylation in human skin fibroblasts. *The FASEB journal 17*, 12 (2003), 1706–1708.

[77] Grier, D. G. A revolution in optical manipulation. *Nature 424* (2003), 810–816.

[78] Grönniger, E., Weber, B., Heil, O., Peters, N., Stäb, F., Wenck, H., Korn, B., Winnefeld, M., and Lyko, F. Aging and chronic sun exposure cause distinct epigenetic changes in human skin. *PLoS Genetics 6*, 5 (2010), e1000971.

[79] Gu, M., Kuriakose, S., and Gan, X. A single beam near-field laser trap for optical stretching, folding and rotation of erythrocytes. *Optics Express 15*, 3 (2007), 1369–1375.

[80] Guck, J., Schinkinger, S., Lincoln, B., Wottawah, F., Ebert, S., Romeyke, M., Lenz, D., Erickson, H. M., Ananthakrishnan, R., Mitchell, D., Kas, J., Ulvick, S., and Bilby, C. Optical deformability as an inherent cell marker for testing malignant transformation and metastatic competence. *Biophysical Journal 88*, 5 (2005), 3689–3698.

[81] Han, T., Wei, M., Wang, C., Wen, M., Chang, S., Huang, W., and Ti, N. Manipulating the deformation of swelling hydrogel models by microparticles. *Multiscale Science and Engineering 2* (2020), 107–113.

[82] Harman, D. The Biologic Clock: The Mitochondria? *Journal of the American Geriatrics Society 20*, 4 (1972), 145–147.

[83] Harris, A. K., Stopak, D., and Wild, P. Fibroblast traction as a mechanism for collagen morphogenesis. *Nature 290* (1981), 249–251.

[84] Harris, A. K., Wild, P., and Stopak, D. Silicone rubber substrata: A new wrinkle in the study of cell locomotion. *Science 208*, 4440 (1980), 177–179.

[85] Hayflick, L., and Moorhead, P. S. The serial cultivation of human diploid cell strains. *Experimental Cell Research 25*, 3 (1961), 585–621.

[86] Heissler, S. M., and Sellers, J. R. Myosin light chains: Teaching old dogs new tricks. *Bioarchitecture 4*, 6 (2014), 169–188.

[87] Herbert, K. M., La Porta, A., Wong, B. J., Mooney, R. A., Neuman, K. C., Landick, R., and Block, S. M. Sequence-Resolved Detection of Pausing by Single RNA Polymerase Molecules. *Cell 126*, 6 (2006), 1083–1094.

[88] Herbig, U., Ferreira, M., Condel, L., Carey, D., and Sedivy, J. M. Cellular senescence in aging primates. *Science 311*, 5765 (2006), 1257.

[89] Herrmann, H., Bär, H., Kreplak, L., Strelkov, S. V., and Aebi, U. Intermediate filaments: From cell architecture to nanomechanics. *Nature Reviews Molecular Cell Biology 8*, 7 (2007), 562–573.

[90] Hertz, H. Ueber die Berührung fester elastischer Körper. *Journal fur die Reine und Angewandte Mathematik 1882*, 92 (1882), 156–171.

[91] Heys, K. R., Cram, S. L., and Truscott, R. J. W. Massive increase in the stiffness of the human lens nucleus with age: The basis for presbyopia? *Molecular Vision 10* (2004), 956–963.

[92] Heys, K. R., and Truscott, R. J. The stiffness of human cataract lenses is a function of both age and the type of cataract. *Experimental Eye Research 86*, 4 (2008), 701–703.

[93] Hirano, Y., Takahashi, H., Kumeta, M., Hizume, K., Hirai, Y., Otsuka, S., Yoshimura, S. H., and Takeyasu, K. Nuclear architecture and chromatin dynamics revealed by atomic force microscopy in combination with biochemistry and cell biology. *Pflugers Archiv European Journal of Physiology 456*, 1 (2008), 139–153.

[94] Hirokawa, N. Kinesin and dynein superfamily proteins and the mechanism of organelle transport. *Science 279*, 5350 (1998), 519–526.

[95] Horie, M., Saito, A., Yamauchi, Y., Mikami, Y., Sakamoto, M., Jo, T., Nakajima, J., Takizawa, H., Nagase, T., and Kohyama, T. Histamine induces human lung fibroblast-mediated collagen gel contraction via histamine H1 receptor. *Experimental Lung Research 40*, 5 (2014), 222–236.

[96] Horton, M., Charras, G., Ballestrem, C., and Lehenkari, P. Integration of Atomic Force and Confocal Microscopy. *Single Molecules 1* (2000), 135–137.

[97] Horvath, S. DNA methylation age of human tissues and cell types. *Genome Biology 14*, 3156 (2013).

[98] Hu, K., Shi, H., Zhu, J., Deng, D., Zhou, G., Zhang, W., Cao, Y., and Liu, W. Compressed collagen gel as the scaffold for skin engineering. *Biomedical Microdevices 12*, 4 (2010), 627–635.

[99] Huang, S., and Ingber, D. E. Cell tension, matrix mechanics, and cancer development. *Cancer Cell 8*, 3 (2005), 175–176.

[100] Humphrey, J. D., Dufresne, E. R., and Schwartz, M. A. Mechanotransduction and extracellular matrix homeostasis. *Nature Reviews Molecular Cell Biology 15*, 12 (2014), 802–812.

[101] Huxley, H., and Hanson, J. Changes in the Cross-striations of muscle during contraction and stretch and their structural interpretation. *Nature 173* (1954), 973–976.

[102] Huxley, H. E. The mechanism of muscular contraction. *Science 164*, 3886 (1969), 1356–1365.

[103] Hwang, E. S., Yoon, G., and Kang, H. T. A comparative analysis of the cell biology of senescence and aging. *Cellular and molecular life sciences : CMLS 66*, 15 (2009), 2503–24.

[104] Imokawa, G., Akasaki, S., Minematsu, Y., and Kawai, M. Importance of intercellular lipids in water-retention properties of the stratum corneum: induction and recovery study of surfactant dry skin. *Archives of Dermatological Research 281* (1989), 45–51.

[105] Iwadate, Y., and Yumura, S. Actin-based propulsive forces and myosin-II-based contractile forces in migrating Dictyostelium cells. *Journal of Cell Science 121* (2008), 1314–1324.

[106] Jaalouk, D. E., and Lammerding, J. Mechanotransduction gone awry. *Nature Reviews Molecular Cell Biology 10* (2009), 63–73.

[107] Jachowicz, R. S., and Senturia, S. D. A thin-film capacitance humidity sensor. *Sensors and Actuators 2* (1981), 171–186.

[108] Jin, T., Li, L., Siow, R. C. M., and Liu, K.-K. A novel collagen gel-based measurement technique for quantitation of cell contraction force. *Journal of The Royal Society Interface 12*, 106 (2015), 20141365.

[109] Jin, T., Li, L., Siow, R. C. M., and Liu, K.-k. Collagen matrix stiffness influences fibroblast contraction force. *Biomedical Physics & Engineering Express 2*, 4 (2016), 047002.

[110] Jonsson, G., and Benavente, J. Determination of some transport coefficients for the skin and porous layer of a composite membrane. *Journal of Membrane Science 69*, 1-2 (1992), 29–42.

[111] Jung, M., and Pfeifer, G. P. Aging and DNA methylation. *BMC Biology 13*, 7 (2015).

[112] Kalyanam, S., Yapp, R. D., and Insana, M. F. Poro-viscoelastic behavior of gelatin hydrogels under compression- implications for bioelasticity imaging. *Journal of Biomechanical Engineering 131*, 8 (2009), 081005.

[113] Khavkin, J., and Ellis, D. A. Aging Skin: Histology, Physiology, and Pathology. *Facial Plastic Surgery Clinics of North America 19*, 2 (2011), 229–234.

[114] Kim, Y. I., Kim, K. S., Ahn, H. J., Kang, I. H., and Shin, M. K. Reduced matrix metalloproteinase and collagen transcription mediated by the TGF-β/Smad pathway in passaged normal human dermal fibroblasts. *Journal of Cosmetic Dermatology 19*, 5 (2020), 1211–1218.

[115] Knott, A., Reuschlein, K., Lucius, R., Stäb, F., Wenck, H., and Gallinat, S. Deregulation of versican and elastin binding protein in solar elastosis. *Biogerontology 10*, 2 (2009), 181–190.

[116] Koch, C. M., Reck, K., Shao, K., Lin, Q., Joussen, S., Ziegler, P., Walenda, G., Drescher, W., Opalka, B., May, T., Brummendorf, T., Zenke, M., Saric, T., and Wagner, W. Pluripotent stem cells escape from senescenceassociated DNA methylation changes. *Genome Research 23*, 2 (2013), 248–259.

[117] Koch, T. M., Münster, S., Bonakdar, N., Butler, J. P., and Fabry, B. 3D traction forces in cancer cell invasion. *PLoS ONE 7*, 3 (2012), 1–8.

[118] Kolodney, M. S., and Wysolmerski, R. B. Isometric contraction by fibroblasts and endothelial cells in tissue culture: A quantitative study. *Journal of Cell Biology 117*, 1 (1992), 73–82.

[119] Kozie, R., Greussing, R., Maier, A. B., Declercq, L., and Jansen-Dürr, P. Functional interplay between mitochondrial and proteasome activity in skin aging. *Journal of Investigative Dermatology 131*, 3 (2011), 594–603.

[120] Krieglstein, K., Miyazono, K., Ten Dijke, P., and Unsicker, K. TGF-β in aging and disease. *Cell and Tissue Research 347*, 1 (2012), 5–9.

[121] Krutmann, J., Morita, A., and Chung, J. H. Sun exposure: What molecular photodermatology tells us about its good and bad sides. *Journal of Investigative Dermatology 132*, 3 (2012), 976–984.

[122] Kurachi, M., Hoshi, M., and Tashiro, H. Buckling of a single microtubule by optical trapping forces: Direct measurement of microtubule rigidity. *Cell Motility and the Cytoskeleton 30*, 3 (1995), 221–228.

[123] Kuznetsova, T. G., Starodubtseva, M. N., Yegorenkov, N. I., Chizhik, S. A., and Zhdanov, R. I. Atomic force microscopy probing of cell elasticity. *Micron 38*, 8 (2007), 824–833.

[124] Lam, W. A., Rosenbluth, M. J., and Fletcher, D. A. Chemotherapy exposure increases leukemia cell stiffness. *Blood 109*, 8 (2007), 3505–3508.

[125] Laplante, C., Huang, F., Tebbs, I. R., Bewersdorf, J., and Pollard, T. D. Molecular organization of cytokinesis nodes and contractile rings by super-resolution fluorescence microscopy of live fission yeast. *Pro-*

ceedings of the National Academy of Sciences of the United States of America 113, 40 (2016), e5876–e5885.

[126] Lee, C. H., Singla, A., and Lee, Y. Biomedical applications of collagen. *International Journal of Pharmaceutics 221*, 1-2 (2001), 1–22.

[127] Legant, W. R., Chen, C. S., and Vogel, V. Force-induced fibronectin assembly and matrix remodeling in a 3D microtissue model of tissue morphogenesis. *Integrative Biology (United Kingdom) 4*, 10 (2012), 1164–1174.

[128] Legant, W. R., Miller, J. S., Blakely, B. L., Cohen, D. M., Genin, G. M., and Chen, C. S. Measurement of mechanical tractions exerted by cells in three-dimensional matrices. *Nature Methods 7*, 12 (2010), 969–973.

[129] Lekka, M., Fornal, M., Pyka-Fościak, G., Lebed, K., Wizner, B., Grodzicki, T., and Styczeń, J. Erythrocyte stiffness probed using atomic force microscope. *Biorheology 42*, 4 (2005), 307–317.

[130] Lenormand, G., Hénon, S., Richert, A., Siméon, J., and Gallet, F. Direct measurement of the area expansion and shear moduli of the human red blood cell membrane skeleton. *Biophysical Journal 81*, 1 (2001), 43–56.

[131] Li, B., and Wang, J. H. C. Fibroblasts and myofibroblasts in wound healing: Force generation and measurement. *Journal of Tissue Viability 20*, 4 (2011), 108–120.

[132] Li, T., Kon, N., Jiang, L., Tan, M., Ludwig, T., Zhao, Y., Baer, R., and Gu, W. Tumor suppression in the absence of p53-mediated cell-cycle arrest, apoptosis, and senescence. *Cell 149*, 6 (2012), 1269–1283.

[133] Lim, C. T., Zhou, E. H., Li, A., Vedula, S. R., and Fu, H. X. Experimental techniques for single cell and single molecule biomechanics. *Materials Science and Engineering C 26*, 8 (2006), 1278–1288.

[134] Lim, C. T., Zhou, E. H., and Quek, S. T. Mechanical models for living cells - A review. *Journal of Biomechanics 39*, 2 (2006), 195–216.

[135] Liu, S. C., Derick, L. H., Zhai, S., and Palek, J. Uncoupling of the spectrin-based skeleton from the lipid bilayer in sickled red cells. *Science 252*, 5005 (1991), 574–576.

[136] Liu, Z., Sniadecki, N. J., and Chen, C. S. Mechanical forces in endothelial cells during firm adhesion and early transmigration of human monocytes. *Cellular and Molecular Bioengineering 3*, 1 (2010), 50–59.

[137] Lombardi, M. L., Knecht, D. A., Dembo, M., and Lee, J. Traction force microscopy in Dictyostelium reveals distinct roles for myosin II motor and actin-crosslinking activity in polarized cell movement. *Journal of Cell Science 120*, 1 (2007), 1624–1634.

[138] López-Otín, C., Blasco, M. A., Partridge, L., Serrano, M., and Kroemer, G. The hallmarks of aging. *Cell 153*, 6 (2013), 1194.

[139] Lu, S., and Wang, Y. Chapter Two - Single-Cell Imaging of Mechanotransduction in Endothelial Cells. In *Mechanotransduction*, A. J. Engler, S. B. T. P. i. M. B. Kumar, and T. Science, Eds., vol. 126. Academic Press, 2014, pp. 25–51.

[140] Luo, K. Ski and SnoN: Negative regulators of TGF-β signaling. *Current Opinion in Genetics and Development 14*, 1 (2004), 65–70.

[141] Ma, X., Kovaćs, M., Conti, M. A., Wang, A., Zhang, Y., Sellers, J. R., and Adelstein, R. S. Nonmuscle myosin II exerts tension but does not translocate actin in vertebrate cytokinesis. *Proceedings of the National Academy of Sciences of the United States of America 109*, 12 (2012), 4509–4514.

[142] Maloney, J. M., Nikova, D., Lautenschläger, F., Clarke, E., Langer, R., Guck, J., and Van Vliet, K. J. Mesenchymal stem cell mechanics from the attached to the suspended state. *Biophysical Journal 99*, 8 (2010), 2479–2487.

[143] Marklein, R. A., and Burdick, J. A. Spatially controlled hydrogel mechanics to modulate stem cell interactions. *Soft Matter 6*, 1 (2010), 136–143.

[144] Maskarinec, S. A., Franck, C., Tirrell, D. A., and Ravichandran, G. Quantifying cellular traction forces in three dimensions. *Proceedings of the National Academy of Sciences of the United States of America 106*, 52 (2009), 22108–22113.

[145] Mattice, J. M., Lau, A. G., Oyen, M. L., and Kent, R. W. Spherical indentation load-relaxation of soft biological tissues. *Journal of Materials Research 21*, 8 (2006), 2003–2010.

[146] McClintock, D., Ratner, D., Lokuge, M., Owens, D. M., Gordon, L. B., Collins, F. S., and Djabali, K. The mutant form of Lamin A that causes Hutchinson-Gilford progeria is a biomarker of cellular aging in human skin. *PLoS ONE 2*, 12 (2007), e1269.

[147] Meigel, W. N., Gay, S., and Weber, L. Dermal architecture and collagen type distribution. *Archives for Dermatological Research 259*, 1 (1977), 1–10.

[148] Metcalf, D. J., García-Arencibia, M., Hochfeld, W. E., and Rubinsztein, D. C. Autophagy and misfolded proteins in neurodegeneration. *Experimental Neurology 238*, 1 (2012), 22–28.

[149] Meunier, S., and Vernos, I. Microtubule assembly during mitosis - from distinct origins to distinct functions? *Journal of Cell Science 125*, 1 (2012), 2805–2814.

[150] Mine, S., Fortunel, N. O., Pageon, H., and Asselineau, D. Aging alters functionally human dermal papillary fibroblasts but not reticular fibroblasts: A new view of skin morphogenesis and aging. *PLoS ONE 3*, 12 (2008), e4066.

[151] Módis, L. *Organization of the Extracellular Matrix: a Polarization Microscopic Approach*, 1 ed. CRC Press, Boca Raton, may 2018.

[152] Moeendarbary, E., and Harris, A. R. Cell mechanics: Principles, practices, and prospects. *Wiley Interdisciplinary Reviews: Systems Biology and Medicine 6*, 5 (2014), 371–388.

[153] Mogford, J. E., Tawil, N., Chen, A., Gies, D., Xia, Y., and Mustoe, T. A. Effect of age and hypoxia on TGFβ1 receptor expression and signal transduction in human dermal fibroblasts: Impact on cell migration. *Journal of Cellular Physiology 190*, 2 (2002), 259–65.

[154] Montesano, R., and Orci, L. Transforming growth factor beta stimulates collagen-matrix contraction by fibroblasts: implications for wound healing. *Proceedings of the National Academy of Sciences of the United States of America 85*, 13 (1988), 4894–4897.

[155] Moon, A. G., and Tranquillo, R. T. Fibroblastpopulated collagen microsphere assay of cell traction force: Part 1. Continuum model. *AIChE Journal 39*, 1 (1993), 163–177.

[156] Moore, S. W., Roca-Cusachs, P., and Sheetz, M. P. Stretchy proteins on stretchy substrates: The important elements of integrin-mediated rigidity sensing. *Developmental Cell 19*, 2 (2010), 194–206.

[157] Morales, S. A., Mareninov, S., Prasad, P., Wadehra, M., Braun, J., and Gordon, L. K. Collagen gel contraction by ARPE-19 cells is mediated

by a FAK-Src dependent pathway. *Experimental Eye Research 85*, 6 (2007), 790–798.

[158] Moulding, D. A., Moeendarbary, E., Valon, L., Record, J., Charras, G. T., and Thrasher, A. J. Excess F-actin mechanically impedes mitosis leading to cytokinesis failure in X-linked neutropenia by exceeding Aurora B kinase error correction capacity. *Blood 120*, 18 (2012), 3803–3811.

[159] Muller, D. J. AFM: A nanotool in membrane biology. *Biochemistry 47*, 31 (2008), 7986–7998.

[160] Mulligan, J. A., Feng, X., and Adie, S. G. Quantitative reconstruction of time-varying 3D cell forces with traction force optical coherence microscopy. *Scientific Reports 9*, 1 (2019), 1–14.

[161] Mullins, R. D., Bieling, P., and Fletcher, D. A. From solution to surface to filament: actin flux into branched networks. *Biophysical Reviews 10*, 6 (2018), 1537–1551.

[162] Munevar, S., Wang, Y. L., and Dembo, M. Traction force microscopy of migrating normal and H-ras transformed 3T3 fibroblasts. *Biophysical Journal 80*, 4 (2001), 1744–1757.

[163] Nadel, E. R., Bullard, R. W., and Stolwijk, J. A. Importance of skin temperature in the regulation of sweating. *Journal of applied physiology 31*, 1 (1971), 80–87.

[164] Nafo, W., and Al-Mayah, A. Characterization of PVA hydrogels' hyperelastic properties by uniaxial tension and cavity expansion tests. *International Journal of Non-Linear Mechanics 124*, 1 (2020), 103515.

[165] Nelson, G., Wordsworth, J., Wang, C., Jurk, D., Lawless, C., Martin-Ruiz, C., and von Zglinicki, T. A senescent cell bystander effect: Senescence-induced senescence. *Aging Cell 11*, 2 (2012), 345–349.

[166] Ng, S. S., Li, C., and Chan, V. Experimental and numerical determination of cellular traction force on polymeric hydrogels. *Interface Focus 1*, 5 (2011), 777–791.

[167] Ngo, P., Ramalingam, P., Phillips, J. A., and Furuta, G. T. *Collagen Gel Contraction Assay.* Humana Press, Totowa, NJ, 2006, pp. 103–109.

[168] Ohshima, S. Centrosome aberrations associated with cellular senescence and p53 localization at supernumerary centrosomes. *Oxidative Medicine and Cellular Longevity 2012*, 1 (2012), 217594.

[169] Pan, M. R., Li, K., Lin, S. Y., and Hung, W. C. Connecting the dots: From DNA damage and repair to aging. *International Journal of Molecular Sciences 17*, 5 (2016), 685.

[170] Park, Y. K., Best, C. A., Badizadegan, K., Dasari, R. R., Feld, M. S., Kuriabova, T., Henle, M. L., Levine, A. J., and Popescu, G. Measurement of red blood cell mechanics during morphological changes. *Proceedings of the National Academy of Sciences of the United States of America 107*, 15 (2010), 6731–6736.

[171] Parrinello, S. Stromal-epithelial interactions in aging and cancer: senescent fibroblasts alter epithelial cell differentiation. *Journal of Cell Science 118*, 3 (2005), 485–496.

[172] Pelham, R. J., and Wang, Y. L. Cell locomotion and focal adhesions are regulated by substrate flexibility. *Proceedings of the National Academy of Sciences of the United States of America 94*, 25 (1997), 13661–13665.

[173] Pena, R. A., Jerdan, J. A., and Glaser, B. M. Effects of TGF-β and TGF-β neutralizing antibodies on fibroblast- induced collagen gel contraction: Implications for proliferative vitreoretinopathy. *Investigative Ophthalmology and Visual Science 35*, 6 (1994), 2804–2808.

[174] Peng, Z., Li, X., Pivkin, I. V., Dao, M., Karniadakis, G. E., and Suresh, S. Lipid bilayer and cytoskeletal interactions in a red blood cell. *Proceedings of the National Academy of Sciences of the United States of America 110*, 33 (2013), 13356–13361.

[175] Peperzak, K. A., Gilbert, T. W., and Wang, J. H. A multi-station dynamic-culture force monitor system to study cell mechanobiology. *Medical Engineering and Physics 26*, 4 (2004), 355–358.

[176] Pesen, D., and Hoh, J. H. Micromechanical architecture of the endothelial cell cortex. *Biophysical Journal 88*, 1 (2005), 670–679.

[177] Petersen, O. W., Ronnov-Jessen, L., Howlett, A. R., and Bissell, M. J. Interaction with basement membrane serves to rapidly distinguish growth and differentiation pattern of normal and malignant human breast epithelial cells. *Proceedings of the National Academy of Sciences of the United States of America 89*, 19 (1992), 9064–9068.

[178] Polacheck, W. J., and Chen, C. S. Measuring cell-generated forces: A guide to the available tools. *Nature Methods 13*, 5 (2016), 415–423.

[179] Putnam, A. J., Schultz, K., and Mooney, D. J. Control of microtubule assembly by extracellular matrix and externally applied strain. *American Journal of Physiology - Cell Physiology 280*, 3 (2001), c556–c564.

[180] Qin, Z., Kreplak, L., and Buehler, M. J. Hierarchical structure controls nanomechanical properties of vimentin intermediate filaments. *PLoS ONE 4*, 10 (2009), e7294.

[181] Quan, T., and Fisher, G. J. Role of age-associated alterations of the dermal extracellular matrix microenvironment in human skin aging: A mini-review. *Gerontology 61*, 5 (2015), 427–434.

[182] Reed, M. J., Ferara, N. S., and Vernon, R. B. Impaired migration, integrin function, and actin cytoskeletal organization in dermal fibroblasts from a subset of aged human donors. *Mechanisms of Ageing and Development 122*, 11 (2001), 1203–1220.

[183] Rhee, S., and Grinnell, F. Fibroblast mechanics in 3D collagen matrices. *Advanced Drug Delivery Reviews 59*, 13 (2007), 1299–1305.

[184] Rhie, G. E., Mi, H. S., Jin, Y. S., Won, W. C., Kwang, H. C., Kyu, H. K., Kyung, C. P., Hee, C. E., and Jin, H. C. Aging- and photoaging-dependent changes of enzymic and nonenzymic antioxidants in the epidermis and dermis of human skin in vivo. *Journal of Investigative Dermatology 117*, 5 (2001), 1212–1217.

[185] Ricart, B. G., Yang, M. T., Hunter, C. A., Chen, C. S., and Hammer, D. A. Measuring traction forces of motile dendritic cells on micropost arrays. *Biophysical Journal 101*, 11 (2011), 2620–2628.

[186] Richards, S. A., Muter, J., Ritchie, P., Lattanzi, G., and Hutchison, C. J. The accumulation of un-repairable DNA damage in laminopathy progeria fibroblasts is caused by ROS generation and is prevented by treatment with N-acetyl cysteine. *Human Molecular Genetics 20*, 20 (2011), 3997–4004.

[187] Rivlin, R. S. Large elastic deformations of isotropic materials IV. further developments of the general theory. *Philosophical Transactions of the Royal Society of London. Series A, Mathematical and Physical Sciences 241*, 835 (1948), 379–397.

[188] Röck, K., Grandoch, M., Majora, M., Krutmann, J., and Fischer, J. W. Collagen fragments inhibit hyaluronan synthesis in skin fibroblasts in response to ultraviolet B (UVB): New insights into mechanisms of matrix remodeling. *Journal of Biological Chemistry 286*, 20 (2011), 18268–18276.

[189] Rodrigo, P. J., Perch-Nielsen, I. R., and Glückstad, J. Three-dimensional forces in GPC-based counterpropagating-beam traps. *Optics Express 14*, 12 (2006), 5812–5822.

[190] Rodriguez, A. G., Han, S. J., Regnier, M., and Sniadecki, N. J. Substrate stiffness increases twitch power of neonatal cardiomyocytes in correlation with changes in myofibril structure and intracellular calcium. *Biophysical Journal 101*, 1 (2011), 2455–2464.

[191] Rodriguez, M. L., McGarry, P. J., and Sniadecki, N. J. Review on cell mechanics: Experimental and modeling approaches. *Applied Mechanics Reviews 65*, 6 (2013), 060801.

[192] Rosa, N., Simoes, R., Magalhães, F. D., and Marques, A. T. From mechanical stimulus to bone formation: A review. *Medical Engineering and Physics 37*, 8 (2015), 719–728.

[193] Rösel, D., Brábek, J., Tolde, O., Mierke, C. T., Zitterbart, D. P., Raupach, C., Bicanová, K., Kollmannsberger, P., Paková, D., Veselý, P., Folk, P., and Fabry, B. Up-regulation of Rho/ROCK signaling in sarcoma cells drives invasion and increased generation of protrusive forces. *Molecular Cancer Research 6*, 9 (2008), 1410–1420.

[194] Rosenbluth, M. J., Lam, W. A., and Fletcher, D. A. Force microscopy of nonadherent cells: a comparison of leukemia cell deformability. *Biophysical journal 90*, 8 (2006), 2994–3003.

[195] Rotsch, C., and Radmacher, M. Drug-induced changes of cytoskeletal structure and mechanics in fibroblasts: an atomic force microscopy study. *Biophysical journal 78*, 1 (2000), 520–535.

[196] Saez, I., and Vilchez, D. The mechanistic links between proteasome activity, aging and age related diseases. *Current Genomics 15*, 1 (2014), 38–51.

[197] Sakar, M. S., Neal, D., Boudou, T., Borochin, M. A., Li, Y., Weiss, R., Kamm, R. D., Chen, C. S., and Asada, H. H. Formation and optogenetic control of engineered 3D skeletal muscle bioactuators. *Lab on a Chip 12*, 23 (2012), 4976–7985.

[198] Sato, M., Suzuki, K., Ueki, Y., and Ohashi, T. Microelastic mapping of living endothelial cells exposed to shear stress in relation to three-dimensional distribution of actin filaments. *Acta Biomaterialia 3*, 3 (2007), 311–319.

[199] Schulze, C., Wetzel, F., Kueper, T., Malsen, A., Muhr, G., Jaspers, S., Blatt, T., Wittern, K. P., Wenck, H., and Käs, J. A. Stiffening of human skin fibroblasts with age. *Clinics in Plastic Surgery 39*, 1 (2012), 9–20.

[200] Schwarz, U. S., Balaban, N. Q., Riveline, D., Bershadsky, A., Geiger, B., and Safran, S. A. Calculation of forces at focal adhesions from elastic substrate data: The effect of localized force and the need for regularization. *Biophysical Journal 83*, 3 (2002), 1380–1394.

[201] Seite, S., Zucchi, H., Septier, D., Igondjo-Tchen, S., Senni, K., and Godeau, G. Elastin changes during chronological and photo-ageing: The important role of lysozyme. *Journal of the European Academy of Dermatology and Venereology 20*, 8 (2006), 980–987.

[202] Shin, J. W., Kwon, S. H., Choi, J. Y., Na, J. I., Huh, C. H., Choi, H. R., and Park, K. C. Molecular mechanisms of dermal aging and anti-

aging approaches. *International Journal of Molecular Sciences 20*, 9 (2019), 2126.

[203] Shin, S., Ku, Y., Babu, N., and Singh, M. Erythrocyte deformability and its variation in diabetes mellitus. *Indian Journal of Experimental Biology 45*, 1 (2007), 121–128.

[204] Shumaker, D. K., Dechat, T., Kohlmaier, A., Adam, S. A., Bozovsky, M. R., Erdos, M. R., Eriksson, M., Goldman, A. E., Khuon, S., Collins, F. S., Jenuwein, T., and Goldman, R. D. Mutant nuclear lamin A leads to progressive alterations of epigenetic control in premature aging. *Proceedings of the National Academy of Sciences of the United States of America 103*, 23 (2006), 8703–8708.

[205] Siamantouras, E., Hills, C. E., Squires, P. E., and Liu, K. K. Quantifying cellular mechanics and adhesion in renal tubular injury using single cell force spectroscopy. *Nanomedicine: Nanotechnology, Biology, and Medicine 12*, 4 (2016), 1013–1021.

[206] Sjerobabski-Masnec, I., and Šitum, M. Skin aging. *Acta Clinica Croatica 49*, 4 (2010), 515–518.

[207] Sneddon, I. N. The relation between load and penetration in the axisymmetric boussinesq problem for a punch of arbitrary profile. *International Journal of Engineering Science 3*, 1 (1965), 47–57.

[208] Stachurski, Z. H. Mechanical behavior of materials. *Materials Today 12*, 3 (2009), 44.

[209] Starodubtseva, M. N. Mechanical properties of cells and ageing. *Ageing Research Reviews 10*, 1 (2011), 16–25.

[210] Sun, Y., Villa-Diaz, L. G., Lam, R. H., Chen, W., Krebsbach, P. H., and Fu, J. Mechanics regulates fate decisions of human embryonic stem cells. *PLoS ONE 7*, 5 (2012), e37178.

[211] Suresh, S., Spatz, J., Mills, J. P., Micoulet, A., Dao, M., Lim, C. T., Beil, M., and Seufferlein, T. Connections between single-cell biomechanics and human disease states: Gastrointestinal cancer and malaria. *Acta Biomaterialia 1*, 1 (2005), 15–30.

[212] Suzuki, T., Fujii, M., and Ayusawa, D. Demethylation of classical satellite 2 and 3 DNA with chromosomal instability in senescent human fibroblasts. *Experimental Gerontology 37*, 8-9 (2002), 1005–1014.

[213] Takahashi, Y., Moriwaki, S. I., Sugiyama, Y., Endo, Y., Yamazaki, K., Mori, T., Takigawa, M., and Inoue, S. Decreased gene expression responsible for post-ultraviolet DNA repair synthesis in aging: A possible mechanism of age-related reduction in DNA repair capacity. *Journal of Investigative Dermatology 124*, 2 (2005), 435–442.

[214] Tamada, M., Sheetz, M. P., and Sawada, Y. Activation of a signaling cascade by cytoskeleton stretch. *Developmental Cell 7*, 5 (2004), 709–718.

[215] Tan, J. C., Kalapesi, F. B., and Coroneo, M. T. Mechanosensitivity and the eye: Cells coping with the pressure. *British Journal of Ophthalmology 90*, 3 (2006), 383–388.

[216] Tan, J. L., Tien, J., Pirone, D. M., Gray, D. S., Bhadriraju, K., and Chen, C. S. Cells lying on a bed of microneedles: An approach to isolate mechanical force. *Proceedings of the National Academy of Sciences of the United States of America 100*, 4 (2003), 1484–1489.

[217] Tang, D. D., and Gerlach, B. D. The roles and regulation of the actin cytoskeleton, intermediate filaments and microtubules in smooth muscle cell migration. *Respiratory Research 18*, 1 (2017), 1–12.

[218] Tanner, R. I. *Engineering Rheology*, 2 ed. Oxford University Press, 1982.

[219] Tatara, Y. On compression of rubber elastic sphere over a large range of displacements-part 1: Theoretical study. *Journal of Engineering Materials and Technology, Transactions of the ASME 113*, 3 (1991), 285–291.

[220] The Open University. Components of the cytoskeleton.

[221] Theocharis, A. D., Skandalis, S. S., Gialeli, C., and Karamanos, N. K. Extracellular matrix structure. *Advanced Drug Delivery Reviews 97*, 1 (2016), 4–27.

[222] Tibbitt, M. W., and Anseth, K. S. Hydrogels as extracellular matrix mimics for 3D cell culture. *Biotechnology and Bioengineering 103*, 4 (2009), 655–663.

[223] Tigges, J., Krutmann, J., Fritsche, E., Haendeler, J., Schaal, H., Fischer, J. W., Kalfalah, F., Reinke, H., Reifenberger, G., Stühler, K., Ventura, N., Gundermann, S., Boukamp, P., and Boege, F. The hallmarks of fibroblast ageing. *Mechanisms of ageing and development 138*, 1 (2014), 26–44.

[224] Tingstrom, A., Heldin, C. H., and Rubin, K. Regulation of fibroblast-mediated collagen gel contraction by platelet-derived growth factor, interleukin-1 α and transforming growth factor-β1. *Journal of Cell Science 102*, 2 (1992), 315–322.

[225] Tirella, A., Mattei, G., and Ahluwalia, A. Strain rate viscoelastic analysis of soft and highly hydrated biomaterials. *Journal of Biomedical Materials Research - Part A 102*, 10 (2014), 3352–3360.

[226] Titushkin, I., and Cho, M. Distinct membrane mechanical properties of human mesenchymal stem cells determined using laser optical tweezers. *Biophysical Journal 90*, 7 (2006), 2582–2591.

[227] Tomasek, J. J., Haaksma, C. J., Eddy, R. J., and Vaughan, M. B. Fibroblast contraction occurs on release of tension in attached collagen lattices: Dependency on an organized actin cytoskeleton and serum. *The Anatomical Record 232*, 3 (1992), 359–368.

[228] Travis, J. A., Hughes, M. G., Wong, J. M., Wagner, W. D., and Geary, R. L. Hyaluronan enhances contraction of collagen by smooth muscle cells and adventitial fibroblasts role of CD44 and implications for constrictive remodeling. *Circulation Research 88*, 1 (2001), 77–83.

[229] Ulrich, T. A., De Juan Pardo, E. M., and Kumar, S. The mechanical rigidity of the extracellular matrix regulates the structure, motility, and proliferation of glioma cells. *Cancer Research 69*, 10 (2009), 4167–4174.

[230] Upadhyay, K., Subhash, G., and Spearot, D. Hyperelastic constitutive modeling of hydrogels based on primary deformation modes and validation under 3D stress states. *International Journal of Engineering Science 154*, 1 (2020), 103314.

[231] Van Vliet, K. J., Bao, G., and Suresh, S. The biomechanics toolbox: Experimental approaches for living cells and biomolecules. *Acta Materialia 51*, 19 (2003), 5881–5905.

[232] Varani, J., Dame, M. K., Rittie, L., Fligiel, S. E., Kang, S., Fisher, G. J., and Voorhees, J. J. Decreased collagen production in chronologically

aged skin: Roles of age-dependent alteration in fibroblast function and defective mechanical stimulation. *American Journal of Pathology 168*, 6 (2006), 1861–1868.

[233] Vedrenne, N., Coulomb, B., Danigo, A., Bonté, F., and Desmoulière, A. The complex dialogue between (myo)fibroblasts and the extracellular matrix during skin repair processes and ageing. *Pathologie Biologie 60*, 1 (2012), 20–27.

[234] Vikhorev, P. G., and Vikhoreva, N. N. Cardiomyopathies and related changes in contractility of human heart muscle. *International Journal of Molecular Sciences 19*, 8 (2018), 2234.

[235] Vinckier, A., and Semenza, G. Measuring elasticity of biological materials by atomic force microscopy. *FEBS Letters 430*, 1-2 (1998), 12–16.

[236] Wang, H. B., Dembo, M., and Wang, Y. L. Substrate flexibility regulates growth and apoptosis of normal but not transformed cells. *American Journal of Physiology - Cell Physiology 279*, 5 (2000), c1345–c1350.

[237] Wang, N., Naruse, K., Stamenović, D., Fredberg, J. J., Mijailovich, S. M., Tolić-Nørrelykke, I. M., Polte, T., Mannix, R., and Ingber, D. E. Mechanical behavior in living cells consistent with the tensegrity model. *Proceedings of the National Academy of Sciences of the United States of America 98*, 14 (2001), 7765–7770.

[238] Wang, Q., Manmi, K., and Liu, K.-K. Cell mechanics in biomedical cavitation. *Interface Focus 5*, 5 (2015), 20150018.

[239] Wang, Y., Botvinick, E. L., Zhao, Y., Berns, M. W., Usami, S., Tsien, R. Y., and Chien, S. Visualizing the mechanical activation of Src. *Nature 434*, 1 (2005), 1040–1045.

[240] Weisenberg, R. C. Microtubule formation in vitro in solutions containing low calcium concentrations. *Science 177*, 4054 (1972), 1104–1105.

[241] West, A. R., Zaman, N., Cole, D. J., Walker, M. J., Legant, W. R., Boudou, T., Chen, C. S., Favreau, J. T., Gaudette, G. R., Cowley, E. A., and Maksym, G. N. Development and characterization of a 3D multicell microtissue culture model of airway smooth muscle. *American Journal of Physiology - Lung Cellular and Molecular Physiology 304*, 1 (2013), L4–L16.

[242] Wilks, B. T., Evans, E. B., Nakhla, M. N., and Morgan, J. R. Directing fibroblast self-assembly to fabricate highly-aligned, collagen-rich matrices. *Acta Biomaterialia 81* (2018), 70–79.

[243] Willett, C. D., Adams, M. J., Johnson, S. A., and Seville, J. P. Capillary bridges between two spherical bodies. *Langmuir 16*, 24 (2000), 9396–9405.

[244] Wingreen, N. S., and Huang, K. C. Physics of Intracellular Organization in Bacteria. *Annual Review of Microbiology 69*, 1 (2015), 361–379.

[245] Xia, S., Zhang, X., Zheng, S., Khanabdali, R., Kalionis, B., Wu, J., Wan, W., and Tai, X. An Update on Inflamm-Aging: Mechanisms, Prevention, and Treatment. *Journal of Immunology Research 2016*, 1 (2016), 8426874.

[246] Xu, Q., and Engquist, B. A mathematical model for fitting and predicting relaxation modulus and simulating viscoelastic responses. *Proceedings of the Royal Society A: Mathematical, Physical and Engineering Sciences 474*, 2213 (2018).

[247] Xue, Z., and Sokac, A. M. Back-to-back mechanisms drive actomyosin ring closure during drosophila embryo cleavage. *Journal of Cell Biology 215*, 3 (2016), 335–344.

[248] Yamato, M., Yamamoto, K., and Hayashi, T. Age-related changes in collagen gel contraction by cultured human lung fibroblasts resulting in cross-over of contraction curves between young and aged cells. *Mechanisms of Ageing and Development 67*, 1-2 (1993), 149–158.

[249] Yang, M. T., Sniadecki, N. J., and Chen, C. S. Geometric considerations of micro- To nanoscale elastomeric post arrays to study cellular traction forces. *Advanced Materials 19*, 20 (2007), 3119–3123.

[250] Yengo, C. M., Takagi, Y., and Sellers, J. R. Temperature dependent measurements reveal similarities between muscle and non-muscle myosin motility. *Journal of Muscle Research and Cell Motility 33*, 6 (2012), 385–394.

[251] Yildiz, O. Vascular smooth muscle and endothelial functions in aging. *Annals of the New York Academy of Sciences 1100*, 1 (2007), 353–360.

[252] Yoshigi, M., Hoffman, L. M., Jensen, C. C., Yost, H. J., and Beckerle, M. C. Mechanical force mobilizes zyxin from focal adhesions to actin filaments and regulates cytoskeletal reinforcement. *Journal of Cell Biology 171*, 2 (2005), 209–215.

[253] Zhang, H., and Liu, K. K. Optical tweezers for single cells. *Journal of the Royal Society Interface 5*, 1 (2008), 671–690.

[254] Zhang, Y., Ng, S. S., Wang, Y., Feng, H., Chen, W. N., Chan-Park, M. B., Li, C., and Chan, V. Collective cell traction force analysis on aligned smooth muscle cell sheet between three-dimensional microwalls. *Interface Focus 4*, 2 (2014), 20130056.

[255] Zhu, J. Bioactive modification of poly(ethylene glycol) hydrogels for tissue engineering. *Biomaterials 31*, 17 (2010), 4639–4656.

[256] Zhu, Y. K., Umino, T., Liu, X. D., Wang, H. J., Romberger, D. J., Spurzem, J. R., Rennard, I., In, S., Cellular, V., Animal, D. B., Jan, N., and Animal, D. B. Contraction of fibroblast-containing collagen cels : initial collagen concentration regulates the degree of contraction and cell survival. *In Vitro Cellular & Developmental Biology. Anima 37*, 1 (2001), 10–16.

[257] Zimmermann, W. H., Fink, C., Kralisch, D., Remmers, U., Weil, J., and Eschenhagen, T. Three-dimensional engineered heart tissue from neonatal rat cardiac myocytes. *Biotechnology and Bioengineering 68*, 1 (2000), 106–114.

Appendix A

This appendix contains a list of publications from the author related with this thesis, supplemental figures and tables that supporting the context.